

Nitrogen in Diamond

Michael N. R. Ashfold,* Jonathan P. Goss, Ben L. Green, Paul W. May, Mark E. Newton,
and Chloe V. PeakerCite This: *Chem. Rev.* 2020, 120, 5745–5794

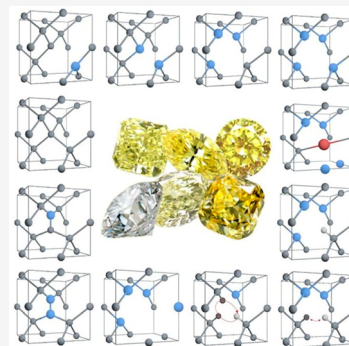
Read Online

ACCESS |

Metrics & More

Article Recommendations

ABSTRACT: Nitrogen is ubiquitous in both natural and laboratory-grown diamond, but the number and nature of the nitrogen-containing defects can have a profound effect on the diamond material and its properties. An ever-growing fraction of the supply of diamond appearing on the world market is now lab-grown. Here, we survey recent progress in two complementary diamond synthesis methods—high pressure high temperature (HPHT) growth and chemical vapor deposition (CVD), how each is allowing ever more precise control of nitrogen incorporation in the resulting diamond, and how the diamond produced by either method can be further processed (e.g., by implantation or annealing) to achieve a particular outcome or property. The burgeoning availability of diamond samples grown under well-defined conditions has also enabled huge advances in the characterization and understanding of nitrogen-containing defects in diamond—alone and in association with vacancies, hydrogen, and transition metal atoms. Among these, the negatively charged nitrogen-vacancy (NV^-) defect in diamond is attracting particular current interest in account of the many new and exciting opportunities it offers for, for example, quantum technologies, nanoscale magnetometry, and biosensing.



CONTENTS

1. Introduction	5746	3.4. Charge Transfer and Photochromism	5760
2. Laboratory-Based Synthesis of Diamond and Nitrogen-Containing Diamond	5748	3.5. Nitrogen-Containing Defects in Diamond	5760
2.1. High-Pressure High-Temperature (HPHT) Methods	5748	3.5.1. Single Substitutional Nitrogen N_s	5761
2.2. Chemical Vapor Deposition (CVD) Methods	5749	3.5.2. N_2^0 (the A-Center) and N_2^+	5762
2.2.1. Growth from C/H Containing Gas Mixtures with or without a Noble Gas	5749	3.5.3. Interstitial Nitrogen Defects	5763
2.2.2. CVD Growth Mechanism	5750	3.5.4. N_nV Family with $n = 1-4$	5763
2.2.3. Effects of Adding Nitrogen to C/H Containing Gas Mixtures	5751	3.5.5. N_nVH Family	5771
2.2.4. Doping CVD Diamond Films with Nitrogen	5753	3.5.6. N_nVH_m Family	5773
2.3. Diamond Particles: Diamondoids, Nanodiamonds, and Microdiamonds	5754	3.6. Selected Aggregates Involving Nitrogen and Another Element	5774
2.3.1. Diamondoids	5754	4. Applications of Nitrogen-Containing Diamond	5775
2.3.2. Nanodiamond	5754	4.1. Incorporation of Nitrogen in Natural Diamond: Applications in Geophysics and Geochemistry	5775
2.3.3. Microdiamond	5755	4.2. Nitrogen Defects and the Identification of Diamond Gemstones	5776
2.4. Implanting Nitrogen into Diamond	5756	4.3. Applications of Nitrogen-Doped Nanodiamonds	5776
3. Properties of Nitrogen-Doped Diamond	5756	4.4. Quantum Technologies Based on the NV^- Defect in Diamond	5777
3.1. Optical Properties	5757	4.4.1. Properties of the NV^- Defect in Diamond That Underpin Its Exploitation in Quantum Technologies	5777
3.1.1. Uniaxial Stress	5757		
3.1.2. Isotopic Enrichment	5758		
3.2. Spin Properties	5758		
3.2.1. Linking Optical Properties and Spin Properties	5758		
3.2.2. Atomistic Modeling	5759		
3.3. Irradiation and Annealing	5759		

Special Issue: Reactivity of Nitrogen from the Ground to the Atmosphere

Received: August 21, 2019

Published: February 12, 2020

4.4.2. NV ⁻ Defect in Diamond and Quantum Networks	5777
4.4.3. NV ⁻ Defect in Diamond and Quantum Computing	5778
4.4.4. NV ⁻ Magnetometry	5778
4.4.5. NV ⁻ Defect and the Future of NMR and MRI	5778
4.4.6. NV ⁻ Defect and Thermometry	5778
4.4.7. NV ⁻ Defect and Electric Field Sensing	5779
4.4.8. Hybrid Quantum Devices Involving a Solid-State Spin and a Macroscopic Mechanical Oscillator	5779
4.4.9. Diamond Masers	5779
5. Summary and Prospective	5779
Author Information	5779
Corresponding Author	5779
Authors	5779
Notes	5779
Biographies	5779
Acknowledgments	5780
References	5780

1. INTRODUCTION

Nitrogen is fundamental to the evolution of Earth. It is the major component of our atmosphere. It is a key element in most of the biomolecules essential to life and is obviously present in the mantle of Earth. Much of our knowledge relating to nitrogen in the mantle comes from analysis of natural diamonds. Most of these diamonds are formed at pressures and temperatures in the respective ranges of 5.5–8.0 GPa and 1000–1400 °C, corresponding to depths of 140–240 km, but some so-called “superdeep” diamonds are deduced to have originated at much greater depths in the lower mantle^{1,2}—as illustrated in Figure 1.

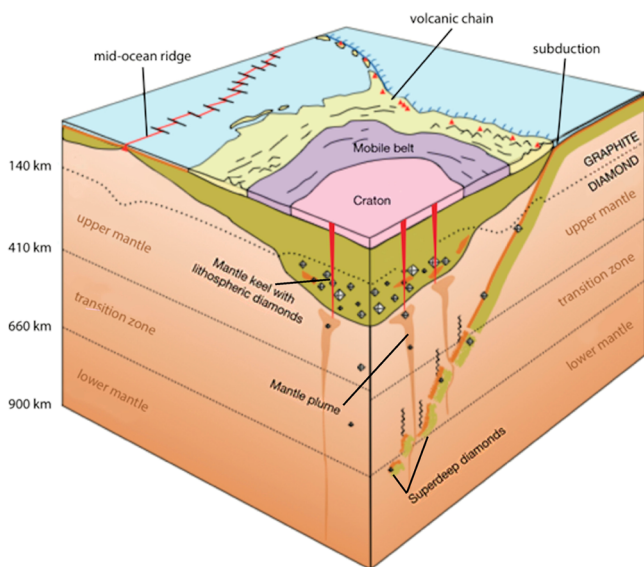


Figure 1. Basic relationship between a continental craton, its lithospheric mantle keel (the thick portion of the lithospheric mantle under the craton), and diamond stability regions in the keel and the mantle. Reprinted with permission from ref 1. Copyright 2013 Gemological Institute of America.

All natural diamonds contain some nitrogen impurities.³ The traditional classification of natural diamonds into types I and II is based on their nitrogen content: Type I samples typically contain hundreds if not thousands of parts per million (ppm) of nitrogen, which will often impart a visible coloration to the diamond and can be characterized (and quantified) by infrared (IR) spectroscopy. Type II diamonds, in contrast, were originally categorized on the basis that they contain too little nitrogen (typically just a few ppm or less) for its presence to be detected by IR absorption. Both types are further subdivided according to how the nitrogen is distributed and the extent, or otherwise, of any boron impurity—as illustrated in Figure 2.

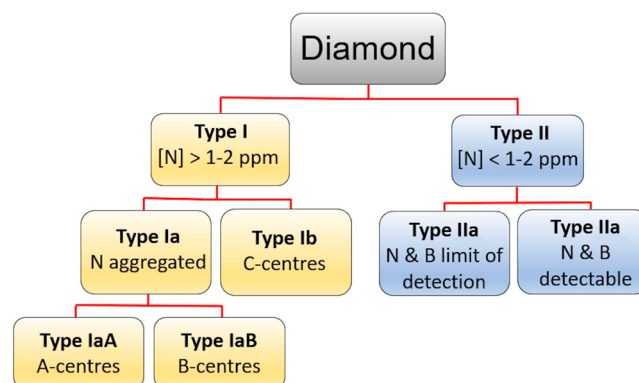


Figure 2. Classification of diamond based on nitrogen content.

Various IR-active N-related defects have long been recognized,^{4–7} and absorption coefficients have been estimated to allow quantification of the amount of nitrogen accommodated in such defects and studies of their interconversion under thermal processing.^{8,9} Such defects were historically labeled alphabetically. Examples include C-centers, wherein a single carbon atom in the diamond lattice has been substituted by a nitrogen atom, A-centers, pairs of substitutional nitrogen atoms, and B-centers, defects comprising four N atoms around a vacancy. A vacancy (henceforth often denoted as V) corresponds to a lattice site from which the carbon is missing. Each of these defects, and the cubic diamond lattice structure are illustrated in Figure 3. Recent advances in our understanding of these and many other N-related defects are surveyed in section 3.

Most (~98%) natural diamonds are type I. Of these, most are classified as type Ia and have a pale yellow or brown color attributable to aggregations of nitrogen atoms within the carbon lattice (see Figure 3). These nitrogen atoms often coexist with hydrogen impurities. As Figure 2 showed, type Ia diamonds are often further subdivided in types IaA, IaB (and even IaAB), reflecting the majority way in which the nitrogen is aggregated. Type Ib stones are much rarer. They also contain substantial nitrogen, but the nitrogen atoms are more widely dispersed throughout the sample. Type Ib diamonds tend to display a wider range of (often more intense) colors that reflect the distribution of nitrogen impurities.

Type IIa diamonds are considered the “purest of the pure”. They contain very low levels of impurity and are transparent throughout the visible and ultraviolet (UV) spectral regions down to wavelengths ~230 nm—thus appearing colorless. Many of the most famous large diamonds (e.g., the Cullinan, Koh-i-Noor, and Lesedi La Rona diamonds) are type IIa. Type IIb diamonds also have very low nitrogen content but, as

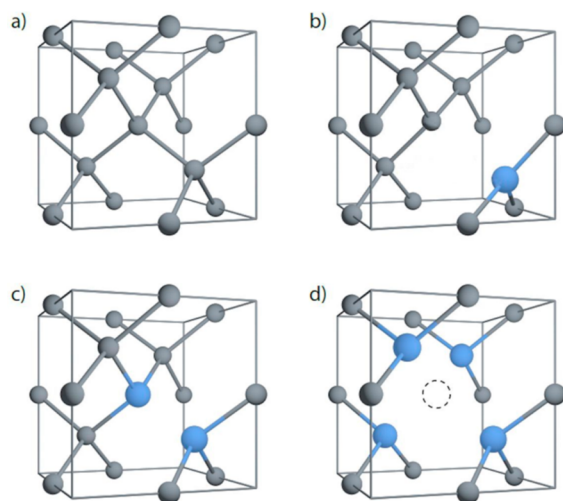


Figure 3. Atomic models of (a) the diamond structure and (b–d) three of the most common nitrogen point defect centers in diamond. The N atoms are blue and slightly larger than the C atoms (gray); a vacant lattice site is indicated by a dashed circle. (b) The C-center with a single substitutional nitrogen, N_s , results in one of the four N–C bonds being extended by $\sim 30\%$ as a result of the additional antibonding electron provided by the nitrogen. (c) The A-center with a nearest-neighbor nitrogen pair, N_2 . (d) The B-center with four nitrogen atoms surrounding a vacancy, N_4V . All defects are depicted in their neutral charge state.

illustrated in Figure 4, often generally appear light blue or gray because of the presence of trace quantities of atomic boron substituted within the lattice. The Hope diamond is a famous example of a type IIb diamond, which are rare in nature. Access to (and study of) type II material has been greatly boosted by the development of rival laboratory-based methods of synthesizing diamond as described in section 2.

Many “nitrogen in diamond” issues continue to exercise the scientific community. For example, the empirical models used by geochemists to trace the behavior of nitrogen in the Earth’s mantle draw disproportionately on analysis of diamond samples—in which nitrogen is the most common and abundant lattice-bound impurity. The analysis is challenging, in part because many of the available samples display multiple growth zones, which likely developed at different times and in different environments (i.e., in different molten fluids and at different

temperatures (T) and pressures (p)). But other fundamental questions also remain, not least how single nitrogen atoms arrive at substitutional sites in the carbon lattice. The substantial nitrogen content in type I diamonds encourages the view that nitrogen is “compatible” in diamond (since nitrogen and carbon have similar atomic sizes and valence shells), but such a statement masks a wealth of complexity. Atomic nitrogen may be compatible in diamond, but molecular nitrogen, ammonium ions, or metallic nitrides (i.e., the forms in which nitrogen is most likely to be present in the Earth’s mantle¹¹) are not. Thus, there remains a pressing need to understand better how the prevailing p , T , and composition affect the speciation of nitrogen under a range of mantle conditions relevant to diamond formation and, then, to understand how that information is encoded in the natural diamonds that are available for analysis. For example, there is growing recognition that many of the highest quality type II diamonds originate from the highly reducing deep mantle,¹² where the pressure and temperature are both more extreme. What is less clear, however, is whether the low N content in such diamonds implies low nitrogen abundance in that region of the mantle or whether the fluid from which such diamonds grew disfavors reactions that release monatomic nitrogen. The reliability of diamond as a reporter of nitrogen abundance in the mantle is thus now under renewed scrutiny.³

The remainder of this Review is structured as follows: We introduce the more popular laboratory-based synthesis routes that now complement nature as a source of diamond. High-pressure high-temperature (HPHT) and chemical vapor deposition (CVD) methods both offer opportunities for investigating single-crystal diamond (SCD) growth under conditions that are much better defined and controlled than in nature. Nanosized diamond particles were first produced by detonation methods,¹³ but the range of potential applications perceived for this material has encouraged alternative synthetic routes; these are also summarized in section 2. The properties and the potential applications of diamond produced by all of these methods can be altered/expanded by strategic introduction of dopant atoms, and this too is discussed in section 2, focusing particularly on doping with nitrogen. Section 3 surveys many of the methods used to reveal and characterize the presence of nitrogen in diamond, and some of the exquisite details about N-containing defects that have now being gleaned from combinations of theory and spectroscopic



Figure 4. Diamonds exhibit many different colors depending on their impurity levels. Reprinted and adapted with permission from ref 10. Copyright 2009 Gemological Institute of America.

analyses of diamonds synthesized under well-defined and controlled laboratory conditions. We outline what such knowledge can tell us about how nitrogen is incorporated in both HPHT and CVD material, and how the presence of nitrogen affects some of the key properties and characteristics of diamond. The Review concludes with section 4, in which some of the many new and exciting applications of nitrogen-doped diamond are summarized.

2. LABORATORY-BASED SYNTHESIS OF DIAMOND AND NITROGEN-CONTAINING DIAMOND

2.1. High-Pressure High-Temperature (HPHT) Methods

Nature was the inspiration for the HPHT method, by which diamond growth was demonstrated by Swedish company ASEA in 1953 (though not reported at that time) and subsequently by US company General Electric in 1955.^{14,15} Most present-day HPHT synthesis exploits the temperature-gradient growth (TGG) method developed later in that decade.¹⁶ However, it took many further years before the design and control of HPHT reactors yielded diamonds of sufficient size and quality to attract much attention from the jewelry industry.^{17–19} Key ingredients for HPHT growth are a carbon source (typically graphite or diamond powder) together with a metal catalyst (e.g., a Fe–Ni or Fe–Ni–Co alloy) that allows diamond formation at lower temperature. These ingredients are placed in a carefully designed reactor chamber such as that illustrated in Figure 5 to facilitate diamond growth on a diamond seed at pressures of 5–6 GPa and temperatures in the range of 1300–1600 °C—that is, just on the diamond side of the Berman–Simon line²⁰ in the carbon phase diagram (Figure 6). Maintaining the carbon source at a slightly higher temperature than the seed ensures net diffusion of carbon atoms through the molten flux and formation of a synthetic diamond crystal on the seed. Early HPHT diamonds were colored, due to impurities (e.g., N, B, or transition metals from the catalyst used) in the growth system. The resulting “industrial” diamonds were too unsightly for gemstone use but ideal for cutting or grinding applications. Nowadays, however, contamination levels can be controlled such that it is possible to grow several colorless gemstone-quality HPHT synthetics simultaneously within the press.

Such improvements in process control have led to similarly impressive advances in our knowledge and understanding of the effects that nitrogen impurities in the metal melts have on the growth, the morphology and the defect and impurity structure in diamonds grown by HPHT methods.²² For example, HPHT diamonds with minimal nitrogen content can be grown by adding aluminum or titanium powder to get the nitrogen in the starting materials. The N-content in the growth medium (and in the resulting HPHT diamond) can then be increased (and controlled) by judicious addition of a suitable nitride (e.g., NaN_3 or P_3N_5)²³ or a substance like melamine ($\text{C}_3\text{N}_6\text{H}_6$) if N–H containing defects are the target for study.²⁴

Pre-existing diamonds (natural or synthetic) can also be subject to further treatment by HPHT methods. One such recent study²⁵ has shown that appropriate annealing of HPHT-grown, N–H codoped SCDs with N content of ~1000 ppm encourages aggregation of the nitrogen atoms (from C-centers to A- and B-centers). Such annealing reduces the visible coloration of these samples, especially in the {111} faces, thereby increasing their potential appeal and value. The IR

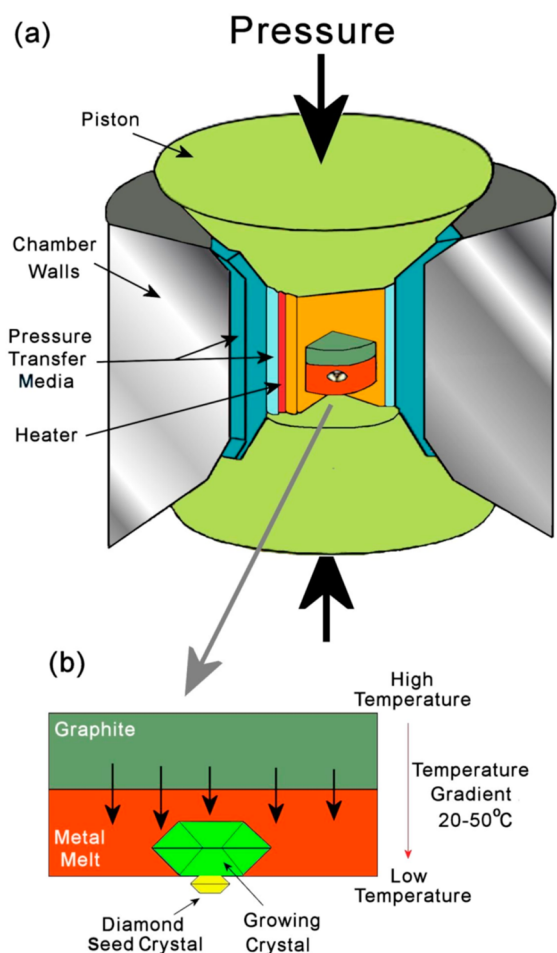


Figure 5. Schematic diagram of (a) an HPHT press, wherein a cell containing graphite, a metal melt, and a diamond seed crystal is subjected to high pressures and temperatures. Under these conditions, (b) the graphite dissolves in the metal and precipitates on the seed crystal, propagating the diamond lattice.

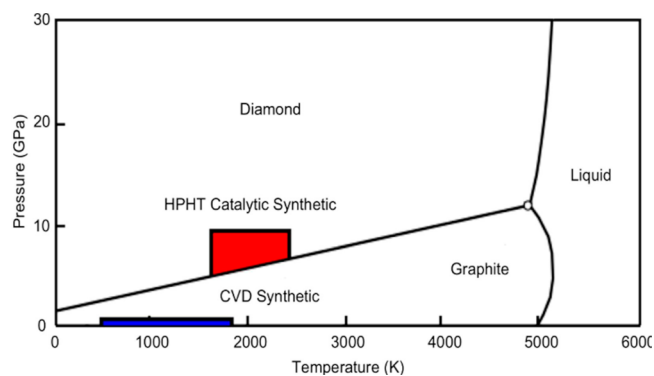


Figure 6. Phase diagram for carbon showing the pressure (p) and temperature (T) regions where HPHT and CVD synthesis can occur. Note that CVD is a nonequilibrium process and that the region illustrating CVD growth has been exaggerated for clarity. Adapted from ref 21. Copyright 2018 University of Newcastle.

absorption signatures of the postannealed samples are also more akin to those of “natural” type Ia and Ib diamonds. Further careful studies of the aggregation mechanism and the mutual interaction of nitrogen and hydrogen (section 3.5) should advance our understanding of how natural diamonds

are formed and of ways in which they can be reliably distinguished from lab-grown diamonds.

2.2. Chemical Vapor Deposition (CVD) Methods

2.2.1. Growth from C/H Containing Gas Mixtures with or without a Noble Gas. In contrast to nature and to the HPHT method, a diamond grown on a suitably heated solid substrate in a CVD reactor starts from a mixture of hot gases at a total pressure below 1 atm. (i.e., below 0.1 MPa). This is a nonequilibrium growth process. Almost inevitably, it favors incorporation of different defects. Attempts at diamond CVD can also be traced back over half a century,^{26,27} but the first deposition protocols that yielded diamonds of reasonable quality at technologically relevant deposition rates only appeared in the early 1980s.^{28–30} The diamond CVD process has been extensively reviewed elsewhere^{31–38} and is, thus, only summarized here. The carbon source is usually methane, diluted (to just a few % input mole fraction) in hydrogen. The gas mixture in most high-quality CVD diamond applications is activated using a microwave (MW) plasma in a specially designed reactor, such as that shown schematically in Figure 7.

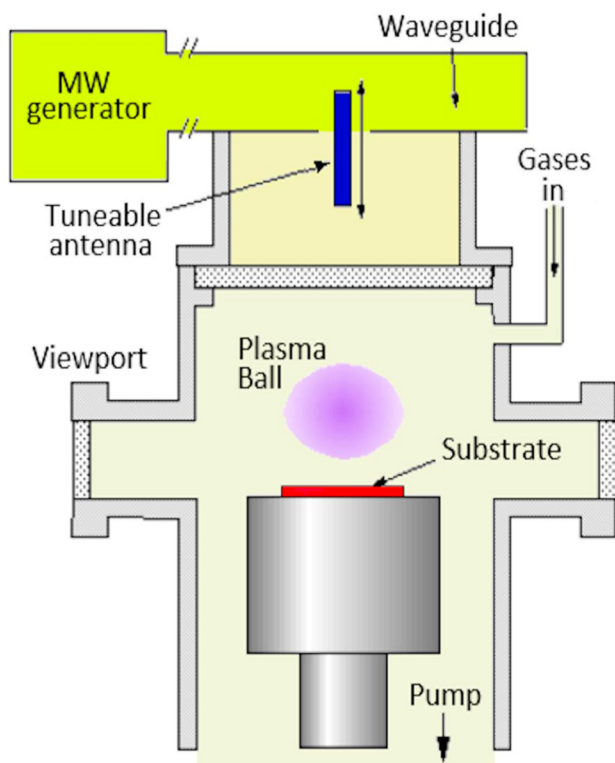


Figure 7. Microwave (MW) plasma CVD reactor. MW radiation enters the chamber via a waveguide and an antenna. The chamber forms a resonant cavity that is tuned by moving the antenna position. The MW power generates a plasma situated just above the substrate surface which activates, ionises and dissociates the input gases, initiating diamond growth on the nearby substrate. Reproduced with permission from ref 39. Copyright 1999 University of Bristol.

Other activation methods include direct current arc jets and hot metal filaments.⁴⁰ Activation in all cases results in the formation of gas-phase H atoms, which play several important roles. They participate in gas-phase reactions with the source hydrocarbon, creating a complex mixture of hydrocarbon species including carbon-containing radicals. The H atoms also participate in abstraction and addition reactions with carbon

atoms on the surface of the growing diamond film. This dynamic equilibrium ensures that most surface atoms at any time are stabilized by terminating C–H bonds, which prevent the surface reconstructing to graphitic carbon. But it also ensures that some fraction (typically a few %) will have an unsatisfied valence (often termed a “dangling” bond) by which an incident carbon-containing radical can be accommodated and thereby grow the diamond lattice. The gas-phase H atoms also preferentially etch any carbonaceous material that deposits in nondiamond form and the recombination of H atoms on any surface contributes to heating of that surface.

Key features of the gas and gas-surface chemistry that enable diamond CVD from MW-activated CH₄/H₂ input gas mixtures are now summarized to paint a background for the later discussion of the effects of adding N₂ to the process gas mixture. Illustrative process conditions are 1–10 kW input MW power (*P*) and total gas pressures (*p*) in the range 100–300 Torr. MW power absorption accelerates electrons (e) in the gas, and the frequency of e-H₂ collisions at the prevailing pressures ensures that this absorbed energy is efficiently transformed into rotational and, particularly, vibrational excitation of H₂. The core of the plasma is characterized by a low (ppm) degree of ionization but a high gas temperature (*T*_{gas} ~ 3000 K or higher). This ensures thermal dissociation of several percent of the H₂ in the hot plasma region to H atoms, which diffuse throughout the reactor and drive the chemistry.

As Figure 7 shows, the MW CVD reactor is designed so that the substrate attains temperatures *T*_{sub} in the range of 1000–1300 K by a combination of radiative and conductive heating from the hot gas, energy released by H atom recombination reactions on its surface, and if necessary, an auxiliary substrate heating/cooling supply. Various constraints limit the choice of substrate material. Self-evidently, the substrate must be able to withstand the prevailing temperature. Many transition metals satisfy this criterion but most are ruled out by their excessive reactivity with carbon-containing species. Molybdenum and, particularly, silicon are popular substrate materials.⁴¹ Both develop a thin interfacial carbide layer at the start of the growth process that helps reduce stresses from lattice mismatch and differences in thermal expansion coefficient but some form of pretreatment is still normally required to encourage diamond nucleation. This can involve abrading the substrate with fine diamond dust (manually or, better, by ultrasonic agitation), or coating the substrate surface with a suspension of nanosized diamond particles prior to positioning it in the growth chamber. Both strategies can be applied to localized areas only and, thus, offer routes to selected area deposition. Bias-enhanced nucleation (BEN) is another strategy—particularly compatible with MW reactors—whereby the substrate is initially negatively biased to encourage bombardment and implantation by carbon-containing ions in the plasma prior to switching to normal plasma-assisted growth.^{42,43}

Diamond growth on a nondiamond substrate starts from numerous nucleation sites. The individual nuclei grow (both axially and radially) and progressively fuse with their immediate neighbors to form a two-dimensional film that then continues to grow along the surface normal. The resulting material will usually be polycrystalline, but its morphology and the average crystallite size can be tuned—from microcrystalline diamond (MCD) through nanocrystalline diamond (NCD)⁴⁴ to ultrananocrystalline diamond (UNCD)^{45,46}—by choosing the appropriate process conditions.⁴⁷ Smaller grain sizes are

avored by increasing the renucleation rate on the growing sample, which can be achieved by raising the C:H ratio in the source gas mixture and, in the case of UNCD, by substituting most of the input hydrogen by argon.

CVD diamond materials present two principal low-index surfaces: the C(111) and C(100) surfaces. The relative (and the absolute) growth rates on these surfaces are also sensitive to factors like the C:H ratio in the source gas and T_{sub} . As illustrated by the scanning electron microscope (SEM) images shown in Figure 8a–c, it is possible to tune the morphology of as-grown MCD films from “rough” (i.e., dominated by {111} facets) to much smoother in the case of a <100>-textured, {100}-faceted film.^{48,49} The inevitable grain boundaries introduce variability and restrict the ultimate potential of all

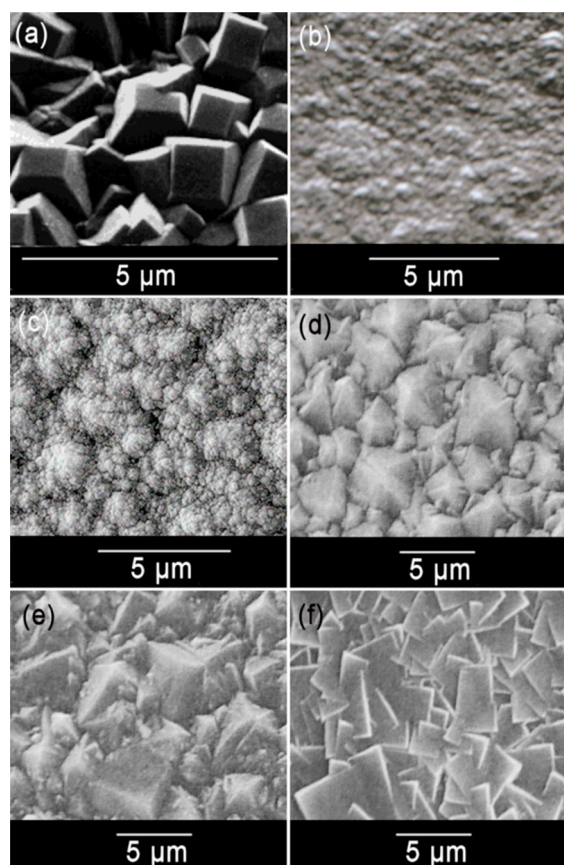


Figure 8. (a–c) Examples of different morphologies of undoped polycrystalline CVD diamond films grown using different C:H ratios in the source gas: (a) faceted microcrystalline diamond typically grown under standard deposition conditions, with <2% CH₄ in H₂, (b) smoother nanocrystalline diamond grown as before, but with >4% CH₄/H₂, and (c) “cauliflower” nanocrystalline diamond grown with >4%CH₄/H₂ but at lower temperatures ($T_{\text{sub}} < 700$ °C). At the scale of these images, UNCD films would be flat and featureless and, thus, are not shown. (d–f) Examples of the different morphologies of polycrystalline CVD diamond grown from MW activated 0.5%CH₄ in H₂ gas mixtures with the following [N]/[C] input mole fractions: (d) 0.1%, when the films are primarily randomly oriented (111) octahedral crystals, (e) 1.0%, where the transition from (111) to square (100) surface morphology starts, and (f) 10%, where the film is predominantly (100) textured. (a–c) Copyright Paul May and the University of Bristol, reproduced with permission. (d–f) Reprinted with permission from ref 49. Copyright 1994 American Institute of Physics.

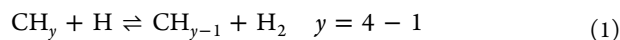
forms of polycrystalline diamond, though not to the extent to preclude its use in an ever-growing range of demanding applications (e.g., heat spreaders, IR and MW windows, wear resistant coatings, etc.).

Turning now to single-crystal diamond (SCD), there are currently two favored approaches to synthesizing larger area SCD by CVD methods.⁵⁰ One involves homoepitaxial growth on a pre-existing SCD substrate, resulting in axial (but minimal transverse) enlargement of the crystal. A subtle variation of this is CVD overgrowth of natural gemstones to make them larger and therefore, of higher value; these “hybrids” can be deceiving as they contain spectroscopic signatures from both natural and synthetic diamond.⁵¹

Such homoepitaxial growth is the driving force behind the burgeoning market in CVD diamond gemstones for the jewelry market and is enabling fabrication of colorless diamonds approaching a centimeter in size.⁵² These recent developments are a direct result of improvements in the technology underlying CVD—notably, higher power MW reactors that enable increased gas dissociation in the plasma (and hence higher growth rates) and improved process management that allows the growth conditions to be precisely controlled and maintained for many days. Cloning (i.e., using a laser to slice off sections from the enlarged crystal) and then carefully positioning the resulting “tiles” prior to further homoepitaxial overgrowth offers a means of increasing the lateral size to fabricate larger area “wafers” of diamond.^{53,54}

The other approach involves heteroepitaxial growth of diamond on another substrate material that is already available in large-area form. The constraints on this substrate material are considerable. In addition to being able to withstand the harsh growth conditions, it must also have appropriate lattice parameters and be available with high quality crystallinity. Iridium is the current substrate of choice, in thin film form (given its scarcity and expense) on, for example, an yttria-stabilized zirconia layer on a Si substrate, and diamond growth is encouraged by an initial BEN stage.^{55,56}

2.2.2. CVD Growth Mechanism. The actual CVD diamond growth relies on a series of fast “H-shifting” radical-forming and radical-interconversion reactions (1) involving, in the hot region of the plasma (or near the filament in a hot filament reactor), abstraction reactions, such as



and, in the cooler regions, additions of the type



(where M is a third body). The relative concentrations of the various CH_y ($y \leq 4$) species depend on the local H atom concentration, [H], and T_{gas} and, thus, show a wide spatial variation within the reactor volume. T_{gas} will often exceed 3000 K in the hot plasma region, yet be not much above room temperature near the reactor walls. CH_y radical recombination reactions yield C₂H_x species, which also cycle through a series of gas-phase H-shifting (abstraction or addition) reactions analogous to processes 1 and 2. Most of the carbon in the hot plasma region is in the form of C₂H₂ (the most stable hydrocarbon at high [H] and T_{gas}), whereas CH₄ (the input hydrocarbon) typically dominates in the cooler periphery of the reactor.⁵⁷ Further recombination and H-shifting reactions can lead to formation of C_nH_x ($n > 2$) species, which are relatively more abundant at higher input CH₄ mole fractions. Since all MW CVD reactors contain steep T_{gas} gradients, it

follows that the total gas-phase number density and the number densities of the H atoms and the various CH_y and C_2H_x species (and thus their interconversion rates) are all sensitive to location within the reactor. The challenge is further compounded by gas–surface reactions (at the growing diamond surface and at the walls of the reactor) and by gas transport, which, in MW CVD reactors, is largely diffusive and thus mass (and species) dependent. Much of this complexity is now understood, however, through a combination of spatially resolved in situ spectroscopic studies of the gas-phase composition as functions of process conditions and complementary plasma modeling.^{31–33,58–68} Radicals containing just one carbon atom are recognized as key to CVD diamond growth, and of these, the methyl (CH_3) radical is generally the most abundant in the immediate vicinity of the growing diamond surface (where T_{gas} is little more than half that in the plasma core).⁶⁹

As noted above, CVD diamond typically presents two principal low-index surfaces—the C(111) and C(100) surfaces—and, given the high H atom flux in the CVD environment, we here focus attention on the fully hydrogenated surfaces. The C(111):H surface has a simple unreconstructed structure with an H atom terminating each surface C atom,⁷⁰ whereas the hydrogenated C(100):H surface has a 2×1 reconstructed structure with rows of surface C atoms paired as dimers^{71,72}—as shown in Figure 9.

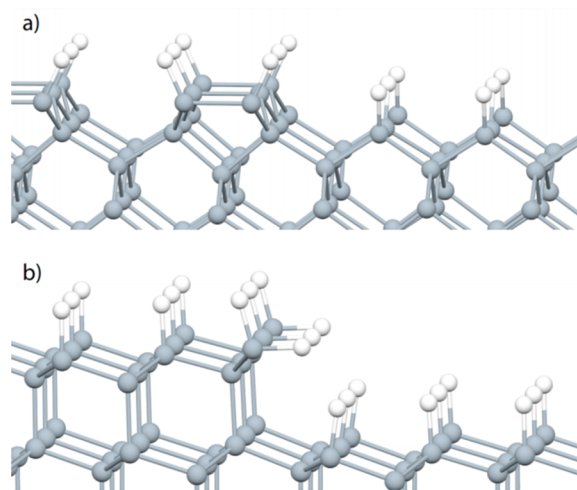


Figure 9. Low-index reconstructed H-terminated diamond surfaces, together with a step edge: (a) (100) and (b) (111). C and H atoms are shown as gray and white spheres, respectively.

Refs 31 and 34 provide overviews of some of the reported CVD diamond growth models, but extensive discussion of these are outside the scope of this Review. By way of illustration, Figure 10 shows a series of elementary steps by which an incident CH_3 radical can insert into a C–C dimer bond on the C(100):H (2×1) surface. The sequence starts with the abstraction of a surface-terminating H atom by an incident gas-phase H atom, thereby creating a surface radical site. Given the relative fluxes of H atoms and CH_3 radicals striking the surface under typical CVD conditions, the most likely next step is chemisorption of another gas-phase H atom, re-terminating the site. Occasionally, however, an incident CH_3 radical will bond at such a site. This carbon atom delivered in this way can then be incorporated into the surface by a

sequence involving another H atom abstraction reaction and a ring-opening/ring-closing rearrangement⁷³ (from structure 3 \rightarrow 6 in Figure 10); a final H atom addition (6 \rightarrow 7) terminates the ultimate radical site and completes the net insertion of a bridging CH_2 group. Several of these steps involve activation barriers, but none are sufficiently large to be prohibitive at typical growth temperatures.⁷⁴ Analogous elementary reaction sequences have been found for other necessary conversions on the C(100):H (2×1) surface, for example, for carbon addition across the trough in a dimer chain, and for (local) migration of a CH_2 group along a dimer chain and along the dimer rows.⁷⁴ Comparable mechanistic studies for growth on the C(111):H surface are rare, though we note one study that identified formation of a four-atom nucleus on this surface as the critical “seed” for next layer growth and recognized that such a nucleus would have a 50/50 chance of forming a stacking fault (a contact twin).⁷⁵

The number of C- and H-containing species in a MW-activated CH_4/H_2 gas mixture and the complexity of their myriad (temperature-dependent) gas and gas–surface reactions is much too large to be included in any mesoscopic model for forming a block of diamond. Most recent models employ kinetic Monte Carlo (KMC) protocols wherein each reaction increment is selected randomly from a (greatly reduced) library of possible reactions using a time-based probability algorithm. Again, a full description of KMC modeling of diamond growth is outside the scope of this Review, but interested readers should consult refs 76 and 77 for details of the types of process that are typically included (or excluded) in such modeling, and the insights such modeling is now beginning to provide.

2.2.3. Effects of Adding Nitrogen to C/H Containing Gas Mixtures. Often undefined levels of nitrogen contamination (a consequence of working with an imperfect vacuum, or from air impurities in the source gases) influenced all early diamond CVD studies, and the community now pays much attention to controlling N_2 (and other) impurities in the activated gas mixture. MW-activated CVD using high purity CH_4 and H_2 source gases and a high-vacuum reactor now offers a straightforward route to forming type IIa diamond in the laboratory, as exemplified by homoepitaxially grown SCD samples with total N defect concentrations below 1 part per billion (ppb).^{37,78} In passing, we note that MW-activated CVD also offers routes to forming essentially monoisotopic diamond; a ^{12}C SCD grown from an isotopically pure $^{12}\text{CH}_4/\text{H}_2$ gas mixture, for example, will display significantly higher thermal conductivity than an equivalent diamond containing ^{12}C and ^{13}C in natural abundance.⁷⁹

Intriguingly, however, many prior studies have shown that adding trace amounts of N_2 to the process gas mixture actually enhances the rate of diamond growth from MW-activated CH_4/H_2 gas mixtures.^{49,80–88} The presence of nitrogen in the process gas mixture also affects the surface morphology, encouraging the preferential formation of {100}-faceted surfaces in the case of polycrystalline diamond films (illustrated in Figure 8d–f)^{49,80,89,90} and macroscopic step-bunching (as illustrated in Figure 11) in the case of SCD samples.^{53,88} Too much nitrogen in the process gas mixture, however, leads to smaller and less well oriented surface facets in polycrystalline films, and ultimately to NCD films or even graphitic deposits.^{49,91} Excessive nitrogen in the input gas mixture has also been shown to disrupt homoepitaxial growth on all but the {100} face in the case of an SCD substrate.⁹²

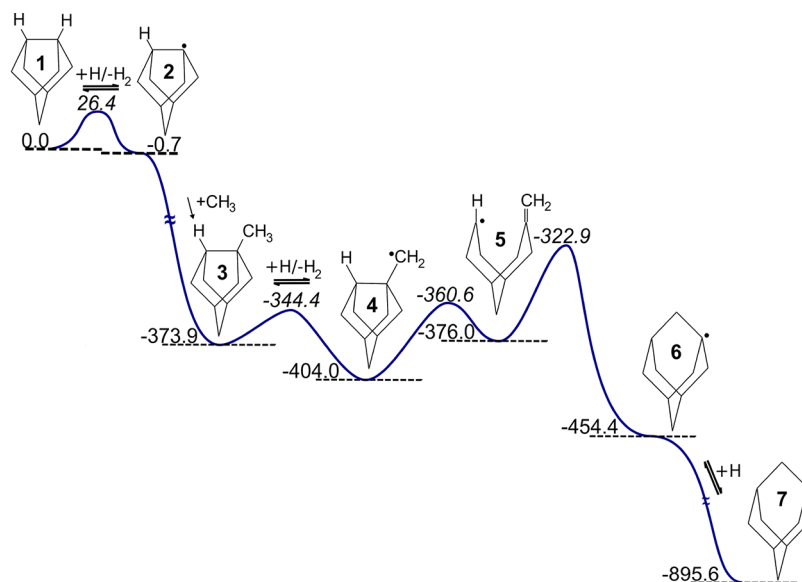


Figure 10. Series of elementary steps by which an incident CH_3 radical can insert into a C–C dimer bond on the C(100):H (2×1) surface. The respective minima (normal font) and transition state (in italics) energies are quoted in kJ mol^{-1} , relative to that of structure 1. Only the atoms treated by quantum mechanics (QM) in these QM/molecular mechanics calculations are shown. Reprinted with permission from ref 74. Copyright 2008 American Chemical Society.

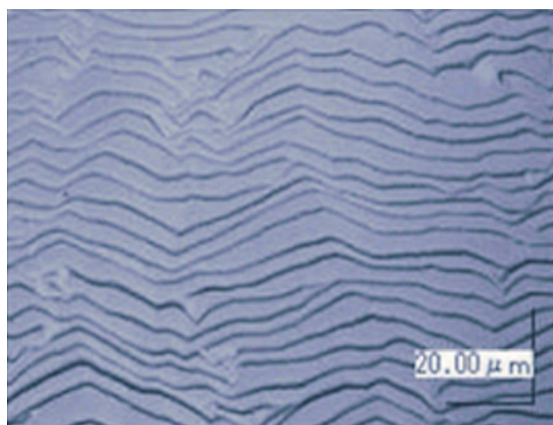


Figure 11. SEM image illustrating the characteristic macroscopic step-bunching seen on the surface of SCD samples grown using nitrogen-containing gas mixtures. Reprinted with permission from ref 88. Copyright 2016 Japan Society of Applied Physics.

How the addition of small amounts of N_2 —a reagent traditionally viewed as rather unreactive—to the process gas mixture can affect the gas and gas–surface chemistry to the extent that it induces a doubling (or more) of the diamond growth rate and obvious changes in the surface morphology is still far from fully understood. Recent plasma diagnostic studies and gas, gas–surface, and solid-state modeling studies have provided several clues, however.

From the gas-phase perspective, a combination of experimental (laser absorption and optical emission spectroscopy) and modeling studies of MW-activated N_2/H_2 (and NH_3/H_2) plasmas operating at process relevant powers and pressures identified the importance of reactions involving excited-state N_2 species.⁹³ N_2 molecules in the hot plasma region are promoted to a range of excited states by electron-impact excitation, the decay of which (by emission of a photon or by collisional relaxation) leads to an overpopulation (relative to that expected on the basis of local thermodynamic

equilibrium) of the metastable first excited triplet ($\text{A}^3\Pi_g$) state. $\text{N}_2(\text{A})$ state molecules have energies ~ 6.2 eV above that of ground (X) state N_2 molecules and, unlike $\text{N}_2(\text{X})$ molecules, react with H atoms. This provides a means of breaking the strong triple bond and allowing N_2 to participate in the plasma chemistry, which, as in the NH_3/H_2 plasma, involves “H-shifting” reactions analogous to eqs 1 and 2 that drive the interconversion between the various NH_x ($x \leq 3$) species.⁹³ This source is complemented by reaction 3



in the hot plasma core of MW-activated $\text{CH}_4/\text{N}_2/\text{H}_2$ gas mixtures.^{94,95} These studies found that most (>99.5%) of the nitrogen in the hot plasma region was still present as N_2 but also recognized that the (modest) reactivity of N_2 could be increased by operating at higher pressures p or microwave powers (P), both of which would increase the maximum T_{gas} .⁹⁵ Less than 0.25% of the input N_2 was converted to HCN under the prevailing experimental conditions, and the relative abundances of all other N-containing species were deduced to be two (or more) orders of magnitude lower. Of those N-containing radical species that might be expected to be reactive during diamond CVD, that is, N atoms and NH , NH_2 , and CN radicals, the near-substrate (ns) concentration of atomic nitrogen, $[\text{N}]_{\text{ns}}$, is higher than $[\text{NH}]_{\text{ns}}$ and $[\text{NH}_2]_{\text{ns}}$, and typically an order of magnitude higher than $[\text{CN}]_{\text{ns}}$.⁹⁵ Changing the N/C ratio in the input gas mixture results in a proportional change in the $[\text{N}]_{\text{ns}}/[\text{CH}_3]_{\text{ns}}$ ratio just above the growing diamond surface, but has little effect on the $[\text{N}]_{\text{ns}}/[\text{NH}]_{\text{ns}}/[\text{NH}_2]_{\text{ns}}/[\text{CN}]_{\text{ns}}$ ratios. The finding that the $[\text{N}]_{\text{ns}}/[\text{CH}_3]_{\text{ns}}$ ratio is much ($\sim 10^{-3}$) smaller than the $[\text{N}_2]/[\text{CH}_4]$ mole fraction ratio in the input gas mixture is further testimony to the inherent stability of N_2 in this plasma environment. Analyses of homoepitaxial diamond layers grown using MW-activated $\text{CH}_4/\text{N}_2/\text{H}_2$ plasmas return N/C ratios consistent with the predicted $[\text{N}]_{\text{ns}}/[\text{CH}_3]_{\text{ns}}$ ratios—suggesting broadly similar incorporation efficiencies for both species—but also show the N content to be sensitive to process conditions;

increasing P and reducing T_{sub} both lead to a higher N content in the deposited material.⁵³

Theory suggests that each of the “potentially reactive” species identified above should be able to insert into a C–C dimer bond on the C(100):H (2×1) surface via a ring opening/ring closing reaction mechanism analogous to that shown in Figure 10 for the case of CH_3 addition.⁹⁶ Of these, CN radical addition appears least probable for several reasons. First, $[\text{CN}]_{\text{ns}}$ is typically less than $[\text{N}]_{\text{ns}}$, though this imbalance is reduced when operating at higher pressures and/or MW powers. Second, a chemisorbed CN species must undergo a further gas-surface reaction step (an H atom addition) to form a surface-bound CNH species (isoelectronic with CO) that is capable of promoting an energetically feasible ring-opening/ring-closing reaction sequence. Third, the N–H bond in the CNH adduct is weak, and the binding energy of the CNH adduct is itself quite low, so this species will be prone to thermal dissociation and desorption.⁹⁶ However, the possibility of incorporating a CNH species remains an intriguing prospect since, if the ring-closed structure is reached, this mechanism alone has the effect of adding two heavy atoms, with the N atom sitting one layer above that of the current growth layer and optimally positioned to nucleate next layer growth. Given that such nucleation is generally viewed as the rate-limiting step in diamond growth, such CN incorporation would be predicted to lead to an enhanced material growth rate—as has been proposed also in the context of possible CN adsorption on the diamond {111} surface.⁷⁵

Theory has also been used to investigate the effect of preadsorbed NH species on the binding of CH_3/CH_2 groups at different step edges on the C(100):H (2×1) surface⁹⁷ and of substitutional N atoms on the energetics (and thus the rates) of the elementary reactions involved in incorporating a gas-phase CH_3 radical on the growing diamond surface.^{98–100} It has been suggested that the additional electron density provided by a near-surface N atom weakens any proximal surface C–H bonds, which should enhance the rate of the H-abstraction step that creates the surface radical site necessary for CH_3 radical addition.¹⁰⁰ Much recent interest in CVD growth from C/N/H gas mixtures on (111)-oriented diamond substrates has focused on the finding that the spontaneously generated nitrogen-vacancy (NV) defects (featured in section 3.5.4.1) are highly oriented along the [111] axis.^{101–107} These findings have been rationalized by atomistic simulations which assume addition of a gas-phase N atom to C(111) growing laterally in step-flow mode,¹⁰⁸ though it has also been suggested that a high alignment of NV defects along the [111] axis could be obtained by thermal annealing if the sample is under an appropriate biaxial compressive strain.¹⁰⁹

2.2.4. Doping CVD Diamond Films with Nitrogen.

Intrinsic, or undoped, diamond is highly insulating. To produce diamond with useful semiconducting properties, it is, thus, necessary to alter its conductivity by adding controlled amounts of impurities. In traditional semiconductor physics, adding an element with one fewer electron (an acceptor) than the bulk, for example, boron in carbon, should produce a p -type semiconducting material, whereas adding an element with one more electron (a donor) should produce an n -type material. Having both p - and n -type material is necessary for forming p – n junctions and the operation of many electronic devices, such as CMOS transistors. Doping diamond with boron can be achieved simply by adding small amounts of boron-containing gases (e.g., B_2H_6 or $\text{B}(\text{CH}_3)_3$) to the gas

mixture during the CVD diamond growth process.¹¹⁰ This readily produces p -type boron-doped diamond (BDD) with conductivities ranging from semiconducting to near metallic¹¹¹ and which can even become superconducting at temperatures < 10 K.¹¹² BDD is already finding application in simple electronic devices,¹¹³ microplasma devices,¹¹⁴ biomedicine,¹¹⁵ and electrochemistry.^{116–119}

In contrast, doping diamond to achieve n -type semiconductivity has proven to be much more challenging. This is because, apart from nitrogen, all potential n -type dopant atoms have a larger atomic radius than carbon. These larger atoms cannot fit easily into the vacancy formed by removing a C atom from a lattice site. Unlike other semiconductor materials (e.g., Si and Ge) the rigid diamond lattice is less able to stretch to accommodate a larger atom in place of C. Most of the potential larger n -type dopant atoms (P, As, Na, Li) have a very low solid-state solubility in diamond, leading to dopant concentrations that are too small to be useful.¹²⁰

Nitrogen is different, in as much that it is a potential electron donor and has an atomic radius less than that of carbon. It incorporates into diamond relatively easily—as evidenced by the naturally occurring type I diamonds and the discoloration of diamonds formed in the early HPHT growth experiments. As shown in section 2.2.3, adding small amounts of N_2 or NH_3 to a CVD gas mixture leads to some N incorporation into the diamond lattice. Unfortunately, the N tends to reside at substitutional sites (C-centers), where—at least in the neutral charge state—it distorts the surrounding diamond lattice due to the preferential formation of a lone-pair on the N atom and a dangling bond on one of its four carbon neighbors. The N still acts as an electron donor, but the distortion generates a donor level that is 1.7 eV below the valence band (see section 3). The energy required to promote an electron from this “deep donor” band into the valence band is much greater than that available at normal semiconductor operating temperatures, with the result that N-doped diamond is ineffective as an n -type semiconductor. Ironically, N-doped diamond can often be even more insulating than undoped diamond because of the N donors compensating for the (mostly) p -type acceptors that arise from defects, surface states or, in the case of polycrystalline CVD diamond films, grain boundaries.

Despite the lack of success for semiconducting N-doped diamond, other applications for this material have been reported, including thermionic emission devices for solar power generation,^{121,122} Fabry–Perot interferometry for optical biosensors,¹²³ thermoluminescence and radiation dosimetry sensors,¹²⁴ and as coatings for microtools.¹²⁵ The N-doping story may not be completely over, however, given recent claims that codoping of diamond with N together with another element, such as B^{126,127} or Li,¹²⁸ in the correct mixing ratio, may yet produce the elusive n -type material—though this has still to be demonstrated conclusively.

UNCD, introduced in section 2.2.1, is a hard, nanosmooth material that is deposited using a CVD process similar to that used for other forms of diamond, but with a much higher C:H ratio in the source gas. UNCD films consist of diamond crystallites < 10 nm in size surrounded by a matrix of enlarged grain boundaries composed of nondiamond sp^2 carbon that can constitute up to 10% of the volume of the film. The physical properties of UNCD are less spectacular than those of larger grained diamond films, but when nitrogen-containing gases are added to the CVD growth mixture, the resulting films exhibit n -type semiconductivity and low resistivity.^{129–131}

Studies have shown that, in this case, the N is not substituting for C in the diamond lattice to act as an electron donor. Instead, the nitrogen atoms are concentrated within the extensive sp^2 grain boundary regions, increasing the thickness of these boundaries and forming conductive regions composed of amorphous carbon nitride or nitrogenated diamond-like carbon. Thus, this is not true n -type doping in the conventional sense, but N-UNCD (as it is known) nevertheless behaves as an n -type semiconductor and has found use in a number of electronic devices.^{132,133}

2.3. Diamond Particles: Diamondoids, Nanodiamonds, and Microdiamonds

Alongside diamond in the form of single-crystal gemstones or thin films, diamond particles of different sizes are another area of considerable current scientific interest. A detailed comparison of the different diamond particle types, their properties, and production methods has appeared recently.¹³⁴ For convenience, diamond particles are usually categorized by size into three broad groups.

2.3.1. Diamondoids. The smallest of these diamond-particle size groups, diamondoids, are hydrocarbon cage molecules of size ~ 1 – 2 nm, in which the carbons all have tetrahedral sp^3 hybridization such that the structures are totally or at least largely superimposable on the cubic diamond lattice.¹³⁵ Adamantane ($C_{10}H_{16}$) is the smallest diamondoid molecule, but by fusing together different numbers of adamantane cage units in different arrangements, a family of structural and isomeric “polymantanes” can be created—the first few of which are illustrated in Figure 12. The smaller

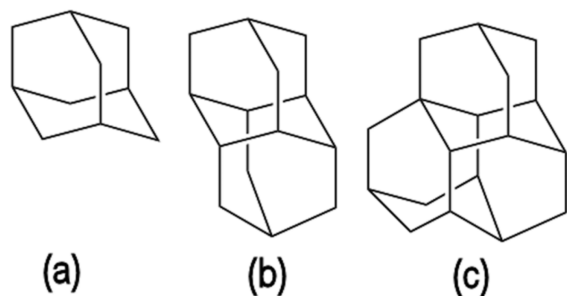


Figure 12. Carbon-cage structures of the first three diamondoid polymantanes: (a) adamantane $C_{10}H_{16}$, (b) diamantane, $C_{14}H_{20}$, and (c) triamantane, $C_{18}H_{24}$. For tetramantane and above, the number of structural isomers increases rapidly. Either one or two hydrogen atoms (not shown) are bonded to every carbon to maintain the carbon valency of 4.

diamondoids, comprising up to four adamantane cages (diamantane, triamantane, and tetramantane), can be synthesized using traditional organic synthetic procedures, but the number of synthetic steps required to make larger diamondoids is prohibitively large. Another production route involves extraction, filtration, and purification of sediments found in petroleum deposits. Millimeter-sized pure crystals of a whole range of polymantane molecules, some comprising ten or more adamantane cages per molecule, have been obtained by this method.^{136,137}

Because diamondoid molecules are simply cage hydrocarbons with an external surface terminated with C–H bonds, it is relatively simple to functionalize the surface by replacing the H with other chemical groups, such as carbonyls, hydroxyls, amines, or cyanides.¹³⁸ It follows that other

molecules, such as proteins, catalysts, or even DNA strands, can then be grafted onto the functionalized surface via, for example, amide or ester links. This has opened up the use of diamondoid molecules for a range of applications, such as pharmaceuticals, catalysis, molecular electronics, and biosensors for DNA sensing.¹³⁹

2.3.2. Nanodiamond. As the number of conjoined cages increases, there comes a point where the diamondoid stops behaving like an individual molecule, but instead adopts the attributes and properties of a more macroscopic material or nanoparticle. As such, nanodiamond (ND) forms the second group of diamond particles, which typically have sizes 2–10 nm.¹⁴⁰ Various ND production methods have been demonstrated,¹⁴¹ the most common of which is via detonation of oxygen-deficient explosives (such as 2,4,6-trinitrotoluene (TNT) and hexahydro-1,3,5-trinitro-1,3,5-triazine (hexogen)) in a nonoxidizing medium (e.g., an inert atmosphere or in water or ice) inside a specially constructed steel detonation chamber.¹⁴² No additional carbon material is required, since carbon is already present in the explosive. The incomplete combustion of the explosives in an oxygen-deficient atmosphere leads to the formation of elemental carbon (in various forms), along with CO, CO₂, water, and nitrogen. The detonation produces a shockwave, which propagates through the reaction mixture at supersonic speeds. The elementary carbon products will condense in the form that is thermodynamically stable at the prevailing temperature and pressure. In this case, the values in the transient shockwave can be $p \sim 10$ – 20 GPa and $T \sim 2000$ – 4000 K, under which conditions diamond is the thermodynamically favored phase of carbon. At all other times, the pressure and temperature conditions favor other forms of carbon. Thus, the explosion produces a mixture of diamond particles, soot and other sp^2 carbon material. The speed with which the gas cools after the shockwave and, hence, the time for which the carbon is in the diamond and graphitic favored regions of the p,T phase diagram (recall Figure 6) is controlled by the cooling properties of the surrounding medium, which controls the composition and yield of the diamond particles.¹⁴³ Because the high explosives used (TNT and hexogen) contain nitro groups, some of the nitrogen inevitably ends up either on the surface of the ND particles or encapsulated within them in substitutional lattice positions,^{144,145} which is important for sensing applications (see section 4.3).

The powdery mixture of products from the detonation is cleaned with various acids and reagents to remove unwanted metallic impurities and soot, and the sp^3 carbon component isolated. The resulting detonation nanodiamond (DND) is commercially available as a powder or as a suspension in water produced at a rate of several tons per year. Unfortunately, partly as a result of their explosive birth, the DND particles tend to fuse into aggregates ~ 100 nm in size. Each DND particle is encased by sp^2 carbonaceous material that binds the composite,¹⁴⁶ as illustrated in Figure 13. The as-supplied material thus usually requires deaggregation into its constituent particles before subsequent processing. Deaggregation can be achieved in many ways, including ball milling, pulverization, high-power sonication, acid treatments, controlled heating in O₂ or H₂, or combinations of these methods.¹⁴⁷ Even after such cleaning and deaggregation, however, the isolated DND particles are not simply larger versions of a perfect polymantane. This is because, as the size of the particle increases, the minimum energy structure is achieved by

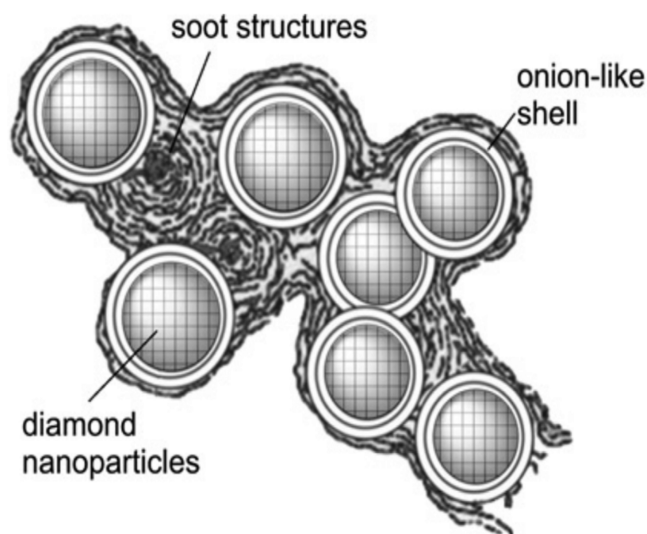


Figure 13. Suggested structure of DND aggregates. The nanodiamond cores are surrounded by fullerene onion-like shells and then fused together by carbonaceous material into a larger composite. Reprinted with permission from ref 146. Copyright 2008 Royal Society of Chemistry.

restructuring the surface carbon atoms to a more sp^2 -like arrangement. DND particles are, thus, viewed as having a diamond core surrounded by a (partially) graphitic or fullerene-like shell and are sometimes described as “bucky-diamonds”.¹⁴⁸ Similar energy minimization arguments suggest that any N atoms present in DND particles will tend to concentrate at the surface.¹⁴⁹

As a result of the various acid treatments and cleaning processes applied following detonation synthesis, the surfaces of DND particles are usually terminated with oxygen containing groups like carboxyl, hydroxyl, or bridging-ether groups. DND particles are thus hydrophilic, which helps their stability when in aqueous suspensions. This surface termination can be modified by standard chemical methods,¹⁵⁰ including direct C–C coupling by photochemical reaction,

diazonium salt coupling, click chemistry, and other routes illustrated in Figure 14. For instance, heating DND in H_2 gives an H-terminated surface, which is mildly hydrophobic,¹⁵¹ while treatment with F_2 yields F-termination, which is superhydrophobic.¹⁵² Amination (addition of NH_2) of the nanodiamond surface is of particular interest because it enables the subsequent binding of a large variety of functional molecules, such as bioactive compounds (proteins, enzymes, DNA), catalysts, drug molecules, or polymer building blocks by amide bond formation or other standard chemical procedures. Adding nitrogen-containing surface groups to DND turns out to be harder than expected, however, with most direct amination reactions proving only partially successful. A better strategy is to establish the amino functions slightly removed from the diamond surface, via a linking molecule—for example, aminated silanes,¹⁵³ Suzuki coupling of aminated aromatic species,¹⁵⁴ or formation of aminomethyl groups.¹⁵⁵ Another approach is to form the amide bond using a highly carboxylated DND surface and a free amino group from the molecule to be tethered. In this way, even large proteins can be immobilized on the carboxylated DND surface via peptide bonds. The peptide link can be made in a single step, enabled by auxiliary reagents, such as EEDQ (*N*-ethoxycarbonyl-2-ethoxy-1,2-dihydroquinoline) or a suitable carbodiimide.¹⁴² Alternatively, thionyl chloride can be used in a two-step method to convert the surface carboxylic acid groups into their respective acid chlorides, which then react readily with any amine groups present in the linking molecule to form amide bonds.¹⁵⁶ Such surface functionalization methods can, of course, be applied to larger (HPHT or CVD grown) diamond samples also but have been most extensively and profitably applied to NDs with their large surface-to-volume ratios.

2.3.3. Microdiamond. Particles larger than ~ 10 nm are also often referred to as nanodiamonds, but when the particle sizes reach 500 nm ($0.5 \mu m$) or larger, it is more appropriate to call them microdiamonds (MDs)—though the labeling convention is often quite relaxed. Unlike the smaller (D)ND particles, which are irregular and shapeless, the larger

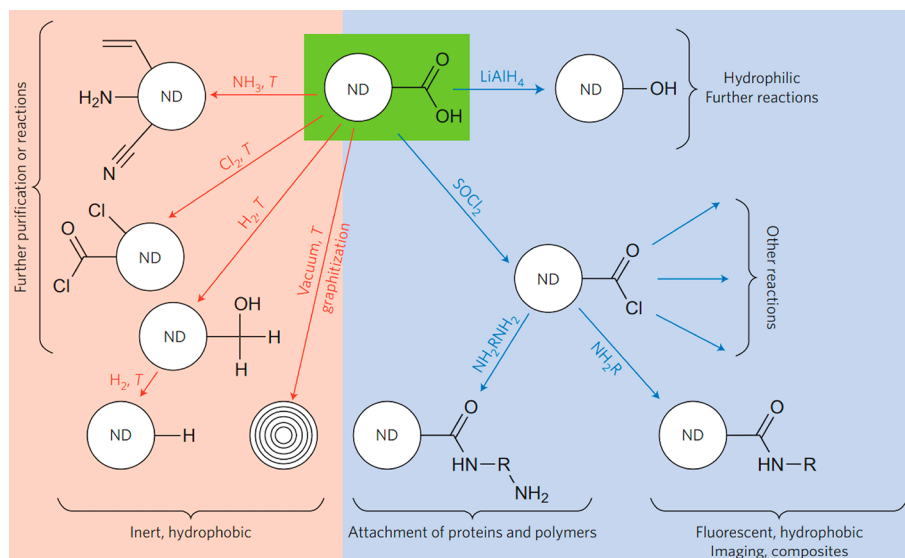


Figure 14. Routes to functionalizing the surface of nanodiamond (ND) particles. Reprinted with permission from ref 140. Copyright 2012 Springer Nature Publishing AG.

nanodiamonds and especially the MDs tend to be more regular in shape and to exhibit facets on one or more faces.

The simplest MD production method is to mill, crush, or pulverize larger lab-grown (HPHT or CVD) or natural diamonds and then size select the fractions by decanting/sieving and centrifuging the suspension in water.¹⁵⁷ The smaller NDs may require repeated cycles of ultracentrifugation and decantation to obtain a reasonably monodisperse sample. Apart from the low cost, one of the advantages of this method is that the nitrogen content in the NDs (or MDs) reflects that in the original uncrushed diamond, which can be as high as a few thousand ppm for some natural type I or HPHT stones. Such high N content in the ND/MD particle greatly increases the chance of finding or creating sufficient NV centers suitable for many of the sensing applications described later in this Review.

Another route to ND/MD synthesis has been to use pulsed laser ablation of graphite in liquid (PLAL), also called liquid-phase pulsed laser ablation.¹⁵⁸ As the name suggests, the output of a high-power pulsed laser is focused onto a graphite target that is immersed in a liquid, usually water. Interaction of the intense laser radiation with both the target and the surrounding liquid creates an ablation plume that is composed of microbubbles of evaporated liquid in which some vaporized target material is trapped. The bubbles expand until they reach a certain critical combination of temperature and pressure, then collapse in a process known as cavitation. During the collapse of the bubble, the entrained materials are subjected to a very high temperature and pressure spike, sufficient to momentarily raise the system into the diamond-stable region of the carbon *p*, *T* phase diagram (see Figure 6). Thus, graphitic material converts into diamond. Analogous to detonation synthesis, because the process is short duration, the resulting diamonds are only of nanometer size. Once viewed only as a low-yield process (10–40% of NDs in the reaction product with an average particle size of 5–15 nm¹⁵⁹), PLAL is now yielding sufficient amounts of monodisperse ND of sufficient purity and homogeneity to make it a commercially viable product.¹⁶⁰

One advantage of the PLAL method is that the composition of the ND can be altered simply by changing the target material or the liquid medium. Thus, magnetic NDs can be produced by incorporating magnetic metals (e.g., cobalt) into the graphite target, and N-containing NDs can be formed by replacing the aqueous medium with ammonia solution. Indeed, PLAL of a graphite target immersed in concentrated ammonia solution has been shown to yield carbon nitride (C₃N₄) nanoparticles.¹⁶¹

2.4. Implanting Nitrogen into Diamond

Ion implantation is widely used in the semiconductor industry to introduce dopants into a material with accurately controlled concentrations and depths in order to modify the electrical conductivity of the material. Doping diamond by ion implantation is more complicated than for many other materials, however, because of its tendency to graphitize when damaged.¹⁶² The reason for this is self-evident from the carbon phase diagram (Figure 6): graphite is the thermodynamically stable form of carbon under normal conditions of *p* and *T*. By its very nature, ion implantation damages the diamond lattice, knocking C atoms from their lattice sites, creating vacancies and interstitials, and forcing impurity atoms (which may be larger than carbon) into the lattice. This

damage can cause localized graphitization or a host of other defects such as vacancies, point defects and dislocations, and create significant lattice strain. For most other materials, such damage and defects can be annealed out by heating for an appropriate time. For diamond, however, all such mechanical damage (and the traditional “solution”) encourages relaxation to the more stable sp² graphitic phase.

A further challenge with diamond is that the energy barriers to diffusion of many implanted impurities through the lattice are sufficiently high to ensure low diffusion probabilities—even at elevated temperatures. Thus, impurities are resistant to moving to the substitutional sites required for electronic doping, while annealing simply accelerates the graphitization process or enables vacancies to cluster, forming extended defect regions. Some of this damage can be reduced if the implantation itself is performed at higher temperatures (>800 K), which encourages instantaneous annealing around the damaged volume. Even so, the number of remaining extended defects and dislocations may still be sufficient to compromise electronic performance.¹⁶³ Implantation has been widely studied as a “brute force” method to obtaining the elusive *n*-type doping of diamond (see section 2.2.4), but the damage created and subsequent graphitization have led to generally unfavorable results.¹⁶⁴

Nitrogen, being smaller than carbon, is actually rather easier to implant into diamond than most other atoms, and N-implantation generally causes less damage.^{165–168} N⁺ ions implanted with keV to MeV energies come to rest mostly on interstitial lattice sites, but a subsequent anneal at *T*_{anneal} > 600 °C encourages their migration to substitutional lattice sites, forming C-centers.¹⁶⁹ Sustained annealing at this (or higher) temperatures, however, encourages proximal vacancies to diffuse through the lattice and become trapped alongside these substitutional nitrogen atoms, forming NV defects.^{170,171} Such diffusion compromises use of N implantation as a route to making *n*-type semiconducting diamond, but NV centers are key to a burgeoning number of magnetometry, biosensing, and quantum information applications, as discussed in section 4.

The past decade has witnessed huge progress in the quality and availability of both HPHT and CVD single crystal diamond grown under well-defined laboratory conditions and in the controlled doping of such material by ion implantation. This, in turn, has led to huge advances in our knowledge and understanding of nitrogen-containing defects in diamond—much of it driven by the many exciting possibilities offered by the NV center. The remainder of this Review is devoted to a comprehensive summary of the current state of knowledge relating to nitrogen-containing defects in diamond and an overview of some of the more chemically oriented applications of nitrogen-doped diamond.

3. PROPERTIES OF NITROGEN-DOPED DIAMOND

Diamond can be viewed as the ideal host for optically active, functional point defects. It has an unusually wide (5.47 eV) optical band gap, which encompasses a very broad range of possible defect-related emission wavelengths. It has a high Debye temperature, meaning that the phonon density-of-states for low-frequency (low-temperature) phonons is low, thus minimizing interactions between point defects and phonons and preventing those interactions from destroying useful quantum properties (like long spin–lattice relaxation times, etc.). It also has a low native spin density (only 1.1% of the

carbon nuclei in a natural-abundance diamond are ^{13}C and thus have nuclear spin $I \neq 0$).

As noted in section 1, nitrogen is the dominant impurity in most natural and lab-grown diamonds.^{5,172} In HPHT-grown diamond, nitrogen is primarily encountered in the isolated substitutional form N_s , whereas in natural diamond the elevated temperatures and geological time scales have caused the nitrogen to aggregate into multi-nitrogen-containing complexes. In this section, we review the properties of the individual nitrogen-containing point defects in isolation and, then, describe their production and interactions induced by treatments, such as irradiation or annealing.

Many techniques are available to study point-defect centers in diamond. The following narrative draws on insights from theory and from the application of many different spectroscopies to samples grown under (better controlled and defined) process conditions. As shown below, further insights can result from studying isotopically enriched samples, and samples under uniaxial stress. Typically, it is the holistic view reached by combining results obtained using multiple techniques that has proven critical for understanding the atomic structure and properties of different defects.

3.1. Optical Properties

The optical properties of diamond defects are a significant part of its historical attraction and form the cornerstone of any future quantum technology applications. Unfortunately, the link between atomic structure and defect emission properties is not straightforward, so that it is not possible to link directly the atomic structure of a defect to a particular optical transition purely by studying its transition frequency. Instead, a number of techniques are employed, often in parallel, to determine structure.

The optical signatures of different processes in diamond typically occur at different energies and have different line widths. In vibrational spectroscopy, one-phonon IR absorption in defect-free diamond is forbidden due to the inversion-symmetric, homonuclear structure of the medium. The addition of point defects can destroy the local symmetry, however, enabling local one-phonon absorption.¹⁷³ The lattice cutoff for a single phonon in diamond is at a wavenumber of 1332 cm^{-1} (165 meV): vibrations at energies below this will propagate through the lattice and are typically broad, with line widths $>40\text{ cm}^{-1}$ (5 meV). Vibrations with energies $\geq 1332\text{ cm}^{-1}$, in contrast, are localized in both frequency and space and will manifest as sharp spectral lines known as local vibrational modes (LVM), with typical line widths $\sim 3\text{ cm}^{-1}$ ($\sim 0.3\text{ meV}$) as illustrated in Figure 15. Most such vibrations appear in the range 1332 and 1500 cm^{-1} , with the notable exception of the C–H (and in principle, N–H) stretch modes, which typically lie in the 2800 – 3350 cm^{-1} region. Overtone transitions will also appear in this higher wavenumber range.

Electronic transitions in diamond occur at energies in the range from $\sim 0.5\text{ eV}$ (4000 cm^{-1}) up to the bandgap at 5.47 eV .¹⁷³ Typically, the spectrum of an electronic transition in diamond will display a sharp, purely electronic feature and a broad phonon-assisted sideband to higher energy in absorption or to lower energy in luminescence. The purely electronic transition is termed a zero-phonon line (ZPL): typical line widths are in the range 0.5 – 5 meV in ensemble measurements at low temperature ($<80\text{ K}$) but can be lifetime-limited ($\sim 20\text{ MHz}$, $60\text{ }\mu\text{eV}$) in measurements of isolated single defect centers. The phonon-assisted sideband may also include

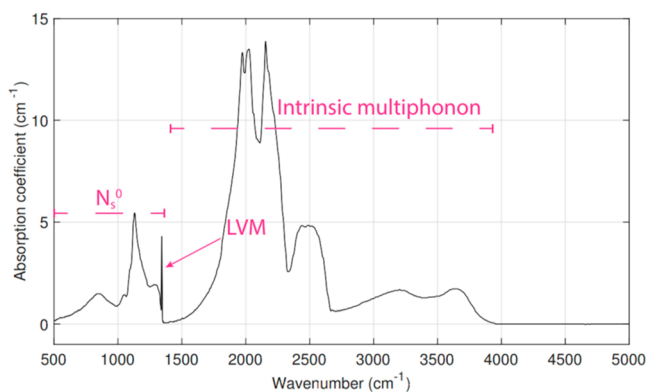


Figure 15. Typical IR absorption spectrum of a nitrogen-doped, HPHT-grown (i.e., type Ib) diamond. The spectrum is dominated by intrinsic multiphonon absorptions, as one-phonon absorption in diamond is forbidden by symmetry in the absence of defects. The introduction of defects, such as nitrogen, can break the local symmetry, introducing extrinsic absorption which will either propagate through the lattice (for vibrations with wavenumbers $<1332\text{ cm}^{-1}$) or remain spatially localized to the defect (a local vibrational mode, LVM, at wavenumbers $>1332\text{ cm}^{-1}$). In the case shown, all the extrinsic absorption is due to neutral substitutional nitrogen atoms. Adapted with permission from data in ref 174.

coupling to a localized vibrational mode, in which case the LVM will be observed offset from the ZPL by an energy corresponding to the LVM frequency. It will prove convenient to discuss such electronic spectral features more fully at the appropriate point in section 3.2.1.

The optical spectrum of a point defect serves as a “fingerprint” of that defect, and the ZPL energy (or wavelength) is often used to label not just the optical spectrum with which it is associated, but also the originating point defect itself (in cases where the atomic constituents are not known). This has led to the compilation of several catalogues of optical transitions in diamond.^{175,176}

Both optical absorption and luminescence measurements are widely employed in the study of diamond. Absorption measurements are typically limited to defects present at concentrations $>100\text{ ppb}$ in samples of thickness 1 mm but are indispensable given their ability to quantify the number of defects present. Luminescence measurements, in contrast, are routinely capable of measuring emission from a single point defect at room temperature, as illustrated below (section 4.4.1).

3.1.1. Uniaxial Stress. Point defects in diamond are necessarily orientationally degenerate (i.e., all equivalent orientations of a defect have identical properties) given the cubic symmetry of the host. However, the application of uniaxial stress to a crystal introduces an anisotropy, the effect of which on any given point defect depends on the angle between the applied stress axis and the symmetry axis of the defect—thereby lifting the orientational degeneracy. Application of a uniaxial stress will generally also lift any degeneracies in the orbitals associated with the defect. Thus, uniaxial stress can eliminate both electronic and orientational degeneracy, with the result that the energy of an optical (or vibrational) transition will shift and, potentially, split into multiple components under the stress-modified local potential. The number of components and their relative intensities provide a unique fingerprint of both the geometric symmetry (i.e., the atomic configuration) of the defect and the orbital symmetries

of the states between which the transition occurs; analogous information can be obtained for the symmetries of vibrational transitions.^{177–181} Uniaxial stress measurements have been critical in the study and identification of many defects in diamond.^{182–189}

3.1.2. Isotopic Enrichment. The development of laboratory growth methods has enabled the routine synthesis of isotopically pure diamond and of samples containing isotopically enriched dopants. The availability of isotopically enriched samples is particularly valuable when exploring defect vibrational properties. The vibration of interest is often modeled as a “diatomic mass on a spring”, with the expected vibration frequency shift under isotopic substitution given by the square-root of the ratio of the reduced masses.¹⁹⁰ The synthesis of mixed-isotope samples allows determination of the number of equivalent nuclei involved in the defect, via the relative intensities of the resulting peaks.¹⁹¹ Although isotopic frequency shift can confirm the presence of an element in a particular defect, lack of shift does not necessarily imply its absence, because if the element in question does not participate in a particular vibration, the frequency of the vibration will be unchanged upon isotopic substitution. As described later, this is the case for the nitrogen atom in the 3107 cm^{-1} C–H stretch mode of the N_3VH^0 defect (see section 3.5.5.3).^{192–194}

In the case of electronic transitions, isotopic substitution may induce a small ZPL energy shift for defects containing the substituted element,^{195,196} which can be critical in assigning the presence of a chemical element to a given optically active defect.^{197–201} As with vibrational spectroscopy, however, the absence of measurable shift under isotopic substitution is not sufficient to conclude that the element itself is absent from the defect.

3.2. Spin Properties

Electron paramagnetic resonance (EPR) spectroscopy has also been pivotal in the identification and probing of point defects in diamond. EPR measures the absorption/emission of microwave radiation between different spin levels of unpaired electrons in a sample held in a magnetic field. Diamond is a covalent solid, so any unpaired electrons in the material are associated with defects. In contrast to EPR measurements of liquid samples, where the measured spectrum depends intimately on the concentration of the radical (among other things), the EPR spectra of point defects in diamond are essentially identical sample-to-sample, as in each case the defect is “frozen” in place and exists in the same environment. This allows the publication of defect-specific spin properties which serve as an unambiguous identifier of a given diamond point defect.

Diamond in natural isotopic abundance is a dilute nuclear spin bath (only 1.1% of the atoms are ^{13}C , with a nuclear spin $I = 1/2$), which yields narrow resonance lines and enables high-resolution paramagnetic spectroscopy. As noted in section 2.2.3, CVD offers a route to essentially pure ^{12}C diamond. Such extreme nuclear-spin-dilute environments are a prerequisite for the superlative spin properties of several diamond defects.^{202–204} There are many in-depth texts covering both the EPR technique,^{205–209} and its specific application to diamond.^{210–214}

The power of EPR relies on the intimate relationship between the spin Hamiltonian parameters measured in an EPR spectrum, and the electronic, chemical, and geometric

structure of the defect. The spectrum of an EPR-active defect reflects its symmetry and orbital structure (via spin–orbit interactions), its chemical constituents (via electron–nuclear hyperfine, and nuclear quadrupole interactions), and spin–phonon coupling at the defect (via its spin relaxation properties). Identification of different chemical elements with similar nuclear spin generally relies on comparison of the spectrum with the natural abundance of different isotopes of each element. For example, nitrogen is a dominant impurity in diamond and is easily identified by its 99.6% abundant $I = 1$ ^{14}N isotope. Where ambiguity exists, the synthesis of samples isotopically enriched in the dopant of interest can be crucial to determining the elements involved, particularly in cases where the dominant isotope has $I = 0$ (as is the case for silicon and oxygen). Even once a dopant has been definitively identified, access to material containing only $I = 1/2$ isotopes (which removes additional spectral complexities associated with the nuclear quadrupole interaction) can be critical in understanding and fully interpreting the EPR spectrum. Studies involving samples enriched with ^{15}N are a good case in point, as illustrated in section 3.5.4.3.

In most EPR measurements, the sample is mounted in a microwave resonator. This affords a very high sensitivity measurement, with a typical noise floor of $\sim 10^{11}$ spins for samples with spin lifetimes as long as those in a material like diamond.^{205,215} In a 40 mg diamond sample, 10^{11} spins corresponds to a defect density of just 0.05 ppb. This sensitivity can be pushed to the ultimate limit—that is, the detection of the spin of a single point defect—in cases where the electronic structure enables spin-state detection through charge collection or luminescence (see section 3.5.4.1).

3.2.1. Linking Optical Properties and Spin Properties.

While EPR is capable of determining the structure and elemental composition of a defect, it does not intrinsically provide any link to the optical properties of that defect. Multiexcitation experiments, such as optical excitation with EPR detection (photoexcited EPR), or optical detection with EPR excitation (optically detected magnetic resonance, ODMR) provide a route to establishing this link. In the former, the sample is illuminated while inside a microwave cavity, and the EPR spectrum of the photoexcited state is monitored. In favorable cases (i.e., in systems where the photoexcited state displays a high intersystem-crossing probability), this approach allows access to excited states with nonzero (electron) spin in defects whose ground states are spin-free. In other cases, the double-resonance excitation may modify the intensity of an existing spectrum as a result of charge transfer with other defects in the diamond (photochromism, see section 3.4). In either case, the double-resonance experiment provides a definitive link between the optical and EPR spectra of a common defect.^{183,216} In some defects, a property of the optical spectrum (e.g., its intensity, polarization, frequency, etc.) is dependent on the defect spin state, and this can be used to measure the spin properties directly, even in cases where the defect does not exhibit ground-state EPR or its spectrum is unknown.^{217–223} This up-conversion from microwave (for typical spin resonance measurements) to visible frequencies, where the photon energies are much higher than any thermal fluctuations and also where single-photon detectors are widely available, has been key to ensuring that studies of the magnetic-resonance properties of single point defects in diamond are almost becoming routine.²²⁴

3.2.2. Atomistic Modeling. Point defects in diamond have been examined by a wide variety of experimental techniques; many directly yield information about the microstructure and chemical constitution of the defects, but others provide information that requires additional assumptions or analysis to be applied. As an example of the latter, IR absorption spectroscopy and Raman scattering both yield the wavenumbers of vibrational modes, which may be in a spectral range typical of a carbon–carbon single or double bond, but the true composition of the oscillator and its arrangement within the diamond crystal will usually not be directly revealed by such measurements. Additionally, direct observation techniques are not able to measure many properties of point defects that one might wish to understand, for example, transition-state structures and electron wave functions.

The use of computational tools to simulate point defects is, thus, a valuable adjunct to experiment, providing confirmation of inferences from observation. However, theory is undoubtedly also an essential quantitatively predictive approach for a wide range of physical properties, serving both to eliminate erroneous microstructure assignments and to reveal information about processes and properties not visible to experiment.

Computational approaches vary in both scale and accuracy. For systems with many thousands of atoms or for simulations that follow processes over time scales in excess of nanoseconds, empirical methods are often used. For implantation cascade damage, relevant to the formation of nitrogen-containing color centers, Monte Carlo simulations can be used, such as embodied in the SRIM (Stopping and Range of Ions in Matter) software. Such simulations²²⁵ (e.g., as shown in section 3.5.4.1.1) can provide insight into the depth profiles of implanted ions, but these approaches do not capture all of the physical processes and conditions, such as heating, channelling, and damage accumulation, nor do they provide direct insight into the microscopic arrangement of the implanted ions.

Atomistic molecular-dynamics simulations are computationally costly but can provide an unbiased assessment of kinetics because reaction mechanisms necessarily must be assumed to determine activation energies. The use of empirical potentials can significantly expedite computational simulations, especially where relatively infrequent processes require long simulation periods to obtain a statistically significant result. The reliability of empirical potentials for point defects is questionable, however, since many of the details of structure and observable properties depend explicitly on the electrons. Hence, the preference for approximate quantum-mechanical (QM) approaches, such as density-functional tight-binding methods, as used to explore the dynamics of impurities in grain boundaries in UNCD.²²⁶

For processes and data that relate directly to the electronic part of the point defects, fully QM-based approaches are needed. This is true not only where the electrons in the system are directly responsible for the observable phenomena but also, more generally, because such approaches are not susceptible to the bias inherent to empirical approaches (e.g., pair potentials). Density functional theory (DFT) is the most common core approach to modeling arrangements of nuclei and electrons. This underpinning theory allows the calculation of total energies and forces based upon the spatial variation of the electron density. To achieve this, additional approximations are typically employed to render the approach tractable. Of these, the separation of the motion of the electrons from the nuclei (the Born–Oppenheimer approximation), the treatment of the

contributions to the total energy from the exchange and correlation terms (the exchange–correlation functional) and the numerical convergence with respect to expansion of the electron states (the wave function basis) are probably the most important. The latter two contribute to the quantitative accuracy of basic properties (e.g., the lattice constant of the underlying diamond structure), while the former removes the electron–phonon coupling from calculations.

The simplest DFT approaches underestimate band gaps and are relatively poor at assessing many-body energies that are so important for many color-centers in diamond. Post-DFT approaches, such as the so-called screened-exchange method,²²⁷ are commonly employed to determine excited-state energies, such as for the NV and SiV centers in bulk diamond^{228,229} and in nanodiamond.²³⁰

Where the calculations are suitably converged, even relatively basic consideration of the derivatives of the total energies obtained using DFT with respect to the nuclear coordinates provides routes to structural optimization (energy minimization yielding binding energies and chemical-reaction energy profiles), as well as spectroscopically observable vibrational modes, with Raman- and IR-active normal-mode frequencies typically within a few percent of the corresponding experimental value.^{194,231,232} Once total energies have been obtained, the dependence upon the chemical potentials of the atoms and electrons provides formation energies and electrical levels^{170,233} (i.e., the equilibrium charge states expected for different locations of the Fermi energy with respect to the valence and conduction bands). Perhaps more importantly, the explicit inclusion of electrons in quantum-chemical modeling, often in tandem with energy correction strategies and hybrid numerical-DFT approaches, has allowed the accurate calculation and prediction of optical and spin properties of many defects in diamond.^{220,231,234–236}

The combination of these factors, in combination with experimental observations, is often the key to unambiguous identification of the microstructure of point defects. The basic energetics provide insight into the likelihood of a given arrangement being stable under growth or subsequent processing conditions,^{100,237,238} and detailed confirmation can then be sought via spectroscopic properties, such as the ionization thresholds predicted at which bleaching of a photoluminescence transition would take place, stress response for vibrational modes,^{194,232} and the magnetic signatures of the hyperfine interaction tensors in paramagnetic centers.^{239–241} Computational data combined with modeling approaches for determination of observables, therefore, represents a powerful toolkit to gain understanding of interactions between defects, their behavior under annealing and subsequent aggregation or destruction.

3.3. Irradiation and Annealing

The study of defects in isolation is frequently insufficient to determine their properties and structure and is only one step along the road to achieving high-quality engineered diamond material containing a target defect in the desired concentration. Knowledge of the interactions between defects, their dynamics, and their creation or destruction routes, are all prerequisites to being able to target material for a particular application.

Common treatments performed on diamond with a view to processing its composition include the introduction of elements through implantation, the introduction of lattice damage through particle irradiation (e.g., with electrons,

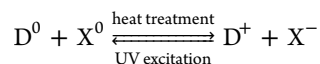
neutrons, or γ rays) and moderate-to-high-temperature annealing of the material. Annealing provides thermal energy required to break bonds within the material, thereby allowing elements, vacancies, or defect complexes to diffuse through the lattice. Moderate annealing at temperatures T_{anneal} up to ~ 1600 °C is achieved using a conventional tube furnace under an inert atmosphere or in ultrahigh vacuum to prevent surface graphitization. Above 1600 °C, stabilizing pressure (>6 GPa) is also required to prevent graphitization; annealing at these temperatures is typically completed in presses used for HPHT diamond synthesis. Anneals can be completed in low-pressure, high-temperature conditions—quickly (<1 min) if the temperature ramp rate is sufficiently high²⁴² or on a more leisurely time scale if significant graphitization of the diamond can be tolerated.^{243,244}

The production route of a defect, which can be crucial in determining its structure, can often be deduced by simultaneously monitoring other known complexes that are created and destroyed in the same treatment. By way of illustration, the defect responsible for emission at 637 nm was originally hypothesized to have the structure of a nitrogen nearest-neighbor to a vacancy following observations that it was produced in material containing substitutional nitrogen and following irradiation and annealing.¹⁸⁷ Such analysis strategies are especially powerful when applied to contemporary lab-grown material, wherein impurity levels can be exquisitely controlled and the range of possible elements involved in any subsequently produced defects thereby restricted. The interactions of different defects are further explored in sections 3.5.4.5 and 3.5.5.4.

3.4. Charge Transfer and Photochromism

Given its wide band gap, diamond at low (\sim ppm) doping levels can be considered an insulator. This allows the same point defect to exist in multiple charge states in the same sample simultaneously (depending on the local environment of each individual defect) and enables dynamic treatments which can redistribute charge between defects and whose effects are pseudostable at room temperature.

For defect charge states dominated by nitrogen donors, a protocol has been developed which allows the same crystal to be measured in two extreme charge states.¹⁸⁹ Optical excitation above the band gap (i.e., at $\lambda < 224$ nm) generates free carriers in the conduction band, which are continuously trapped and re-emitted until the excitation is removed, at which point a charge distribution is essentially “frozen in” (barring highly local effects such as charge tunnelling). Typically, this maximizes the concentration of neutral substitutional nitrogen and, in turn, tends to maximize the concentration of the neutral charge state of other defects in the crystal. Conversely, heating at ~ 550 °C in the dark gives enough thermal energy to allow electrons to redistribute from metastable states (but not enough to modify the atomic configuration of the vast majority of point defects), maximizing the concentrations of positively charged nitrogen donors and negatively charged codefects. Schematically, for a donor D and defect X, this process can be written



This protocol has successfully demonstrated charge transfer between $\text{SiV}^{0/-}$,²⁰¹ $\text{NVH}^{0/-}$,²⁴⁵ and $\text{NV}^{0/-}$,²⁴⁶ and these effects can be an extremely powerful diagnostic when used in

conjunction with other methods. For example, if the two stable charge states of a given defect differ by a single electron, then at least one of them can be expected to be EPR-active, and hence, this enables a route to identify the atomic constituents. If the defect has associated optical transitions, then changes in the relative concentrations of the defect charge state can have a dramatic effect on the overall color of the sample—an effect known as photochromism (for an example, see section 3.5.4.2). By correlating the gain of one optical transition with the loss of the other, it is possible to identify two different charge states of the same defect.

3.5. Nitrogen-Containing Defects in Diamond

The notation used to describe defects in diamond is not universal, and the historic descriptors can be confusing. The traditional, alphabetical labels were introduced along with the A-, B-, and C-centers in section 1, but such descriptors are not systematic. The notation used in the present Review is as follows: A *substitutional* defect is one where a host atom (here carbon) is replaced by another element and will be denoted by the element followed by a subscript “s”. Thus, the systematic label for the single substitutional nitrogen defect historically termed the C-center (Figure 3) would be N_s , with the associated charge (e.g., +, −, 0) indicated by the appropriate superscript. The A-center (Figure 3), involving two substitutional N atoms in nearest-neighbor positions, would in the systematic notation be labeled N_2 . The “s” in this case and in many larger substitutional defects is implicit and not normally specified. Defects involving two substitutional nitrogen atoms separated by, respectively, one and two carbon atoms—for example, the $\text{N}_s^0\text{—C—N}_s^+$ and $\text{N}_s^0\text{—C—C—N}_s^+$ centers—are also known^{239,247–249} but are only likely to be found in HPHT diamond samples containing high levels of substitutional nitrogen. *Interstitial* defects, where the defect element is additional to the host lattice, also exist and are here denoted using a subscript “i”. The dinitrogen interstitial discussed in section 3.5.3 is thus denoted as N_{2i} to avoid confusion with the N_2 defect.

Another family of defects considered in this section revolve around the vacancy, where a carbon atom is missing from the host lattice and four unstable radicals remain. The vacancy is labeled “V” (and is sometimes found italicized in the literature to avoid any possible confusion with the element vanadium). Any, or all, of the four carbon radicals surrounding the vacancy may be substituted by nitrogen to yield the defects labeled N_nV , where the number of nitrogen atoms n ranges from 1 to 4. The B-center introduced previously in Figure 3 is a member of this family; with four nitrogens surrounding a vacancy, it is labeled the N_4V defect. The vacancy and its associated radicals can also be decorated with hydrogen atoms; for example, the N_nVH family, with $n = 1\text{--}3$. There is also potential for nitrogen to form multi-hydrogen-containing defects labeled N_nVH_m , where $n \geq 1$, $m \geq 2$, and $n + m = 4$ (section 3.5.6). The hierarchy of defects involving nitrogen and hydrogen atoms around a vacancy is summarized in Table 1.

Other known nitrogen-based defects include, for example, $\text{N}_3\text{V}_2\text{N}$. This defect is based on a divacancy structure with six surrounding carbon radicals, three at each end. To achieve the $\text{N}_3\text{V}_2\text{N}$ defect, the three radicals at one end are substituted by nitrogen, along with one of the radicals at the other end.

Many other nitrogen-containing defects involving species other than vacancies and hydrogen atoms are known in diamond, but space limitations dictate that these receive only

Table 1. Family of N_nVH_m Defects with $n + m \leq 4^a$

V	NV	N ₂ V	N ₃ V	N ₄ V
VH	NVH	N ₂ VH	N ₃ VH	
VH ₂	NVH ₂	N ₂ VH ₂		
VH ₃	NVH ₃			
VH ₄				

Adapted with permission from ref 21. Copyright 2018 University of Newcastle. ^aThose highlighted in orange are viewed as being fully saturated.

passing mention. The $N_s^0CN_s^+$ and $N_s^0CCN_s^+$ centers were noted above and are complemented by hydrogen-containing analogues like N_sHC . This is a neutral defect (and thus has $S = 0$), wherein the hydrogen is bonded to the carbon and proximal to the nitrogen lone pair,²⁵⁰ that has been linked with a vibrational mode at 3324 cm^{-1} by comparing theoretical stress parameters with experiment.¹⁹⁴

Another major class of defects arises when a larger element (e.g., Ni) moves from a substitutional site around a vacancy into the space created. The remaining carbon sites around the incorporated defect can be further saturated with nitrogen to form defects up to and including, for example, the $NiVN_4$ split-vacancy defect discussed in section 3.5.6.

Our understanding of nitrogen-containing defects in diamond and their interconversion upon exposure to temperature and pressure has advanced hugely in the recent past. Thus, following this short preamble, we now summarize the current state of knowledge regarding many of the better characterized defects.

3.5.1. Single Substitutional Nitrogen N_s . The single substitutional nitrogen defect, N_s (Figure 3b), readily incorporates into lab-grown diamond produced by CVD or HPHT synthesis, and in natural diamond. The probability of N_s incorporation is growth-sector dependent. In HPHT material, the nitrogen incorporation probabilities typically follow the trend: $\{111\} > \{100\} > \{113\} > \{110\}$,²⁵¹ whereas in CVD-grown diamond, N_s usually preferentially incorporates into $\{111\}$ rather than $\{100\}$ growth sectors,²⁵² with incorporation into $\{113\}$ and $\{110\}$ intermediate. In CVD diamond, N_s usually greatly outweighs the incorporation of nitrogen in the form of other defects (e.g., NV, NVH).²⁵³ Three charge states ($-/0/+$) of this defect are known.

3.5.1.1. N_s^0 . The N_s^0 center (termed the P1 center in the EPR literature) was first reported in 1959 and identified as involving nitrogen since this is the only naturally occurring atom with an almost 100% abundant $I = 1$ isotope.²⁵⁴ This, and the observation of ^{13}C satellites from a unique carbon neighbor, established the model of a single substitutional N atom, with a unique N–C “broken” (or stretched) bond to accommodate the unpaired electron density substantially localized in an N–C antibonding orbital. EPR measurements established that the electronic g -tensor is axially symmetric about the unique N–C bond, but that the departure from an isotropic g -value is very small.²⁵⁵

^{14}N and ^{15}N hyperfine coupling parameters for the N_s^0 center have been determined accurately by electron nuclear double resonance (ENDOR) spectroscopy, and ^{13}C hyperfine coupling of the unpaired electron observed with neighboring

carbon atoms in several different positions.^{256–258} The interactions between the electron and nuclear spins provide important insights into the defect structure. In the case of the N_s^0 center, the assignment of a ^{13}C hyperfine coupling to a specific site is determined by the ^{13}C relative intensities of the EPR satellites (which reflects the number of equivalent neighbors) and the magnitude, sign and symmetry of the interaction. Theory is now able to predict both the principal values and directions of these interactions quantitatively,²⁴¹ enabling a detailed picture of the unpaired-electron probability distribution. Analysis reveals that $\sim 25\%$ of the unpaired-electron density is localized on the nitrogen, with the remaining $\sim 75\%$ on the unique carbon; the localization on other carbon neighbors is very small. The ^{14}N quadrupole interaction is axially symmetric about the $\langle 111 \rangle$ axis of the defect and analysis of the quadrupole and hyperfine interaction data shows the unique N–C separation to be $\sim 30\%$ greater than the normal C–C bond length,^{241,259} see Figure 3b.

Motional averaging of the N_s^0 EPR spectrum is observed at temperatures $> 600\text{ K}$, as the “hopping” rate of the unpaired-electron probability density between the four possible N–C antibonding orbitals becomes comparable with the microwave frequency. By 1200 K , the EPR spectrum is truly isotropic, since the unpaired electron is “hopping” so quickly that it samples an average of all possible sites. Measurements at intermediate temperatures have allowed determination of the reorientation activation energy, $0.7(1)\text{ eV}$.²⁶⁰ The rate at which stress-induced ordering of the N_s^0 center is annealed out has been investigated by EPR methods at lower temperatures ($78\text{--}200\text{ K}$), as a function of the relative alignment of the defect and the applied stress. These data highlight the importance of tunnelling between thermally populated excited vibrational states.^{261–263}

Three EPR spectra originating from distinct coupled pairs of N_s^0 defects have been reported for diamonds containing high concentrations of N_s^0 centers.²⁶⁴ With the external Zeeman field aligned parallel to a $[100]$ crystallographic axis, the hyperfine interaction with the two N_s^0 centers gives rise to a characteristic 1:2:3:2:1 peak intensity pattern for each center. Another group of lines observed at about half the magnetic field of the N_s^0 center was attributed to a superposition of several spectra originating from weakly coupled pairs of N_s^0 centers separated by more than $\sim 0.7\text{ nm}$. The coupling is too weak for satellites from the component spectra to be observable, but the forbidden transitions from all these pairs contribute to the half-field spectrum. Further, at high N_s^0 concentrations, a replica of the N_s^0 EPR spectrum observed at roughly twice the magnetic field of the usual N_s^0 EPR spectrum is attributable to a two-photon transition at isolated N_s^0 centers.

The IR absorption spectrum associated with the N_s^0 defect in diamond grown from elements in natural isotopic abundance shows a maximum at 1130 cm^{-1} and a sharp LVM at 1344 cm^{-1} (Figure 16). $25 \pm 2\text{ ppm}$ of N_s^0 centers equates to 1 cm^{-1} of absorption at 1130 cm^{-1} .²⁶⁵ The 1130 cm^{-1} peak shifts $\sim 9\text{ cm}^{-1}$ to lower wavenumber upon replacing ^{14}N with ^{15}N ,^{266,267} and the 1130:1121 ratio matches that expected for a C–N vibration. Changing the nitrogen isotope has no detectable effect on the sharp mode at 1344 cm^{-1} , but this mode shifts to 1292 cm^{-1} in diamonds made of ^{13}C atoms—implying that this mode is not associated with N atom motion but is a pure carbon vibration associated with the strengthened C–C bonds adjacent to the nitrogen.²⁶⁶

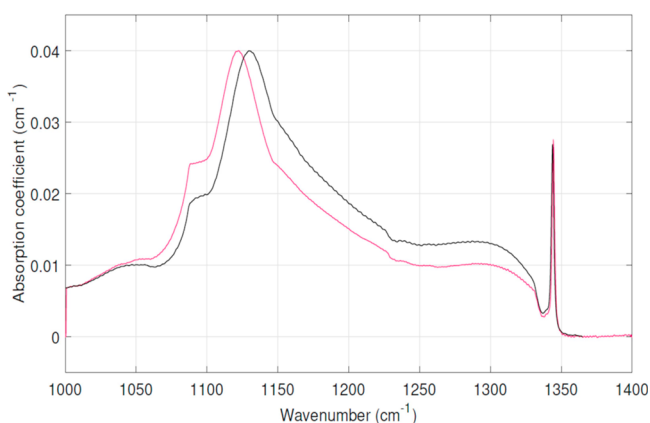


Figure 16. One-phonon spectrum of uncharged substitutional nitrogen in diamond doped with ^{14}N (black) and ^{15}N (red). The spectrum shows a broad absorption at 1130 cm^{-1} , which is predominantly due to nitrogen (as demonstrated by the strong nitrogen isotope shift), and an LVM at 1344 cm^{-1} associated with the vibration of carbon atoms adjacent to the nitrogen. Figure adapted with permission from ref 269. Copyright 2011, University of Warwick, used with permission.

Theory²⁶⁸ predicts atomic displacements consistent with the observed isotopic dependences and confirms the experimental finding (from measured uniaxial stress-induced splittings²⁶⁹) that the 1344 cm^{-1} LVM is an $A \leftrightarrow E$ transition in a defect of trigonal symmetry, as depicted in Figure 3.

The electronic absorption attributable to the N_s^0 defect shows an onset at energies $\sim 1.7\text{ eV}$ and rises continuously to the band edge. The concentration of N_s^0 centers correlates with the integrated intensity of a broad feature at 4.6 eV (270 nm)¹⁷² though uncertainties associated with background absorption may handicap concentration estimates derived in this way. Measurements of the onset of optical absorption and thermoconductivity measurements place the deep nitrogen-donor level at 1.7 eV below the conduction band (E_C)²⁷⁰ and suggest a photoionization energy of N_s^0 of 2.2 eV .²⁷¹

3.5.1.2. N_s^- . This center was identified as the carrier of a transient IR absorption at 1349 cm^{-1} induced by ultrafast $\sim 400\text{ nm}$ photoexcitation of N-doped diamond samples.²⁷² N_s^- defect formation was attributed to initial excitation of electrons from N_s^0 defects into the conduction band and the subsequent preferential recombination of these electrons with other N_s^0 centers (rather than with the original ionized nitrogen defects). Assignment of the 1349 cm^{-1} to a LVM of N_s^- was supported by DFT calculations,²⁷² which also suggest that N_s^- possesses an acceptor level $\sim 1.1\text{ eV}$ below the bottom of the conduction band.²⁷³ Further, in diamond samples in which the dominant N-containing defect is N_s^0 , it was proposed that the 270 nm absorption is accompanied by N_s^- creation via the reaction, $\text{N}_s^0 + h\nu \rightarrow \text{N}_s^- + h^+$, where h^+ is a hole in the valence band.²⁷³

3.5.1.3. N_s^+ . N_s^0 can also donate an electron if the diamond contains a suitable acceptor (e.g., a vacancy, a nitrogen-vacancy defect or a substitutional boron atom). An N_s^+ center results, with the N atom sitting on the lattice site and four identical bonds to the neighboring carbon atoms.⁹² N_s^+ is diamagnetic, so an EPR signal is neither expected nor observed. The N_s^+ defect does give rise to IR absorption, however, with a sharp peak at 1332 cm^{-1} accompanied by further features at 1115 , 1046 , and 950 cm^{-1} .²⁷⁴ The lower-wavenumber peaks shift (to 1040 and 940 cm^{-1} , respectively) upon substituting ^{14}N by

^{15}N , consistent with their assignment to N_s^+ , but the 1332 cm^{-1} does not shift upon changing the nitrogen isotope.²⁶⁹ 1 cm^{-1} of absorption at 1332 cm^{-1} is induced by $5.5 \pm 1\text{ ppm}$ of N_s^+ defects,²⁷⁴ but quantifying N_s^+ concentrations from IR absorption spectra requires care because many defects contribute to absorption at 1332 cm^{-1} and other absorptions in the one-phonon region can also influence the spectral deconvolution.

Jones et al.²⁷³ also proposed that N_s^+ can contribute to the absorption at 270 nm ($\text{N}_s^+ + h\nu \rightarrow \text{N}_s^0 + h^+$) but, given the large lattice relaxation (T_d to C_{3v}), recognized that such a transition would likely yield a structureless absorption feature. When multiple defects are present, substantial changes in the concentrations of N_s^+ (and N_s^0) can be produced by optical excitation (in the visible) and by heating in the dark to relatively modest temperatures (e.g., $550\text{ }^\circ\text{C}$). The N_s^+ concentration in as-grown N-doped CVD diamond can far exceed that of N_s^0 , indicating that there are a great many electron traps.

3.5.2. N_2^0 (the A-Center) and N_2^+ . The aggregation of N_s^0 centers to form A-centers has been much studied.^{8,275} The formation rate of A-centers in thermal annealing studies of type Ib synthetic diamonds was shown to scale with the square of the initial concentration of single substitutional N atoms, implying that the A-center involves two nitrogen atoms.²⁷⁵ The structure of the A-center is now accepted as comprising a pair of adjacent substitutional atoms with trigonal symmetry,²⁷⁶ as shown in Figure 3. N_2^0 centers give rise to IR absorption at 1282 , 1203 , 1093 , and 480 cm^{-1} ,²⁷⁷ as illustrated in Figure 17;

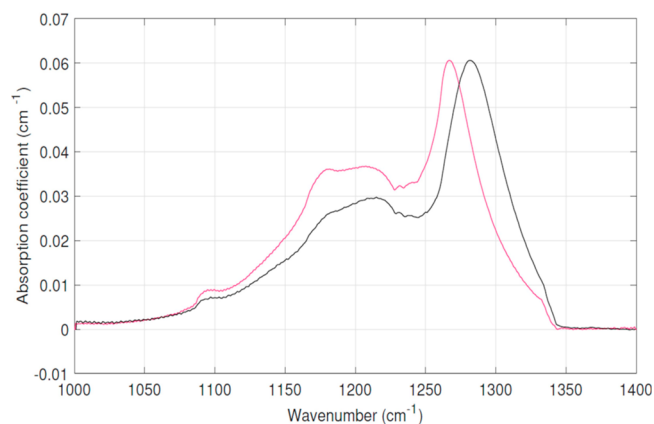


Figure 17. IR absorption spectra of the N_2^0 (A-center) defect in diamond. The primary peak at 1282 cm^{-1} in a natural abundance sample (black) shifts to lower wavenumber in ^{15}N -enriched diamond (red). Figure adapted with permission from ref 269.

1 cm^{-1} of absorption at 1282 cm^{-1} is produced by $16.5 \pm 2\text{ ppm}$ of N_2^0 centers.⁷ These IR absorptions are satisfactorily reproduced by modeling²⁵³ based on the foregoing N_2^0 structure, which also returns a doubly occupied level around midgap that accounts for the 3.8 eV absorption edge seen in type IaA diamonds.

N_2^0 is diamagnetic and thus not amenable to study by EPR, while the N_2^- defect would be energetically unfavorable and therefore unlikely to form. However, the N_2^+ center is paramagnetic and has been created in some natural single crystal diamonds by illumination with photons of energy $>3.0\text{ eV}$.²⁵⁹ N_2^+ defects could be created via electron capture by N_2^{2+} (diamagnetic), by ionization of N_2^0 centers, or possibly

both, depending on the traps and donors available. The ^{14}N and ^{13}C hyperfine coupling matrices for the N_2^+ defect show that essentially all the unpaired-electron population is in the lowest-energy antibonding orbital formed between the two N atoms, which are equivalent.

Using orthogonality and simple geometric considerations, the ^{14}N hyperfine interaction parameters allow estimation of the N–N separation in the N_2^+ center. The returned distance is similar to the unique N–C separation in N_s^0 . This seems reasonable, given that the N_s^0 and N_2^+ centers are isoelectronic, and that the main cause of the bond extension is the placement of an electron in the antibonding orbital.²⁵⁹ Studies on the number of N_2^+ centers remaining after cessation of the optical excitation return a wide distribution of lifetimes, reflecting the large variation in the separation between any particular N_2^+ center and its electron trap or donor. In micron-sized powered diamond and nanocrystalline diamond, N_2^+ can be observed without illumination, suggesting that a defect created near the surface can act as a trap or donor.^{259,278}

3.5.3. Interstitial Nitrogen Defects. There are no definitive assignments to any spectroscopic signature of single interstitial nitrogen-related defect structures in diamond.²⁷⁹ The EPR spectra of two defects observed in ^{15}N -doped material have been assigned to interstitial nitrogen defects (Figure 18a).²⁸⁰ These assignments are not supported by DFT,

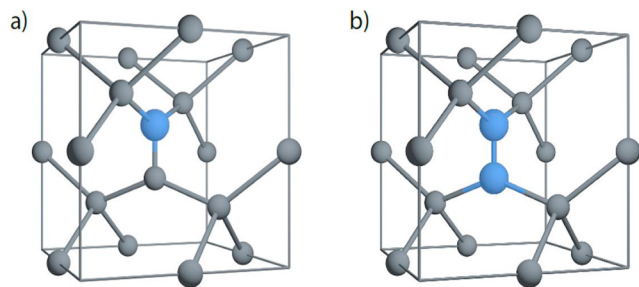


Figure 18. Structure of (a) N_i and (b) N_{2i} in diamond. The interstitial atoms in both cases share a common $\langle 100 \rangle$ axis, and the respective defects possess C_{2v} and D_{2d} symmetry.²³² N_i has been tentatively identified by EPR,²⁸⁰ but its assignment is not supported by DFT.²⁸¹ In contrast, a combination of uniaxial stress IR measurements and DFT have definitively identified N_{2i} .²³²

however, which also failed to find atomic structures which satisfactorily explained the experimental data:²⁸¹ further work is required in this area.

The $\langle 001 \rangle$ -split dinitrogen interstitial, N_{2iv} (Figure 18b)²³² is now assigned to the so-called H1a LVM transition at 1450 cm^{-1} through a combination of uniaxial stress measurements and theory,²³² notwithstanding earlier nitrogen isotopic substitution experiments that identified the 1450 cm^{-1} mode as containing two equivalent carbons and only a single nitrogen atom.^{191,197,282} The confusion arises because the 1450 cm^{-1} transition originates at a pair of degenerate modes, each of which does indeed involve one nitrogen and two carbon atoms.

The 1450 cm^{-1} mode is visible immediately following irradiation of natural type Ia diamond and is strengthened in type IaA diamond by annealing at $T_{\text{anneal}} > 250\text{ }^\circ\text{C}$.¹⁹¹ In this material, it seems probable that the low annealing temperature is a result of carbon interstitials migrating (at $\sim 300\text{ }^\circ\text{C}$)²⁸³ and subsequently being captured at N_2 , that is, $\text{C}_i + \text{N}_2 \rightarrow \text{N}_{2i}$. In type Ib diamond, the defect is produced following irradiation and subsequent annealing at $600\text{ }^\circ\text{C}$. Here, it is hypothesized

that its production is via single nitrogen interstitials, N_i , being captured at remaining substitutional nitrogen centers.²⁸⁴ H1a is stable to $\sim 1400\text{ }^\circ\text{C}$.^{232,285}

3.5.4. N_nV Family with $n = 1-4$. As noted at the start of this Review, nitrogen is the dominant impurity in most natural diamond, and forms the basis of the natural diamond classification system. Many natural diamonds also possess significant concentrations of defects in the N_nV form, with $n = 1-4$. These defects are generally considered to form via processes involving the capture of vacancy and nitrogen-vacancy complexes, where the vacancies are generated at growth defects, and during natural (or artificial) irradiation.

To a good approximation, the electronic structure of the N_nV family of defects can be described using the “vacancy-cage” model.^{283,284} This model assumes that the gross properties of a vacancy-type defect in diamond can be derived by considering only those electronic orbitals that “point into” the vacancy. Since the radicals are unstable, the electronic states that result are localized on the defect and lie in the band gap. For the N_nV family, therefore, the vacancy-cage model encourages us to focus on the symmetry (and valence) changes when up to four of the C atoms around a vacancy are substituted by N atoms. The structures of the N_nV ($n = 1-4$) defects are collected in Figure 19.

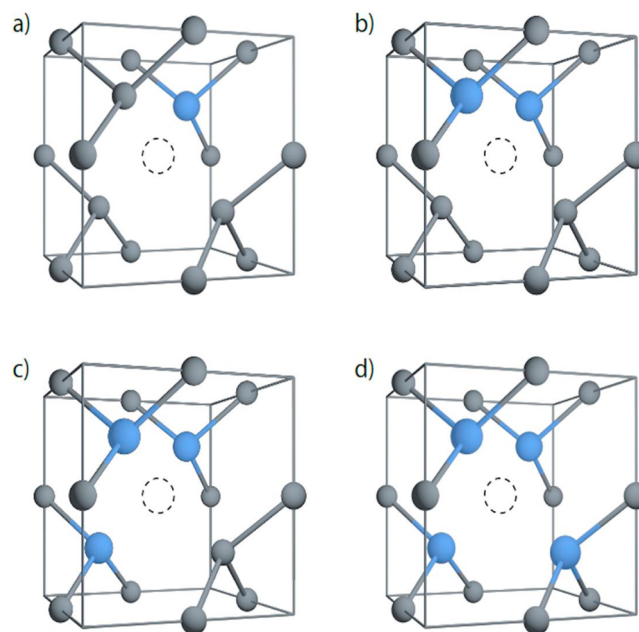


Figure 19. Structures of the N_nV defects in diamond. (a) The N atom in the NV center remains approximately on the lattice site of carbon (in undoped diamond) and does not relax significantly toward the vacant lattice site, giving an axial C_{3v} symmetry. (b) The two N atoms and the vacancy in the N_2V defect are retained in a $\{110\}$ plane, giving the defect rhombic (C_{2v}) symmetry. (c) The N_3V^0 defect has the same (C_{3v}) symmetry as NV, so the same vacancy-cage-based one-electron levels apply in both defects. (d) The N_4V defect maintains the T_d symmetry of the diamond lattice.

3.5.4.1. NV. The nitrogen vacancy center, NV, comprises a single substitutional N atom adjacent to a vacant lattice site as shown in Figure 19a, giving the defect a trigonal C_{3v} symmetry. Three charge states of NV are known, +, 0, and −, with total ground-state spin $S = 0, 1/2,$ and $1,$ respectively.^{235,285-287} NV defects have been subjected to huge recent attention owing to

their potential applications in quantum computing, quantum communication and magnetometry (see section 4). These applications stem from the spin-dependent fluorescence of the NV^- center,²³⁶ which, remarkably, reaches 30% contrast between different spin states, not just at cryogenic temperatures but also at room temperature,²⁸⁸ its spin-selective optical transitions that are accessible below ~ 10 K,²⁸⁹ and long spin-coherence times, even at room temperature.^{202,290} Such properties are rare in solid-state systems, though we note other rival candidates that have been identified in diamond,^{291,292} silicon carbide^{293,294} and hexagonal boron nitride (h-BN).²⁹⁵ The properties of the NV^- center have been the subject of several in-depth reviews.^{287,296,297} Here, we look to summarize the properties of all charge states of the NV center.

The NV^- and NV^0 states exhibit optical ZPLs at 637 and 575 nm, respectively (Figure 20).^{187,299} In both cases, the ZPL accounts for <5% of the total emission or absorption, with the remainder associated with a broad phonon-assisted sideband. NV^- also shows an IR transition at 1042 nm, between a pair of

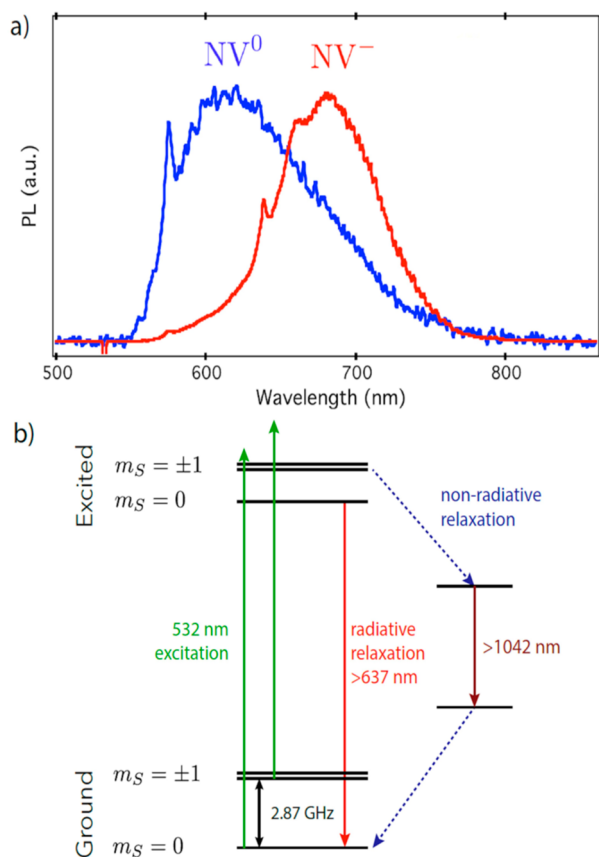


Figure 20. (a) Room-temperature emission spectra of NV^0 and NV^- . These defects have weak ZPLs at 575 and 637 nm, respectively, with broad phonon-assisted sidebands contributing the majority of emission (and absorption). (b) Simplified energy-level structure of the NV^- center in diamond. Optical transitions between the ground and excited state are bright (cycling) if the center is in the $m_S = 0$ spin sublevel, and dark (noncycling) if the center is in the $m_S = \pm 1$ state. The spin-dependent difference in excited-state radiative versus nonradiative transition probabilities results in both spin-dependent fluorescence intensity (optically detected magnetic resonance) and optical spin polarization approaching 100%, even at room temperature. Panel a: Reprinted with permission from ref 298. Copyright 2010 American Physical Society.

spin singlet states.^{184,300} No optical transition has been definitively assigned to NV^+ , and its presence is inferred only through the lack of emission from $NV^{0/-}$ in active or passive charge control experiments.^{235,286,301} DFT calculations predict that the NV^+ defect has an $S = 0$ (rather than $S = 1$) ground state.²³⁵ This state is thus unlikely to be observed by EPR. However, an optically accessible triplet state of NV^+ has also been predicted (~ 1 eV above the ground state)³⁰² but not yet observed.

NV^0 possesses an $S = 1/2$ ground state, but no EPR has ever been detected from this state. The orbital structure of NV^0 has been revealed by recent magnetic circular dichroism measurements and shown to involve a relatively small spin-orbit interaction in the ground state.³⁰³ Historically, the lack of EPR from the orbitally degenerate NV^0 ground state has been attributed to dynamic Jahn-Teller distortion,^{285,298} but recent measurements suggest it may be more a result of strain-broadening.³⁰³ A high-spin $S = 3/2$ excited NV^0 state is observed when suitable samples are illuminated with light of energy ≥ 2.2 eV.^{285,304}

The most stable charge state of any particular NV defect depends on its local doping environment. We note that the concept of a Fermi level is not strictly applicable to a moderately doped wide-band gap semiconductor, such as diamond.³⁰⁵ Nonetheless, the concept is useful to illustrate differences in the local charge environments. In the case of diamond doped with >100 ppb concentrations of substitutional nitrogen, the Fermi level is ~ 1.7 eV below the conduction band²⁷⁰ and NV^- is the dominant charge state.²³³ In “electronic-grade” material, however, where the primary dopant is substitutional nitrogen at concentrations ~ 1 ppb, it is possible to probe single isolated NV centers optically, typically using a confocal microscope.³⁰⁶ Both neutral and negative charge states are observed in the latter material, with the “stable” charge state of a particular center depending both on the local donor/acceptor density and the excitation wavelength used to probe the center.^{307,308} Active charge state control has been demonstrated for near-surface NV centers using electrodes formed by patterning oxygen and hydrogen termination of a diamond surface.^{235,286,301} As Figure 21a shows, under typical NV excitation conditions using a laser operating in the green spectral region (520–532 nm range, which excites both the NV^0 and NV^- charge states), any given center will be in a pseudostable equilibrium with NV^- being photoionized to NV^0 and photoexcitation of an electron from the valence band to the ground state of NV^0 , recovering NV^- . Under higher laser intensity, this generates a detectable photocurrent that has allowed photoelectric readout of both NV ensembles^{309–311} and single NV centers.³¹²

3.5.4.1.1. Fabrication of NV Defects. NV is very rarely observed in natural diamonds in any charge state, though it can be produced by electron irradiation and subsequent annealing in rare type Ib and some type Ia natural diamonds.¹⁸⁷ However, synthetic nanodiamond particles naturally contain small concentrations of NV centers, which can be sufficient for some applications. Most applications require much higher concentrations of NVs, however, and so, their concentration in the diamond must be increased in some way. Further, to make use of the optical and magnetic properties of these NV centers, they often must be located very near (within a few tens of nanometers) of the surface and, for some applications, also in well-defined lateral positions.

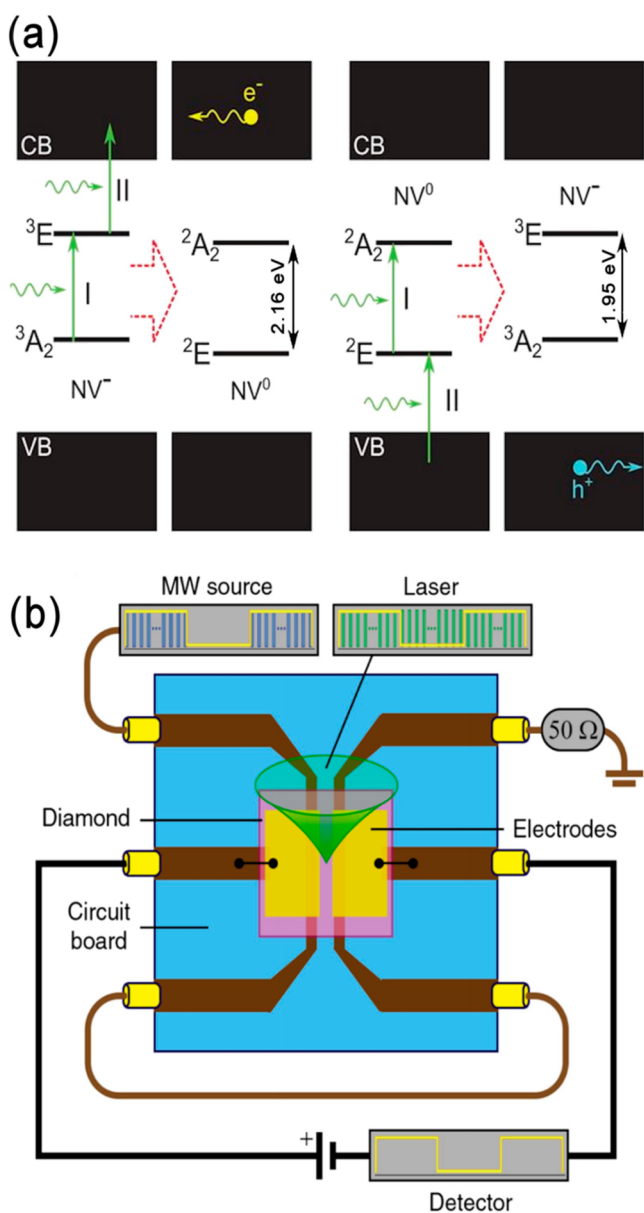


Figure 21. (a) Photoelectric readout scheme from NV^{-/0}. Intense green light causes a spin-dependent two-photon ionization of NV⁻, emitting an electron. Subsequently, a two-photon, spin-independent repumping process recovers NV⁻ and emits a hole. (b) Schematic diagram of a device used to perform photoelectric readout of NV. Panel a: Reprinted with permission from ref 312. Copyright 2019 American Association for the Advancement of Science. Panel b: Reprinted with permission from ref 311. Copyright 2017 American Physical Society.

NV defects are typically produced by the capture of vacancies at substitutional nitrogen atoms. The activation energy for movement of vacancies in diamond is ~ 2.3 eV^{313,314} (corresponding to experimental temperatures of ~ 600 – 700 °C). The nitrogen may be native (i.e., grown-in) or implanted to produce near-surface NV centers.^{165,168,315–318} In the latter case, the required vacancies are introduced during the implantation process itself (Figure 22a). In low N-containing material, the spatial periodicity of the resulting array of NV centers illustrated in Figure 22b is limited not just by the precision of the implantation event but also by the requirement of a vacancy that is able to diffuse to the implanted species.

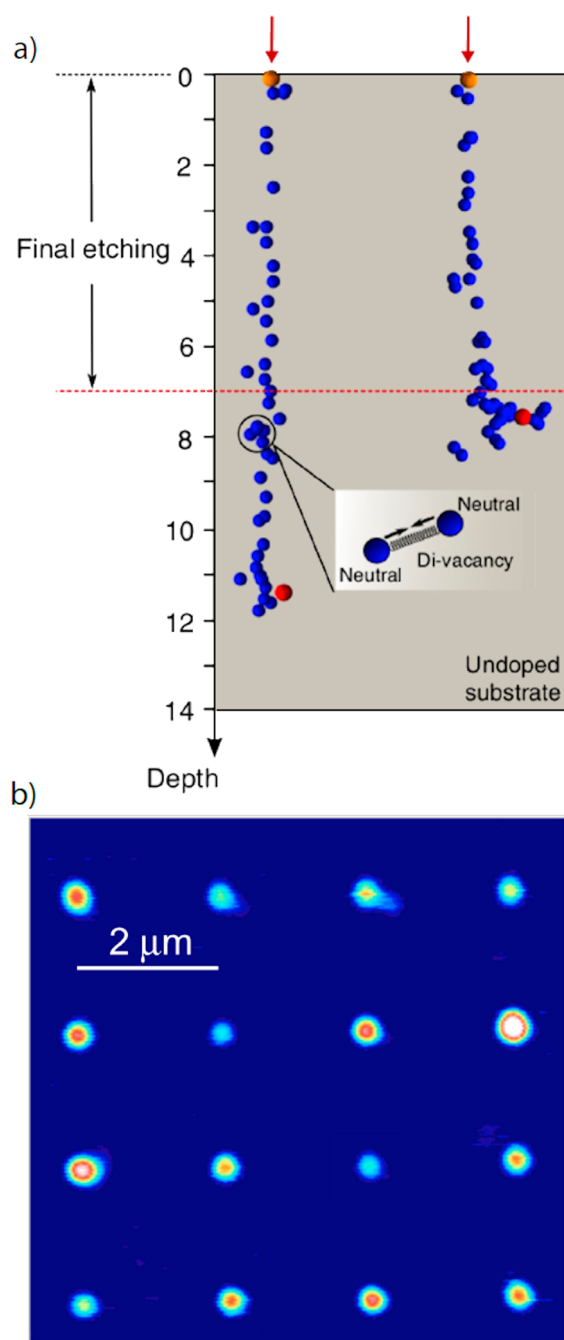


Figure 22. (a) Monte Carlo simulations of N⁺ ion implantation into diamond. Blue and red spheres indicate vacancies created by the implantation and the final stopping location of the ion, respectively. (b) Array of single NV⁻ centers created by ion implantation and imaged with a confocal microscope. Panel a: Adapted from ref 331 under CC BY 4.0 license. Copyright 2017 de Oliveira et al. Panel b: Copyright Deutsche Physikalische Gesellschaft. Reproduced by permission of IOP Publishing. CC BY-NC-SA license, adapted from ref 332.

When exploiting native nitrogen, the vacancies may be introduced by irradiation with electrons, protons, or neutrons,^{187,319–321} by ion implantation with helium/carbon^{322,323} or by plasma processing.³²⁴ An alternative method to produce the NV centers with high spatial precision is to use a high-power femtosecond laser pulse to displace carbon atoms in a vacancy “laser writing” process, and then anneal the

diamond to allow these vacancies to diffuse to any nearby N atoms. This can even be achieved using the same laser but operating at lower pulse powers.^{325–327} This method has great potential for the placement of defects at desired locations with an accuracy of 10 nm–1 μm with minimal residual lattice damage.

The conversion yield of N_s to NV has been shown to be much higher when electron irradiating at elevated temperature (740 °C) than when using the equivalent irradiation dose and then annealing postirradiation.³²⁸ The precise mechanism is not yet clear, but it seems likely to be the result of a reduction in vacancy recombination and vacancy aggregation.³¹⁴ Most of these techniques provide better depth than in-plane resolution, but the latter can be improved by using delta-doping during growth to confine a narrow nitrogen-doped layer within intrinsic buffer layers, achieving layer depth resolutions as thin as 4 nm.^{321,329} Implanted nitrogen has been the historic focus in this area, but recent results suggest that those NV⁻ defects that achieve lifetime-limited coherent optical transitions are actually formed by vacancy capture at native nitrogen, rather than at the implanted nitrogen atoms.³³⁰

Nanodiamonds made by pulverizing larger CVD, HPHT, or natural diamonds often contain a high concentration of nitrogen as a result of the N present in the original stones, while DND often contains N atoms from the N-containing high explosives used in their fabrication (see section 2.3.2). These NDs also usually contain a significant number of vacancies; annealing at high temperatures (>800 °C) allows these vacancies to migrate and become trapped at substitutional N sites (C-centers), forming the desired NV centers. The number of initial vacancies can be increased if required by high-energy electron irradiation. For NDs with little or no N content, ion implantation of nitrogen both adds additional N atoms and creates vacancies, such that subsequent annealing produces the NVs at the desired high concentrations. Conversion efficiencies from nitrogen to NV have been reported to be ~10%, producing NV densities of tens of parts per million.^{157,333} This corresponds to a few NV centers within a 10 nm ND particle.

For other types of lab-grown diamond, NV centers can be grown-in as a unit during CVD or HPHT growth. In the former, NV defects typically account for <1% of the total nitrogen incorporated during growth,²⁵³ though the nitrogen incorporation rate and the N:NV ratio is highly growth temperature-dependent.³³⁴ As noted in section 2.2.3, NV centers formed during CVD growth are sensitive to the plasma conditions and the crystallographic surface presented to the plasma. Growth on substrate planes other than {100} (for which all <111> directions are equivalent) can result in nonequilibrium populations of NV with the four possible <111> orientations (so-called “preferential orientation”, see Figure 23). For growth on <111> surfaces, it has been shown that, in the majority of cases, nitrogen is incorporated first, and the vacancy is subsequently grown over the nitrogen on the next epitaxial layer.¹⁰²

In {110} growth, only NV centers whose primary <111> axis is not in the substrate plane are occupied,²⁵³ while growth on {111} substrates produces NV centers whose symmetry axes are all perpendicular to the surface (the other three orientations are effectively unoccupied).^{102,103,105} Such preferential orientation of NV centers has also been reported on the <111> surfaces of HPHT-grown crystals.³³⁵ At moderate temperatures (1500–1600 °C), NV defects are thought to

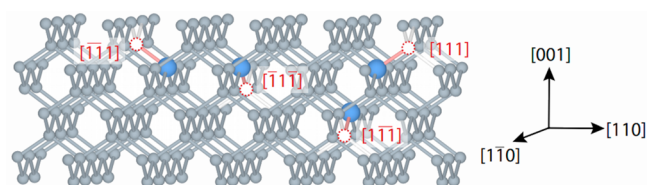


Figure 23. Illustration of different NV orientations within the diamond lattice. There are four equivalent <111> directions in diamond: in typical production methods (e.g., ion implantation and annealing or CVD growth on <100> substrates, where the angle between each <111> and <100> is identical), all four orientations will be populated equally, that is, 25% each. However, CVD growth on substrates which present different relative angles between each <111> and the growth surface (e.g., growth on <111> or <110> substrates) can lead to nonequilibrium population of the four equivalent directions (so-called “preferential orientation” of defects). Preferential orientation is preferred for scalable fabrication of NV-based photonic devices and can increase the sensitivity of NV-based magnetometers (see section 4).

move through the lattice as a unit (section 3.5.4.5.2).³³⁶ Recent experiments have demonstrated loss of preferential orientation upon annealing at 1500 °C, but it is not yet clear whether this is due to the creation of additional NV centers or to the loss of preferential orientation in existing defect centers.³³⁷

Another strategy to get around the problem of positioning the NV centers with nm precision and within a few nanometers of a surface is to pattern the surface around the NVs. In this approach, shallow NV centers are created by implantation and annealing, as before, but then the surface is patterned into nanophotonic structures, such as columns or pillars by standard lithography and anisotropic etching processes (see Figure 24). By optimizing the density of NVs and the column widths, it is possible to fabricate a device where approximately one out of three pillars contain a single NV center.³³⁸ This approach has the advantage of not only locating the NV centers precisely but also enhancing the photon rates from these centers by directing the light out of the substrate rather than into the bulk, which can be a problem for NV centers buried under flat surfaces.^{339,340}

3.5.4.2. N_2V . The N_2V center comprises two nitrogen atoms surrounding a vacancy in a {110} plane (Figure 19), giving the defect overall rhombic (C_{2v}) symmetry.³⁴² As with NV, only the neutral and negative charge states of N_2V have been directly observed, with their respective ZPLs at 503 nm (2.465 eV, also commonly labeled H3, where the H indicates a defect that is observed after irradiation and heating) and at 986 nm (1.257 eV, traditionally labeled H2) as shown in Figure 25. Given the low symmetry, no electronic degeneracy is possible in any charge state.

The ground state of the N_2V^0 defect has 1A_1 symmetry^{342,344} and is thus EPR-inactive. This symmetry was confirmed via uniaxial stress measurements, and the structural form inferred from the production routes in natural diamond samples.^{276,344} The atomic structure responsible for the H3 feature was confirmed when photoexcited EPR measurements of H3-containing diamonds identified a spin-triplet excited state with the rhombic symmetry and equivalent nitrogen hyperfine interactions consistent with the N_2V model.³⁴⁵

H3 is one of the most common luminescence centers observed in natural diamond (usually accompanied by N3 luminescence, see section 3.5.4.3) and is readily introduced by

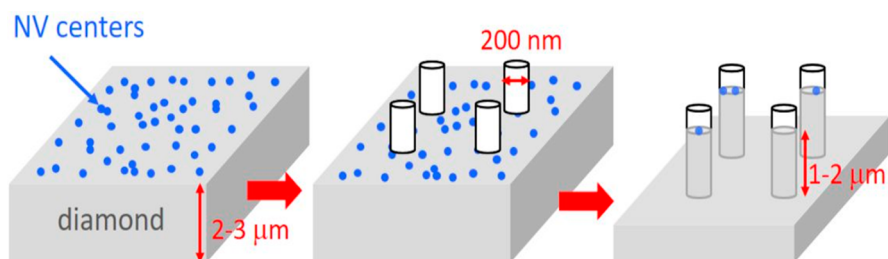


Figure 24. Example of a fabrication process for positioning NV centers in cylindrical diamond pillars. Similar processes can be used to fabricate columns, cones, or pyramid structures. Shallow NV centers are created in single-crystal diamond by implantation and annealing. Electron-beam lithography methods are then used to define ~ 100 nm diameter features on the surface. The diamond is etched into pillars $\sim 1\text{--}2\ \mu\text{m}$ deep using an O_2 -based plasma in an anisotropic dry etch process, thereby removing all NVs that are not protected under the resist. The resist is removed, revealing pillars with between 0 and 3 embedded NVs close to the top surface of the pillar. Figure adapted from ref 341 under CC BY 4.0 license. Copyright 2017 E. Bernardi, R. Nelz, S. Sonusen, E. Neu.

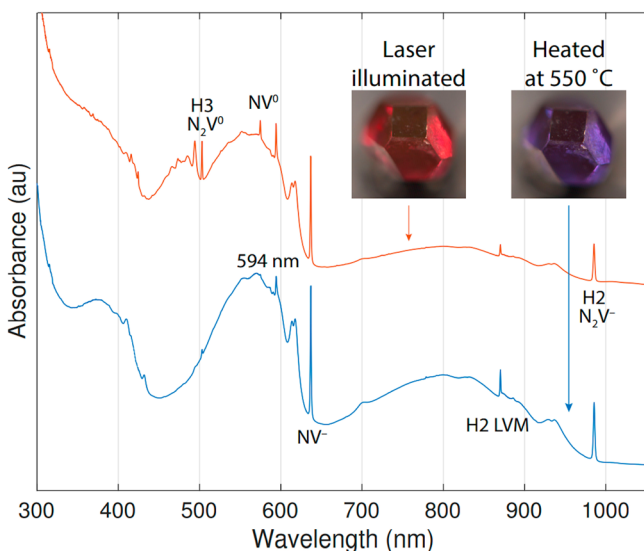


Figure 25. UV-vis absorption spectra of a treated HPHT-grown diamond. The sample contains several common defects of the $\text{N}_n\text{V}^{0/-}$ family, many of which are photochromic. The sample is shown in two extreme charge states (laser illuminated and heated), induced using the charge-transfer protocols described in section 3.4. The process is reversible and does not create or destroy defects. The 594 nm defect originates at a trigonal center observed in irradiated, nitrogen-doped samples.¹⁸⁰ Its atomic structure has yet to be determined, with the current suggestion that it may be a negatively charged divacancy.³⁴² Adapted with permission from ref 343. Copyright 2015 University of Warwick.

irradiation and subsequent annealing ($800\text{--}1600\ \text{°C}$) of type IaA diamond.³⁴⁶ In such material, H3 formation is attributed to the trapping of a vacancy at an A-center (nearest-neighbor nitrogen pair) through the route $\text{N}\text{--}\text{N}\text{--}\text{V} \rightarrow \text{N}\text{--}\text{V}\text{--}\text{N}$.³⁴⁷ As a result, the spatial locations of N_2V centers are correlated with the location of nitrogen pairs, leading to ZPL broadening³⁴⁸ and H3 luminescence quenching via resonant transfer to proximal A-centers.^{349,350} N_2V is also easily produced by irradiating and annealing HPHT-grown type Ib material (see section 3.5.4.5). The defect formation in this case is understood to be dominated by mobile NV centers moving as a unit via emission and recapture of the same vacancy.³³⁶ In turn, the NV center is captured at an N_s center, forming N_2V .^{351–353} The window of stability for N_2V production in type Ib material is, therefore, relatively narrow, beginning when the NV center becomes mobile at $\sim 1500\ \text{°C}$ and ending when

N_2V breaks up via the emission of a vacancy to form A-centers.³⁵² N_2V can also be created during HPHT synthesis. In this case, the defect is observed to be preferentially oriented on the $\{001\}$ growth surfaces, with only the two possible orientations (of six) whose principal axis are in the growth plane identified postsynthesis.^{354–356}

In natural diamond, H3 has been observed decorating platelets (interstitial aggregates frequently found in natural diamond) and dislocations,³⁵⁷ resulting in striations of H3 luminescence that follow the local dislocation direction (Figure 26).³⁵⁸ High-temperature annealing of brown natural dia-



Figure 26. Above-band gap fluorescence imaging shows dislocation networks decorated with H3 fluorescence (green) in a natural type Ib diamond. Reprinted with permission from ref 10. Copyright 2009 Mike Breeding and the Gemological Institute of America.

monds (whose color originates at dislocations introduced by plastic deformation³⁵⁹ and which constitute the largest population of natural diamonds by color³⁶⁰) can result in the generation of N_2V centers by the release of vacancies from slip planes.³⁶¹ Dislocations are frequently introduced to natural diamond during their violent transport to the surface, and their form and defect decoration play a crucial role in distinguishing natural and lab-grown diamond.³⁶²

H3 has attracted attention on account of its relatively short radiative lifetime ($\tau = 17.5\ \text{ns}$) combined with high fluorescence quantum yield under pulsed excitation.³⁵⁰ Thus, there are several reports of the observation of single, isolated N_2V^0 centers—making it a potential single-photon source.^{363–365} The optical properties of H3 are exploited in a proposal for an N_2V^0 quantum memory³⁶⁶ based around the previously mentioned triplet excited state,³⁴⁵ though leakage into these same states also limits the quantum yield of a continuous wave (CW) photon source.^{367,368} Nevertheless, H3

is unique among diamond color centers as being the only one to have been reported as a viable laser-gain color center.³⁶⁹

In contrast to H3, only the ground and one excited state have been identified for the N_2V^- (H2) defect. H2 possesses a distinctive LVM 167 meV from the ZPL, which is associated with the vibration of carbon atoms local to the defect.³⁴² The H2 and H3 bands were first linked via photochromic effects observed in optical absorption measurements,^{370–372} while subsequent uniaxial stress measurements showed that H2 and H3 possess the same symmetry.³⁴² The assignment of H2 to N_2V^- was not definitive, however, until the recent observation of EPR from the 2B_1 ground state that correlated with the strength of H2 absorption.³⁵³ These measurements demonstrated that the unpaired-electron spin density is mostly distributed between the two carbon atoms (and away from the lone pair on each nitrogen atom) and experiences only a weak dipolar interaction with the equivalent nitrogen atoms. Such behavior is now recognized as common to the ground states of all the N_nV (and N_nVH) defects and reflects the fact that the difference in valence between nitrogen and carbon means that it is energetically unfavorable for the unpaired electron spin to be localized on the nitrogen itself.

N_2V^0 is the stable charge state over a large range of Fermi levels (E_F), with N_2V^- stable only for moderately *n*-type (i.e., $E_F \sim (E_C - 2 \text{ eV})$) material.¹⁷⁰ The existence of N_2V^+ has been predicted,¹⁷⁰ but its observation would require, simultaneously, enough nitrogen to form nitrogen aggregates and enough acceptors to overwhelm any remaining substitutional nitrogen (donors).²¹

3.5.4.3. N_3V . Unlike NV and N_2V , only the neutral charge state of N_3V^0 has been identified experimentally, via both optical and EPR spectra that have been labeled N3 and P2, respectively. N3 shows a distinctive optical spectrum (Figure 27), with a ZPL at 415 nm (2.985 eV) observed in both

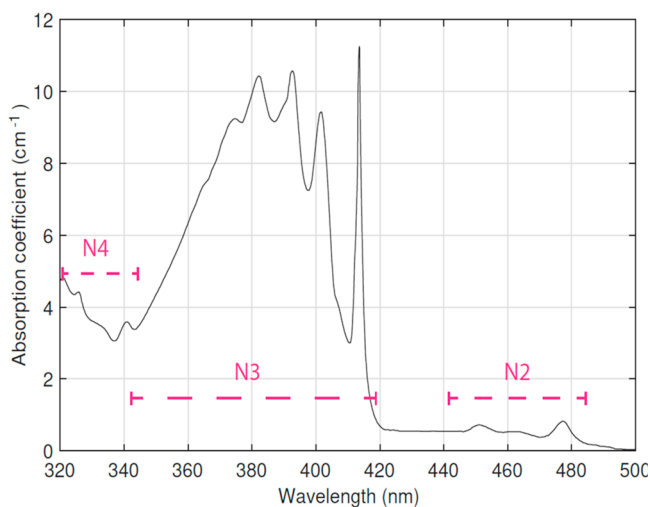


Figure 27. Typical absorption spectrum of a natural diamond containing strong N2–N4 features. Adapted with permission from ref 376. Copyright 2005 Gemological Institute of America.

absorption and emission. The N3 absorption is accompanied by weak bands to higher ($\sim 3.7 \text{ eV}$) and lower ($\sim 2.6 \text{ eV}$) energy labeled N4 and N2, respectively, as shown in Figure 27.³⁷³ The reported N3 fluorescence lifetime $\tau = 41 \text{ ns}$ at 80 K, but this value is specimen dependent and decreases with increasing concentrations of N_2^0 centers.³⁷⁴ The N3 center is

the most common color center encountered in natural diamond,^{172,375} to the extent that it is one of the primary markers employed in the identification of natural and synthetic diamond.³⁶² N3 contributes to the characteristic blue emission yielded by most natural diamonds under above-band gap excitation, in combination with so-called “Band A” emission from dislocation networks.^{357,362}

N_3V^0 retains the C_{3v} symmetry of NV, with the carbon and nitrogen elements nearest-neighbor to the vacancy interchanged (Figure 19). Thus, it shares the same one-electron group theoretical levels as NV, implying that, within the vacancy-cage model, there is only a single hole in the N_3V^0 charge state (i.e., $S = 1/2$) and that N_3V^- should be closed-shell and inactive to all but vibrational spectroscopy. Nevertheless, the seemingly simple N_3V defect has generated much discussion regarding its electronic structure and, in particular, the origin of the N2 absorption transition.^{374,377} This may have been resolved by recent thermochromism experiments, which indicate that the N2 and N3 transitions may not share a common origin despite their correlation across several orders of magnitude in strength and large numbers of samples.³⁷⁸

The atomic structure of N_3V^0 was determined via its ground-state EPR spectrum,^{379–381} which was subsequently correlated with the N3 absorption spectrum.³⁷⁸ The EPR spectrum of N_3V^0 (Figure 28) is complex, due to the similar magnitude of the hyperfine and quadrupole interactions with each of the three equivalent nitrogen atoms. Though the predicted structure based on the atomic model was not in doubt, it was not until $^{15}N_3V^0$ in ^{15}N -enriched synthetic diamond

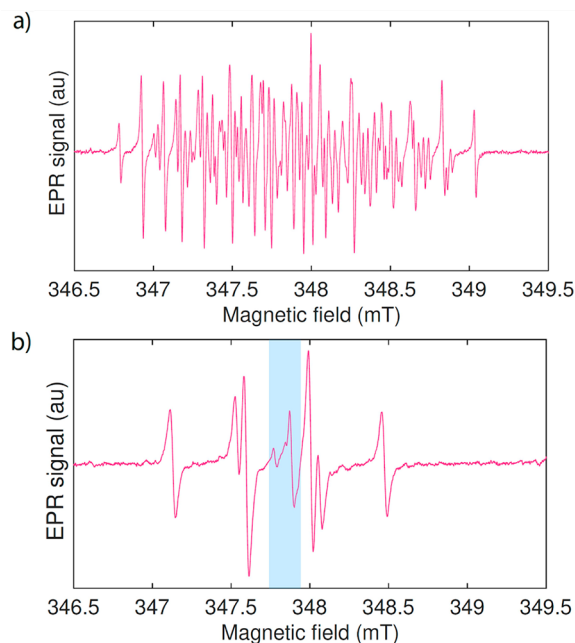
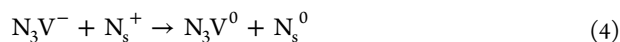


Figure 28. EPR spectra of the N_3V^0 center measured with the magnetic field parallel to the $\langle 001 \rangle$ direction in (a) natural abundance (essentially 100% ^{14}N) and (b) ^{15}N -enriched samples. The signal in the area shaded in blue arises from unrelated defects. The change from ^{14}N ($I = 1$) to ^{15}N ($I = 1/2$) removes the nuclear quadrupole interaction (arising from the inhomogeneity of charge within the nucleus itself) and greatly reduces the complexity of the N_3V^0 spectrum. Adapted with permission from ref 384. Copyright 2017 American Physical Society.

became available that the ground-state spin Hamiltonian parameters could be determined satisfactorily.³⁸²

There is limited (indirect) evidence suggesting the existence of N_3V^- . In particular, photochromism measurements of samples containing both N_s and N_3V defects show a simultaneous increase in the intensities of both N3 absorption and of IR absorption due to N_s^0 when the samples are illuminated with red/green light.^{382,383} This can be understood if the N_3V^- is acting as a donor via the process



and indicates a photoionization threshold for N_3V^- in the range 1.65–2.2 eV.³⁸² This is consistent with the results of DFT calculations, which suggest a value ~ 1.9 eV.³⁸⁴ It is also similar to the photoionization threshold of N_s^0 , implying that samples containing both N_s^0 and N_3V^- will be in metastable equilibrium when exposed to green light.³⁸⁴ The recent observation of simultaneous electronic and nuclear spin polarization of N_3V^0 and N_s^0 has been attributed to spin-selective relaxation in an excited triplet state of N_3V^- , with local N_s^0 spin polarized via the emission of a spin-polarized current from N_3V^- .³⁸⁴ The additional one-electron states required to generate a triplet state in N_3V^- are derived from the conduction band, rather than the one-electron states of the defect itself,³⁸⁴ though this is not corroborated by DFT calculations employing different functionals.²¹ In the latter work, the presence of N_3V^+ is also predicted, with an optical transition at ~ 0.6 eV.²¹ These results should serve to motivate further investigation of the structure and properties of N_3V^- .

3.5.4.4. N_4V . With lone pairs on each of the four nitrogen atoms, N_4V^0 is a closed-shell center. Thus, no optical or EPR transitions are anticipated. The addition or removal of charge from the defect increases its overall energy, so only the neutral charge state would be expected to be stable. Indeed, N_4V^0 (the B-center) is one of the dominant forms of nitrogen defect in natural (type Ia) diamond, revealed by its distinctive IR absorption in the one-phonon region (Figure 29). The B-center has been weakly correlated with the N9 optical absorption band at 5.26 eV.³⁸⁵ If this association proves correct, it would provide a measure of the photoionization energy of N_4V^0 .

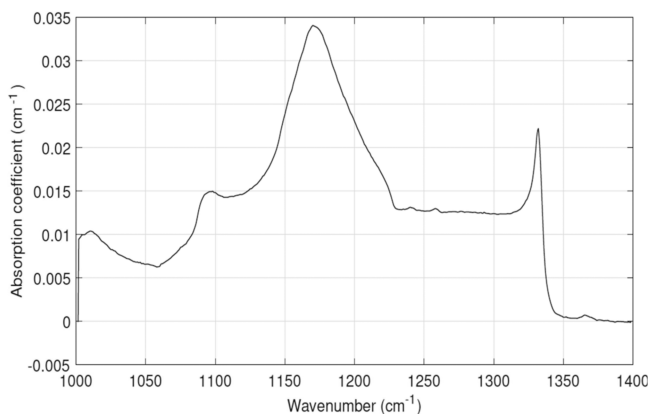


Figure 29. Infrared absorption spectrum of a natural diamond for which the one-phonon region is dominated by the contribution from B-centers. The spectrum shows a characteristic peak at 1170 cm^{-1} and a sharp pseudo-LVM at the lattice cutoff wavenumber (1332 cm^{-1}). Adapted with permission from ref 10. Copyright 2009 Gemological Institute of America.

Given the difficulties in identifying $S = 0$, luminescence-free centers, assignment of the B-center spectrum to N_4V^0 relies on a combination of DFT calculations²⁶⁸ and circumstantial evidence from annealing studies.^{275,344} Uniaxial stress studies struggle to produce resolvable splittings of the lattice-broadened, one-phonon continuum absorption.

Heat treatment of natural, brown IaB diamond can lead to near-colorless samples, whereas heat treating brown IaA or IaAB samples does not.^{386,387} The B-center is produced in nitrogen-doped diamond via heat treatment at high temperatures ($T_{\text{anneal}} > 2200$ °C) under stabilizing pressure.^{275,388} This is understood to occur via migration of NV to N_3V and subsequent emission of a vacancy center, $NV + N_3V \rightarrow N_4V + V$ (via an N_3V_2N intermediate, as discussed below).

Irradiation of type IaB diamond to introduce vacancies, followed by low-temperature ($T_{\text{anneal}} \sim 800$ °C) annealing to make them mobile, results in production of the related luminescence center, H4 (Figure 30), which emits at 496

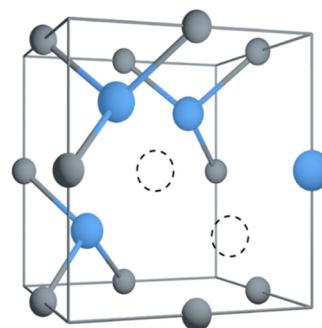


Figure 30. H4 defect structure.

nm.^{185,346,389} H4 is produced by capture of a vacancy at N_4V ^{352,389} and subsequent N–V exchange to place the two vacancies nearest-neighbor to each other, resulting in the atomic configuration $N_4V-V \rightarrow N_3V_2N$.³⁴⁵ The structure of H4 was determined through its optically accessible excited state:³⁴⁵ uniaxial stress measurements identified H4 as having the same C_{1h} symmetry as revealed by the EPR spectrum.¹⁸⁵ H4 itself is destroyed by annealing at 1600 °C.^{347,375} In passing, we note how, for both the A-center (N_2)^{185,276} and B-center (N_4V),³⁴⁵ the observation and identification of EPR spectra related to vacancy capture at the defect (i.e., H3/ N_2V^0 for the A-center and H4/ $N_3V_2N^0$ for the B-center) has been instrumental in advancing understanding of the precursor defect.

3.5.4.5. Production and Aggregation of the N_nV Family. In general, the aggregation of the N_nV family toward N_4V is driven by the reduction in Gibbs energy associated with reducing the number of dangling bonds.³⁵¹ The energy required for direct substitutional nitrogen–carbon exchange is high^{282,390} and the migration and aggregation of nitrogen is thus mediated by the diffusion of intrinsic and nitrogen-containing defect complexes. Irradiation of diamond with electrons, neutrons, or γ radiation results in lattice damage in the form of the self-interstitial C_i (visible in both optical absorption¹⁸⁸ and EPR³⁹¹) and vacancies (detected optically in the neutral state³⁹² and both optically³⁹³ and by EPR³⁹⁴ in the negative state); the $[V^0]:[V^-]$ ratio is defined by the relative concentrations of $[V]$ and the donor $[N_s]$. Interstitial production rates during irradiation are unaffected by the presence of N_s (within 10% experimental error).³⁹⁵ Histor-

ically, aggregation has been considered to be dominated by vacancy-driven processes, but more recent works have included contributions involving self-interstitials and nitrogen–carbon interstitials.³⁵¹ The narrative that follows is limited to cases where nitrogen is the dominant impurity.

3.5.4.5.1. Interstitial-Driven Processes. C_i atoms become mobile at temperatures of $\sim 300\text{--}400\text{ }^\circ\text{C}$.^{141,396} Strain fields introduced around the vacancy introduce an additional energy barrier (over and above the diffusion energy), which C_i must overcome to enable vacancy–interstitial recombination.³⁹⁷ Closely located, highly strained Frenkel pairs (close interstitial–vacancy pairs) will self-annihilate,³⁹⁸ while the remainder of the C_i centers diffuse to other traps. Interstitials trapped at N_s form N_i ^{279,284}



where the (+C) represents a carbon on its natural lattice site. The reverse process is unlikely due to the high binding energy of N_i .²⁸² The diamagnetic nature of N_i^- and the spectral overlap of N_s^0 and N_i^0 in EPR²⁸⁵ make it hard to quantify the concentration of these interstitials, $[N_i]$. The diffusion barrier of $N_i^{0/-}$ is calculated to be similar to, or lower than, that for C_i , allowing $N_i^{0/-}$ to migrate at similar temperatures—yielding N_{2i} via



Experimentally, N_{2i} is observed (via the H1a line at 1450 cm^{-1}) to anneal in at $\sim 650\text{ }^\circ\text{C}$ in irradiated type Ib material³⁹⁹—consistent with process 6. In irradiated type IaA diamond, N_{2i} centers are produced at $T_{\text{anneal}} \geq 300\text{ }^\circ\text{C}$,⁴⁰⁰ presumably via interstitial capture at A-centers^{59,109}



Therefore, the limiting step in the production of N_{2i} in type Ib and type IaA diamond is the diffusion barrier to N_i and C_i , respectively. N_{2i} is destroyed at $\sim 1400\text{--}1500\text{ }^\circ\text{C}$,^{232,401} by conversion to N_2 and emission of an interstitial³⁵¹



i.e., the reverse of reaction 7. In this manner, the original interstitial can be recycled, with the carbon interstitial effectively behaving as a catalyst in the aggregation from N_s to N_2 .

In the absence of irradiation damage, the interstitial population is negligible and the interconversion between defects is dominated by vacancy-related aggregation. Note, however, that the presence of transition metals from the growth solvent in HPHT-synthesized diamond is understood to provide another source of self-interstitials, even in the absence of irradiation,^{351,400} see section 3.6.

3.5.4.5.2. Vacancy-Driven Processes. Following irradiation, the first vacancy-related processes are observed at $T_{\text{anneal}} \sim 700\text{--}800\text{ }^\circ\text{C}$, when the vacancy becomes mobile.³¹³ These vacancies are trapped by whatever is the dominant form of nitrogen present, i.e.



in type Ib, type IaA, and type IaB diamond, respectively. All these complexes are stable until $\sim 1400\text{ }^\circ\text{C}$, where NV begins

to migrate. The energy required to completely break an NV defect (i.e., for the vacancy to escape Coulombic attraction and the nitrogen-induced strain field) is greater than that required for a sequence of local vacancy emission and retrapping steps, as illustrated in Figure 31. In this scenario, V first interchanges

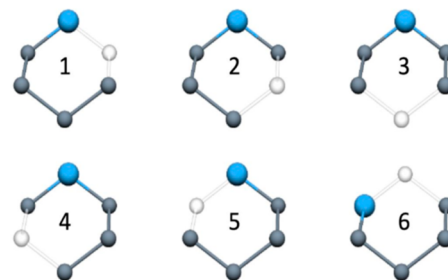


Figure 31. Motion of the vacancy associated with an NV defect through the lattice, resulting in net motion of the NV defect itself. At temperatures of $1500\text{--}1600\text{ }^\circ\text{C}$, the defect breaks up (2) but the vacancy is trapped by the strain field from the nitrogen. The vacancy locally migrates through the lattice, eventually approaching the nitrogen from the opposite side (5). By interchange of the nitrogen and the vacancy (6), the defect has translated through the lattice.

with a neighboring C, while the N atom becomes a substitutional defect. The next two steps move V progressively further from the N atom, from whence it could then return to a different site neighboring the N atom. To effect a diffusion jump, the N atom must swap places with one of the C atoms bordering the vacancy. This last step results in the net movement of the N atom from one atomic site to a neighboring site. Further migration events can occur repeatedly.³³⁶ Any remaining N_s defects will trap migrating NV to produce N_2V .



A-center formation by the breakup of N_2V defects ($N_2V \rightleftharpoons N_2 + V$) is observed experimentally at $\sim 1700\text{ }^\circ\text{C}$.^{8,275,375} The production of N_2 in irradiated type Ib material when annealed at $1500\text{ }^\circ\text{C}$ has traditionally been attributed to vacancy-enhanced aggregation through reuse of a vacancy (i.e., $NV + N_s \rightarrow N_2V \rightarrow N_2 + V$; $V + N_s \rightarrow NV$).³⁵² This process requires the dissociation of N_2V , transiently increasing the number of dangling bonds, and so should only become significant at $T_{\text{anneal}} \geq 1600\text{ }^\circ\text{C}$. Thus, current opinion favors low-temperature aggregation of N_2 being driven by interstitial migration, as discussed in section 3.5.4.5.1.

The precise production mechanisms for N_3V and N_4V are unclear. N_3V can be formed in type Ib and IaA material at $T_{\text{anneal}} \sim 1800\text{--}1900\text{ }^\circ\text{C}$,^{382,402} at which temperatures several formation routes can be envisaged, for example



Dissociation of N_2 at high temperature ($\sim 2000\text{ }^\circ\text{C}$)^{275,361,403} supplies a population of substitutional nitrogen during annealing. Vacancies may be emitted from interstitial aggregates (platelets),⁴⁰⁴ by the breakup of multivacancy clusters,⁴⁰⁵ or be continually emitted and retrapped by the creation and destruction of NV and N_2V defects.¹⁷⁷ Typically,

the concentrations of N_2V and N_3V at all points in the aggregation process are significantly lower than the final concentrations of N_2 and N_4V centers. This might imply that they are not significant contributors to the final N_2 and N_4V aggregation mechanisms or simply that they are relatively less stable under high-temperature ($T_{\text{anneal}} > 1800$ °C) annealing.

3.5.4.6. Summary. The specific route to producing any particular member of the N_nV family most efficiently can define the choice of starting material. Both the interstitial- and vacancy-mediated aggregation mechanisms are considered viable and could thus operate simultaneously, with the dominant mechanism for any given sample depending strongly on the relative concentrations of different impurities and intrinsic defects. Further care is also needed when targeting a particular final charge state. In the context of this section, which focuses on diamond samples wherein nitrogen is the dominant electrically active dopant, we require the presence of substitutional nitrogen to stabilize negative charge states of the N_nV defects (via $N_s^0 + X^0 \rightarrow N_s^+ + X^-$), but its absence is necessary to stabilize the corresponding neutral charge state. Table 2 presents a summary of the principal aggregation processes, in conjunction with their activation energies and experimental annealing behavior (if known).

3.5.5. N_nVH Family. Hydrogen is a common impurity in many types of diamond, with concentrations in excess of 1000

Table 2. List of Aggregation Processes, Their Activation Energies, E_a , and Experimental Annealing Behavior (Where Known)^a

process	possible mechanism	E_a (eV)	T_{anneal} (°C)
vacancy			
$N_s + V \rightarrow NV$	V migration	2.3 ³¹³	700
$N_2 + V \rightarrow N_2V$	V migration	2.3	700
$N_s + NV \rightarrow N_2V$	NV migration	4.9 ³³⁶	1400–1500
$NV \rightarrow N_s + V$	NV dissociation	5.8 ³³⁶	
$N_2V \rightarrow N_2 + V$	N_2V dissociation		1600–1700
$N_2V + NV \rightarrow N_3V + V$	NV migration	4.9	1400–1500
$N_2 + NV \rightarrow N_3V$	NV migration		
interstitial			
$N_s + C_i \rightarrow N_i + (C)$	C_i migration	1.6 ⁴⁰⁴	300–400 ³¹⁴
$N_s + N_i \rightarrow N_{2i}$	N_i migration	0.8–2.4 ²⁸²	650 ³⁹⁹
$N_{2i} + (C) \rightarrow N_2 + C_i$	N_{2i} dissociation	5.9 ³⁵¹	1400–1500 ^{269,280}
vacancy–interstitial			
$V + C_i \rightarrow (C)$	C_i migration	1.6	300–400
$NV + C_i \rightarrow N_s + (C)$	C_i migration	1.6	300–400
$N_2V + C_i \rightarrow N_2 + (C)$	C_i migration	1.6	300–400
$N_2 + C_i \rightarrow N_{2i} + (C)$	C_i migration	1.6	300–400
$N_i + V \rightarrow N_s$	V or N_i migration	1.6	650–700
$NV + N_i \rightarrow N_2$	N_i migration	1.6	650

Adapted from ref 343. Copyright 2015 University of Warwick, used with permission. ^aAggregation from N to N_2V is relatively well-understood in both the vacancy- and interstitial-dominated regimes, but the dominant formation routes to N_3V and N_4V remain under debate. E_a values (where given) refer to the process stated on the left. Note there may be an additional energy barrier to recombination of different reactants—for example, the strain barrier around the vacancy which requires additional energy above the interstitial migration energy to enable vacancy–interstitial recombination.³⁹⁷

ppm reported in natural diamonds,⁴⁰⁶ in the range 200–900 ppm for HPHT grown samples, but typically <50 ppm in CVD-grown single-crystal diamond.⁴⁰⁷ These relative values might appear surprising, given that H_2 is the dominant source gas used in the CVD process, but can be understood if the hydrogen is trapped at defects or inclusions in natural and HPHT samples (which do not exist in good quality SCD films). In this and the following section, we summarize current knowledge relating to the structure, properties, and inter-conversion of defects in diamond that contain both N and H.

3.5.5.1. NVH. The NVH defect (Figure 32a) was first identified in its negative charge state in untreated CVD-grown

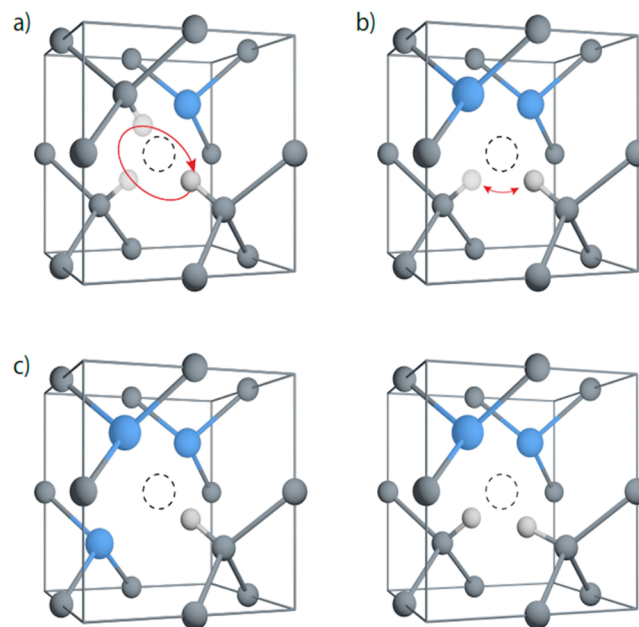


Figure 32. Structures of the (a) NVH, (b) N_2VH , (c) N_3VH , and (d) N_2VH_2 centers. The H atoms tunnel between the three equivalent carbon bonding sites in panel a and the two equivalent sites in panel b, giving the defects time-averaged (on EPR time scales) trigonal (C_{3v}) and rhombic (C_{2v}) symmetry, respectively.

single crystal diamond, via its ground state $S = 1/2$ EPR spectrum, which also identified interactions with a nitrogen and a hydrogen atom.⁴⁰⁸ This spectrum, and the hyperfine interactions, all imply C_{3v} symmetry, that is, the defect retains a $\langle 111 \rangle$ symmetry axis. Initially, it was hypothesized that the hydrogen was directly bonded to the N atom,⁴⁰⁸ but the lone pair on the nitrogen make this configuration chemically unfavorable.⁴⁰⁹ Statically bonding the hydrogen to one of the three nearest-neighbor carbon atoms results in a defect with C_{1h} symmetry, in contradiction to the experimental data.⁴⁰⁸ This problem was solved by identifying the hydrogen as being dynamically bonded, with the hydrogen atom tunnelling between the three equivalent carbon bonding sites, resulting in a time-averaged C_{3v} axial symmetry.^{410,411} Further experiments using cryogenic multifrequency EPR failed to measure a static C_{1h} spectrum, though transition-dependent line width broadening was observed, strengthening the case for the dynamic model and yielding an estimated tunnelling rate of order 10^8 s⁻¹.⁴¹²

The concentration of NVH⁻ ($[NVH^-]$, as measured by EPR) has been shown to correlate with a broad visible absorption band at 520 nm^{231,413,414} and with a sharp IR

absorption feature at 3123 cm^{-1} ⁴¹⁵ that is commonly observed in CVD diamond grown with moderate nitrogen in the source-gas mixture.^{416,417} Subsequent photochromism measurements demonstrated anticorrelation between $[\text{NVH}^-]$ and the intensity of the 3123 cm^{-1} feature,^{413,415} allowing the latter to be assigned to NVH^0 .^{245,414} The IR transition wavenumber is invariant under nitrogen isotope substitution⁴¹⁷ and is thus assigned to a C–H stretch mode within the defect—an assignment supported by DFT calculations.¹⁹⁴ Uniaxial stress measurements of the 3123 cm^{-1} transition imply a defect with C_{1h} symmetry, however, rather than the C_{3v} symmetry observed for the NVH^- center in EPR.⁴¹⁵ This apparent paradox is resolved by recognizing that the tunnelling rate of the hydrogen atom must be faster than the standard EPR time scale ($\sim 50\text{ GHz}$), in which the time-averaged C_{3v} symmetry is observed, but slower than the optical time scale ($\sim 100\text{ THz}$), which yields the static C_{1h} symmetry. The NVH^0 concentration $[\text{NVH}^0]$ can be derived from the integrated intensity or height of the 3123 cm^{-1} feature.

NVH is a common defect in CVD-grown diamond, where it can comprise up to 10% of the total identified nitrogen content.¹⁰¹ As with NV , preferential orientation of native NVH defects has been measured for CVD growth on (110) surfaces,¹⁰¹ but it is not yet clear if the NVH grows as a unit or as NV , which subsequently traps hydrogen. Either way, the presence of the hydrogen results in much shorter spin lifetimes; NVH defects are thus unlikely to prove useful in spin-based quantum communications or quantum computing applications.

NVH is formed in hydrogen-containing, nitrogen-doped material when subjected to $T_{\text{anneal}} \geq 800\text{ }^\circ\text{C}$. Under these conditions, the vacancies are thought to trap hydrogen and move as a VH unit,²¹ before being trapped at a substitutional nitrogen to form NVH . NVH appears to be more stable than NV itself, as it anneals at a higher temperature ($\sim 1800\text{ }^\circ\text{C}$,⁴¹³ cf., $1500\text{--}1600\text{ }^\circ\text{C}$ for NV).

3.5.5.2. N_2VH . N_2VH^0 was recently identified by EPR in moderately nitrogen-doped ($[\text{N}_s] = 3\text{--}15\text{ ppm}$) CVD-grown samples.⁴¹⁸ The defect has an $S = 1/2$ ground state and, as with NVH (section 3.5.5.1), the hydrogen atom is found to reorientate between the equivalent carbon bonding locations at a rate that is fast compared to the EPR time scale, leading to a time-averaged rhombic C_{2v} symmetry (Figure 32b), as opposed to the static C_{1h} symmetry.^{419,420} Nitrogen isotopic substitution confirms the presence of nitrogen in the defect.

Table 3 collects together the hyperfine parameters, percent unpaired-spin density localized on each N atom, and the

Table 3. Comparison of the Hyperfine Parameters (A /MHz), Percent Unpaired-Spin Density Localized on Each Nitrogen Atom, and Principal Quadrupole Parameter (P_{\parallel} /MHz) for the EPR-Measured N_nV and N_nVH Defects^a

	A_1	A_2	A_3	% localized on each N	P_{\parallel}	ref
NV^-	-2.70		-2.14	<1	-5.0	422
NVH^-	-2.36		-2.09	0	-4.8	408
N_2V^-	-2.92	-3.22	-2.47	1	-5.0	353
N_2VH^0	+3.91	+4.24	+6.51	2	-4.6	418
N_3V^0	+7.45		+11.30	<i>b</i>	-4.7	382

^aFor defects that possess axial symmetry, $A_1 = A_2$ by symmetry. ^bFor N_3V , the similar magnitude of the anisotropic hyperfine and dipolar interactions make localization estimates inaccurate.⁴²³

principal quadrupole parameter for the various EPR-measured N_nV and N_nVH defects. Like other N_nV and N_nVH defects, N_2VH is photochromic.⁴¹⁸ Calculations suggest the other stable charge state in n -type material is N_2VH^- ,⁴²⁰ which is predicted to be both $S = 0$ and optically inert.²¹ Two IR bend-mode absorption peaks at 1375 and 1378 cm^{-1} , which have previously been observed in irradiated and annealed pink CVD diamond,⁴²¹ correlate in intensity with N_2VH^0 , and their assignment to N_2VH^0 is supported by DFT calculations.^{21,419} If correct, the integrated intensity of the 1378 cm^{-1} transition can be used to provide a measure of the N_2VH^0 concentration, $[\text{N}_2\text{VH}^0]$.⁴¹⁸ N_2VH^0 is also produced in nitrogen- and hydrogen-containing samples by HPHT annealing at $T_{\text{anneal}} \geq 1800\text{ }^\circ\text{C}$. By analogy with the N_nV family, its destruction at achievable temperatures is expected to occur by capture of additional defects, rather than by thermal breakup of the defect itself.²¹

3.5.5.3. N_3VH . N_3VH is considered the terminus of the N_nVH family, as all bonds into the vacancy are saturated. The formation energy of N_4VH is extremely high, making its formation unlikely.²¹ As with N_4V , only the neutral form of N_3VH is considered stable, irrespective of the pseudo-Fermi level. IR absorption features at 1405 and 3107 cm^{-1} (corresponding to bend and stretch modes, respectively) have recently been assigned to N_3VH^0 through a mixture of DFT^{194,424} and uniaxial stress studies.^{269,415} The defect possesses C_{3v} symmetry, with the hydrogen bonded to the sole carbon (Figure 32c) and has $S = 0$ in the stable, neutral form.

The 3107 cm^{-1} peak is often prominent in the IR spectra of type Ia natural diamond,^{192,421,425–427} and its intensity may exceed the intrinsic diamond multiphonon absorption in so-called “hydrogen-rich” diamond.⁴²⁸ The 3107 cm^{-1} peak shifts to 3098 cm^{-1} in ^{13}C -enriched samples, and shows no shift under nitrogen isotopic enrichment.^{192,193} N_3VH^0 concentrations in natural diamond have been estimated by assuming that the 3107 cm^{-1} peak has an oscillator strength similar to that reported for the 3123 cm^{-1} C–H stretch mode in NVH^0 (see section 3.5.5.1). On that basis, the observation of 3107 cm^{-1} peak absorption coefficients as large as 30 cm^{-1} in many natural samples⁴²⁹ implies N_3VH^0 concentrations $>20\text{ ppm}$, that is, that the N_3VH^0 defect accounts for a significant proportion of the total measured nitrogen in these samples.

The 3107 cm^{-1} absorption feature is observed in hydrogen- and nitrogen-containing CVD diamond samples postannealing at $T_{\text{anneal}} \geq 1800\text{ }^\circ\text{C}$,⁴⁰¹ with a relative intensity that increases up to $2300\text{ }^\circ\text{C}$.^{269,430} A weak 3107 cm^{-1} absorption (corresponding to approximately 2 ppm of N_3VH^0) has also been observed after annealing HPHT-grown samples (containing $>200\text{ ppm}$ nitrogen) at $T_{\text{anneal}} \geq 2100\text{ }^\circ\text{C}$.¹⁹³ No hydrogen-related absorption was identified in these HPHT samples before the high-temperature anneal, so the hydrogen must be incorporated in an (as yet) unidentified form. It is likely that N_3VH production in CVD-grown samples is typically nitrogen-limited, whereas, in HPHT samples, the production of this defect is more likely to be hydrogen-limited. The same annealing conditions can destroy the 3107 cm^{-1} absorption feature in some natural diamonds, suggesting that it can interact with other defects in the crystal at these temperatures.⁴³¹

3.5.5.4. Production and Aggregation of the N_nVH Family. The annealing behavior of CVD diamond samples containing high levels of both nitrogen and hydrogen does not follow the

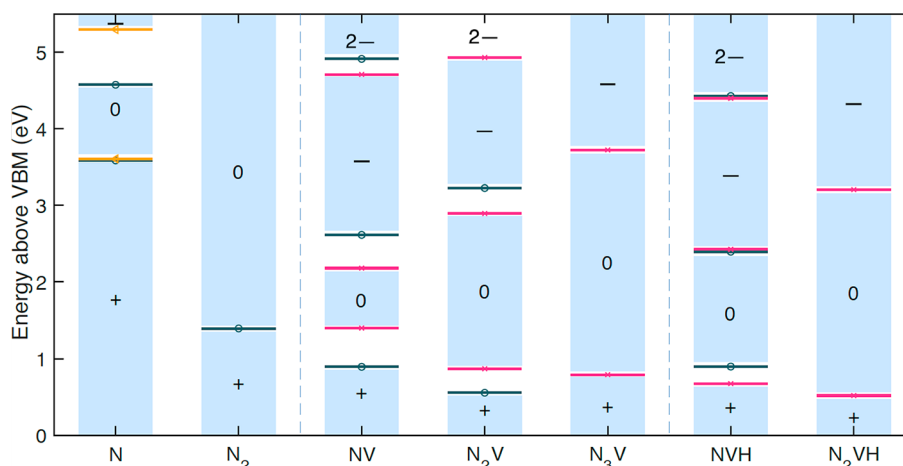


Figure 33. Theoretical charge transition levels for various N_nV and N_nVH complexes: in each region, the dominant charge state at a given chemical potential (pseudo-Fermi) level (referenced to the valence band maximum (VBM)) is given—regions where all available sources agree are shaded in blue. Energy levels shown in green, red, and orange are taken from refs 21, 170, and 436, respectively, and have been scaled to correct for the band gap error in these works. N_4V and N_3VH have been omitted as they are both predicted to be stable only in the neutral charge state. The dominant substitutional dopants in diamond are nitrogen (n -type, $E_F \sim (E_C - 1.7 \text{ eV})$) and boron (p -type, $E_F \sim (E_V + 0.37 \text{ eV})$).

accepted nitrogen-aggregation route described in §3.5.4.5, as the presence of hydrogen within the N_nVH defects significantly modifies their binding energies, and thus the temperatures at which different defects become mobile. In general, aggregation within the N_nV family is driven by decreasing the number of dangling bonds into the vacancy.³⁵¹ This holds true for N_nVH also: the addition of, first, hydrogen and then nitrogen increases the thermodynamic stability of the defect,²¹ but the current understanding of N_nVH aggregation is significantly less advanced than for the N_nV family. Below, we summarize the current state of knowledge.

NVH is introduced during CVD growth of nitrogen-doped diamond,¹⁰¹ with reported $[NVH]:[N_s]$ concentration ratios in the range from $\sim 1:15$ to $1:5$.⁴¹³ As noted previously (section 3.5.5.1), NVH can also be grown-in preferentially oriented but, unlike NV, the presence of the hydrogen results in much shorter spin lifetimes. NVH defects are thus unlikely to prove useful in spin-based quantum communications or quantum computing applications. Typically, the higher the nitrogen concentration, the higher the charge trap density and the lower the observed $[N_s^0]:[N_s^+]$. This material is typically brown in color, which seems to originate at dislocations,^{413,432} which in conjunction with typically high concentrations of vacancy-clusters in this material,^{246,359} provide a source of vacancies for aggregation, even in the absence of irradiation.

NVH is thermodynamically more stable than NV and anneals out at $T_{\text{anneal}} \sim 1600\text{--}1800 \text{ }^\circ\text{C}$ (cf., $\sim 1500 \text{ }^\circ\text{C}$ for the NV defect).⁴¹⁵ N_2VH^0 was observed at low concentrations in an annealing study of a CVD-grown diamond (with initial $[N_s] = 3.6 \text{ ppm}$) following a 4-h anneal at $T_{\text{anneal}} = 1800 \text{ }^\circ\text{C}$.⁴¹⁸ The N_2VH^0 concentration was seen to increase further after treatment at $T_{\text{anneal}} = 2000 \text{ }^\circ\text{C}$, but showed no further detectable change after treatment at $T_{\text{anneal}} = 2200 \text{ }^\circ\text{C}$. Annealing at $1800 \text{ }^\circ\text{C}$ completely removed all signal associated with $NVH^{0/+}$. Thus, the observation that $[N_2VH^0]$ increased further after annealing at $2000 \text{ }^\circ\text{C}$ suggests the presence of an intermediate step in the annealing process between NVH and N_2VH . This might be mediated by VH, which is predicted to diffuse as a unit before dissociating,⁴¹⁹ or by interstitial hydrogen.^{433,434} Critically, no infrared absorption from N_2 or N_4V defects was observed at any stage, despite the production of N_3VH^0 after annealing at

$\geq 1800 \text{ }^\circ\text{C}$. This is at odds with the annealing behavior of N_nV , where a significant concentration of N_2 would be expected in any type Ib diamond that had been annealed to produce N_3V .

N_3VH is common in natural diamond, whereas NVH and N_2VH have not been reported.⁴³⁵ It seems likely that this reflects aggregation toward N_3VH over geological time scales. But, in summary, the aggregation mechanisms and kinetics of high-nitrogen, high-hydrogen containing diamond clearly require further study. Such studies are particularly important given the production of nitrogen-doped CVD diamond for magnetometry applications—discussed in section 4.

3.5.6. N_nVH_m Family. Figure 32d shows an example of the multihydrogen N_nVH_m group, where $n + m = 3$ or 4 and $n \geq 1$. Multi-hydrogen-containing point defects in diamond have thus far evaded detection, but where there is a radical remaining in the N_nV family, there is potential for it to be saturated with a hydrogen, as illustrated above with the N_nVH group of defects. Similar arguments might be expected to apply in the case of radical forms of N_nVH defects.

Defects in the first and second rows of Table 1 have been discussed above. The following three rows contain more than one hydrogen. The defects highlighted in orange are viewed as being fully saturated. These would be neutral defects, so have $S = 0$ and are thus undetectable in EPR. They support no allowed optical transitions but might be detectable by IR absorption—the necessary stretch and bend wavenumbers have been predicted and are tabulated in ref 21.

The only remaining defect in this family is NVH_2 . The ground state of the neutral defect would have $S = 1/2$, but the negatively and positively charged versions of the defect will both have $S = 0$ ground states. Thus, the neutral NVH_2 defect should be EPR active, and all charge states of the NVH_2 defect should also be IR active. The simplest explanation for the nondetection of such multiple-hydrogen-containing defects is that they are not present. Given the range of other nitrogen-containing defects discussed above, however, this might be surprising. Alternatively, the concentrations of these defects might be below current detection limits if, for example, they are transient species. Or, the hydrogen concentration might be insufficient to create the defects or the hydrogen may not be

accessible to aggregate further if it is already held in a deeper trap, like N_3VH , for example.

Future searches for N_nVH_m defects with $m > 1$ might usefully employ samples prepared with lower N:H contents—thereby, potentially, favoring aggregation to multiple-hydrogen-containing (rather than multiple-nitrogen-containing) defects. There is also a possibility that annealing at lower temperature for longer times might encourage formation of multiple-hydrogen-containing defects. Hydrogen implantation would result in hydrogen incorporation after growth, which might be another way of altering the aggregation process. Boron acts as an acceptor in B-doped diamond and, therefore, creates positively charged defects, which might be a route to creating a more mobile H^+ species that could aggregate more easily. But boron could also trap hydrogen, or unintended complexes containing boron, nitrogen, and hydrogen may be formed. Furthermore, were NVH_2 defects to be formed in this way, they might well be in their positive-charge state and thus, again, only amenable to IR detection.

3.6. Selected Aggregates Involving Nitrogen and Another Element

There is a ceaseless drive in commercial HPHT synthesis toward greater process efficiency, seeking to reduce the temperature and pressure required for growth (and thus the price) of commercially viable diamonds.¹⁹ The addition of the metal catalyst (section 2.1) enables growth at lower temperatures and the formation of larger single crystal diamonds. The catalyst/solvent of choice is usually a transition metal, either as the element or as an alloy, such as Fe–Ni–C or Fe–Co–C. Thus, metallic flux (a tell-tale sign of HPHT growth) and point defects associated with material in the melt can be incorporated into HPHT diamond. Both Ni and Co are incorporated into $\{111\}$ but not $\{100\}$ or minor growth sectors.⁴⁰⁰ This introduces a new family of aggregates that contain both transition metals and nitrogen, many of which have now been identified by applying EPR spectroscopy to HPHT material grown with known transition-metal catalysts and annealed to facilitate nitrogen aggregation. Defects identified by EPR have in some cases been correlated with optical signatures.^{214,437–439} Transition-metal–nitrogen aggregates are also occasionally found in natural diamond but at much lower concentrations than found in lab-grown diamond.⁴⁴⁰

Ni-related defects have attracted particular interest as a potential rival to NV centers as a single-photon source⁴⁴¹ and in vivo biomarker/thermometry^{442,443} applications, though more recent measurements indicate their optical properties are less favorable than the group-IV-vacancy defects (see below).⁴⁴⁴ Ni is readily incorporated substitutionally during HPHT growth.⁴⁴⁵ Co is much less readily incorporated, and there is no clear evidence for incorporation of Fe into the diamond lattice. This might seem surprising, given the relative atomic sizes: silicon, for example, with a smaller atomic radius, is incorporated in diamond in a split-vacancy structure.⁴⁴⁶ It can be understood, however, by recognizing the tetrahedral crystal-field stabilization of the 3d-orbitals into e and t_2 states. In the case of Ni_s , for example, four electrons participate in bonding with the surrounding carbons leaving a $3d^6$ (i.e., $e^4t_2^2$) configuration on the Ni_s center. The Ni–C bond lengths are 2.04 Å, which is not atypical of a metal–ligand bond but highly strained relative to the surrounding diamond construct.⁴³⁸ This substitutional defect is incorporated in the negative charge

state because of the presence of nitrogen acting as a donor making it $S = 3/2$.⁴⁴⁷

This structure is highly strained, however, and can be removed by annealing at $T_{\text{anneal}} \sim 1400\text{--}1500$ °C).^{438,448} In the case of Ni_s , it is thought that a carbon interstitial is created thermally, local to the nickel, and the substitutional defect relaxes into the vacancy, yielding a NiV defect (Figure 34a)

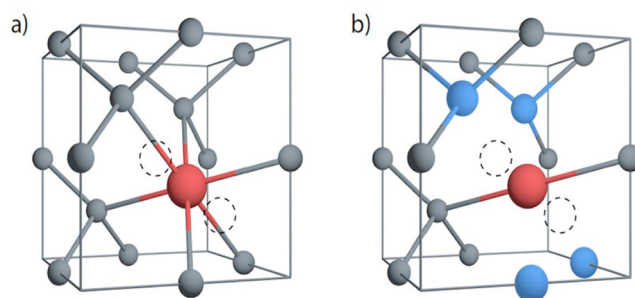


Figure 34. (a) NiV defect—the Ni adopts an interstitial position in the center of the split-vacancy. (b) The NE8 defect— $NiVN_4$, where the nickel adopts a similar location.

with lower elastic strain. Note that the V in this descriptor can also be found described in the literature as a split-vacancy, double semivacancy, semivacancy pair, or confusingly termed a divacancy. The NiV defect is labeled NE4/AB1 in EPR when in the negative charge state^{449–453} and NE4* when neutral,⁴⁵⁴ the Ni has the electronic configuration $3d^5$ and is $S = 1/2$.⁴⁴⁰ The symmetry was determined to be D_{3d} , with the Ni atom surrounded by six carbons arranged in a distorted octahedral arrangement with Ni–C bond lengths ~ 1.8 Å.^{440,455} At temperatures where Ni_s converts to NiV with emission of a carbon interstitial, the interstitial is highly mobile. It is trapped by N_s^0 , converting this to the mobile N_i , which itself is trapped releasing the carbon interstitial so that the process can be repeated (see section 3.5.4.5.1). The diffusion of nitrogen is thus greatly enhanced. The NiV defect is a relatively stable trap of nitrogen and defects have been identified where 2, 3, and 4 of the 6 nearest-neighbor carbon atoms have been replaced with N atoms. This leads to a suite of defects identified using EPR (Table 4, where the “NE” prefix stands for “nickel exhibition”), and in some cases linked with specific optical signals. Figure 34b illustrates the structure of the $NiVN_4$ (NE8) defect.

Of those $NiVN_n$ aggregates listed in Table 4, NE8 has attracted most interest as it has the potential to be used in quantum information processing^{444,461} and biological applications.⁴⁴² The NE8 defect is correlated with a strong luminescence peak in the near IR at 793.6 nm, where commercial low-loss fiber optics are available to enable long-range quantum communication.⁴⁶² This defect also has a higher intensity and narrower bandwidth than rival NV defects, and a shorter lifetime of 3 ns.^{444,462} Although there have been reports of the NE8 defects being grown into CVD diamond, these results should be treated with some caution as it is difficult to envisage how such a complex defect could be formed during growth.^{462–465} Attempts at co-implantation have failed.⁴⁶⁶ Despite its photophysical advantages, however, the recent literature suggests a shift back to NV as the favored quantum defect because of its ease of production and controlled formation or to other group-IV-vacancy defects, such as SiV,²⁹² GeV,⁴⁶⁷ and SnV.⁴⁶⁸

Table 4. Summary of Nickel-Vacancy-Nitrogen Aggregates

EPR label	defect	spin, S	symmetry	optical	T_{anneal} (°C)
NE1 ⁴⁵⁶	NiVN ₂ ⁻	1/2	C_s , C_{2h}	S3 optical ⁴⁵⁷	
NE2 ⁴⁵⁶	NiVN ₃ ⁰	1/2	C_1	S2 optical ^{457,458}	1950
NE3 ⁴⁵⁶	NiVN ₃ ⁰	1/2	C_s	S2 optical ⁴⁵⁷	1950
NE4 ^{449–453}	NiV ⁻	1/2	D_{3d}	1.72 eV (721 nm)	1550
NE4* ⁴⁵⁴	NiV ⁰	1	C_{2h}	1.83 eV (678 nm)	
NE5 ⁴⁵⁶	NiVN ₂ ⁻	1/2	C_s , C_{2h}		1850
NE6 ⁴⁴⁸		1/2	C_2		
NE7 ^{438,448}	NiVN ₂ ²⁻	1/2	C_s		
NE8 ⁴⁵⁶	NiV ₂ N ₄ ⁺	1/2	C_{2h}	1.56 eV (793.6 nm) ⁴⁵⁹	2050
NE9 ⁴⁵⁶	NiVN ₃ ⁰	1/2	C_{3v}		2050
AB5 ⁴⁵²	Ni _s ²⁻ N _s ⁺	1	C_{3v}		
ME1 ⁴⁶⁰	Ni _s ⁻ + N _s ^{+α}	3/2	cubic		

^aDefect speculated to involve Ni_s⁻ with N_s⁺ in a fourth-nearest-neighbor position, found in rare blue Argyle diamonds that are often highly strained.

More generally, the presence of nickel changes the nitrogen aggregation process (Table 2) and also catalyzes nitrogen diffusion by enhancing the Coulombic attraction between the defects⁴⁶⁹ and the release of interstitials and vacancies.^{400,469,470} In line with earlier studies,⁴⁰⁰ the aggregation of C- to A-centers is greatly enhanced by the presence of Ni defects. As seen in Table 4, at subsequent higher annealing temperatures more nitrogen saturates the split-vacancy surrounding the Ni.

Other transition metals can also be incorporated in diamond but generally to a lesser degree and less aggregated with nitrogen. CoVN-related centers are found in HPHT-grown samples but at much lower concentrations than their Ni counterparts;⁴⁷¹ it is generally accepted that Ni is incorporated more easily due to its size.⁴⁷² A defect comprising a substitutional pair of Co and N, analogous to N₂, has been associated with a 2.367 eV ZPL, and a CoVN defect, analogous to NiVN, is thought to be the O4 defect found in EPR^{473,474} (although O4 has also been assigned to the Co–N substitutional pair⁴⁷⁵). Two other EPR centers labeled NLO2 and NWO1 have no direct evidence of nitrogen, but are thought to be CoV defects with varying numbers of proximal nitrogens in different positions.⁴⁵⁶ Optical analogues of these defects and Co–N-related peaks have been investigated in ref 471. On annealing at $T_{\text{anneal}} > 2050$ °C, all three of these Co-related EPR centers are removed; it is speculated that this is due to capture of an additional N to form a diamagnetic defect that is EPR inactive.⁴⁵⁶ Co is also thought to have a lesser impact on the aggregation processes when compared to Ni.⁴⁷⁶

Titanium is added as a nitrogen getter in the HPHT production of colorless stones (low nitrogen) but may also be incorporated into diamond because Ti is carbide-forming.⁴⁷⁷ It has recently been suggested that two paramagnetic defects occasionally observed in natural type Ib diamond could incorporate both N and Ti.⁴⁷⁸ Further, it is postulated that a TiVN defect (analogous to the NiVN defect, see Figure 34a) could be produced by HPHT annealing of Ti-containing diamonds.⁴⁷⁹ It has also been speculated that the NU1/485 nm defect is a $\langle 100 \rangle$ Ti–N split interstitial.⁴⁷⁸

Along with Co and Ni, iron is commonly used as a solvent/catalyst during HPHT growth. The natural abundance of Fe is also considerably higher than that of Ni and Co, but Fe has been calculated to be unstable in diamond,⁴⁷² and no FeN point defects have been successfully identified. It is perhaps also surprising that FeVN centers analogous to those identified for Co and Ni have not been detected in diamond, given the common usage of Fe in HTHP synthesis. Iron nitride inclusions have, however, been found in HPHT diamonds grown with Fe₉₀Ni₁₀ and NaN₃.⁴⁸⁰

Of the remaining first-row transition metals there have been attempts to incorporate chromium,^{481,482} copper,⁴⁸³ and zinc⁴⁸² via ion implantation but no corresponding N aggregates have been identified. There is, however, a possibility for them to form if further HPHT annealing were to be used to drive aggregation.

During CVD growth, there is potential for Si to be incorporated into the diamond, either unintentionally via contamination from the quartz optical windows on the reactor (Figure 7) or by intentionally doping by adding a trace of SiH₄ to the process gas mixture.⁴⁸⁴ Si can also be incorporated during HPHT growth and with ion implantation. The SiV⁰ defect identified in EPR and confirmed with theory can also act as a trap for nitrogen, and the SiVN defect is believed to have been identified.⁴⁸⁵

Speculations have also appeared concerning nitrogen–phosphorus aggregates, which are not based around a vacancy but rather resemble substitutional pairs of nitrogen and phosphorus atoms. After 10 min annealing at 2350 °C, the initial group of defects (labeled NP1–NP3) disappear and are succeeded by NP4–NP6. The latter group are proposed to involve a P atom in a vacancy structure analogous to NiV, with N in varying coordination spheres.²¹⁴

4. APPLICATIONS OF NITROGEN-CONTAINING DIAMOND

4.1. Incorporation of Nitrogen in Natural Diamond: Applications in Geophysics and Geochemistry

As noted in section 1, geochemical studies on mineral inclusions in diamonds have fundamentally shaped our understanding of where natural diamonds come from and the geological history of our planet.⁴⁸⁶ The chemical composition of inclusions provides information about diamond formation, mantle storage and distribution. The early studies of inclusions in diamonds led to two important discoveries—first, that diamonds form long before the kimberlite (or lamproite) in which they are transported to the near surface and, second, that minerals included in diamonds can be related to rock types that are characteristic of depths 150–200 km underlying ancient cratons (old and stable parts of the continental lithosphere, which comprises the Earth's two topmost layers, the crust and the uppermost mantle (recall Figure 1)).^{487–489}

The state of nitrogen aggregation in natural diamond depends on nitrogen concentration, mantle residence time and mantle temperature. Under the temperature conditions prevailing in the Earth's mantle, aggregation of nitrogen from single substitutional atoms to pairs (A-centers, see Figure 3) typically happens very quickly, but aggregation from the A-center to the B-center occurs at a much slower rate.⁴⁹⁰ Rare natural type Ib diamonds have not experienced temperatures above ~850 °C for any extended geological period, suggesting that after formation they were rapidly transported to shallower

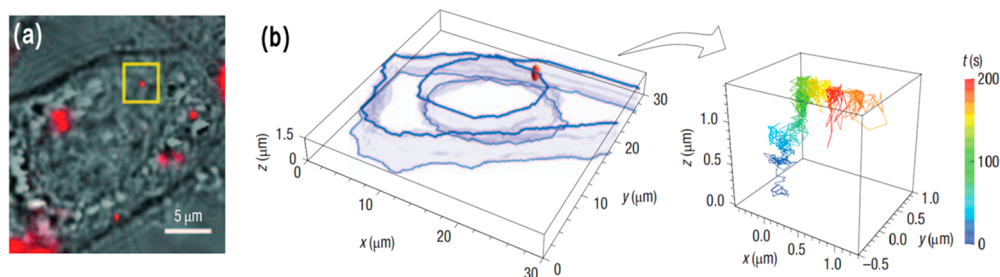


Figure 35. (a) Combined bright-field and epifluorescence images of nanodiamonds in a live HeLa cell. The yellow box identifies a single 35 nm ND that is tracked. (b) A reconstruction of the cell (left) and 3-dimensional tracking of the selected ND over a period of 200 s (right). Reprinted with permission from ref 514. Copyright 2008 Nature Publishing Group.

and cooler depths.⁴⁹¹ The very high sensitivity to temperature and relatively weak dependence on residence time makes nitrogen A- to B-center aggregation a useful geo-thermometer but a very poor geo-chronometer.

Radiogenic dating of inclusions trapped during growth gives a much more reliable measure of the age of natural diamonds (most have ages between 90 million and 3.5 billion years),^{492–494} so the aggregation state can be used to determine the mantle residence temperature experienced by the diamond.⁴⁹⁰ It is important to note that the temperature determined by nitrogen aggregation is not simply an average over the period of residence; a short period of elevated temperature will have had a disproportionately large effect on nitrogen aggregation. Spatially resolved mapping of nitrogen incorporation and aggregation provides valuable information on the history of diamond growth events and the residence time in the mantle.^{427,495}

In geochemistry, the ratio $\delta^{13}\text{C} = \left\{ \left(\frac{^{13}\text{C}/^{12}\text{C}}{^{13}\text{C}/^{12}\text{C}} \right)_{\text{sample}} / \left(\frac{^{13}\text{C}/^{12}\text{C}}{^{13}\text{C}/^{12}\text{C}} \right)_{\text{ref}} - 1 \right\} \times 1000\text{‰}$ is used to infer the origin of the carbon. Worldwide natural diamonds have a carbon isotopic composition $\delta^{13}\text{C}$ ranging from -41 to $+5.0\text{‰}$ ^{496,497} with $\sim 72\%$ contained in the narrow interval between -8 and -2‰ , which is within the range of mantle values. $\delta^{15}\text{N}$ values for nitrogen in diamond spread over a large range, from -40 to $+18\text{‰}$, and with other data have been used to develop an understanding of the mechanisms of natural diamond formation.⁴⁹⁷

4.2. Nitrogen Defects and the Identification of Diamond Gemstones

Given the value of natural diamond gem stones an arsenal of diamond verification instruments have been developed to separate or to identify natural diamonds from lab-grown diamonds and simulants. The *Diamond Producers Association* has developed a protocol to test the performance of diamond verification instruments in a consistent manner.⁴⁹⁸ Although such instruments operate in a variety of different ways, most use one or more spectroscopic techniques to identify the nature of the gem under test. For example, the *Diamond-Sure*^{361,415} instrument (produced by *De Beers Technologies*) interrogates the optical absorption of the sample, looking for the presence or absence of different defects, including the N_3V^0 (N_3) defect observed in 98% of natural diamonds. Other instruments make use of photoluminescence or photoluminescence imaging. Again, it is often the presence, absence, or relative concentrations of different nitrogen related defects in the diamond that are used to determine whether the stone is natural, treated (e.g., HPHT annealed to remove unwanted defects that affect the color, or irradiated and annealed to introduce defects that give the diamond a desirable color, etc.)

or lab-grown. Usually it is the combinations of nitrogen defects present that are used to determine the origin (natural/lab-grown) and treatment history of the diamond, but the presence/absence of other defects (notably those incorporating transition metals, silicon, and hydrogen) also provides very useful information.

4.3. Applications of Nitrogen-Doped Nanodiamonds

As shown in section 2.3.2, there is a confusing array of nanodiamonds available, produced by a variety of methods.¹⁴⁰ Strategies for removing unwanted sp^2 carbon (as well as other materials used in the synthesis), for deagglomeration and for modification/functionalization of the diamond surface all remain very active research areas. There has been much discussion regarding the biocompatibility and fate of nanodiamonds in the body⁴⁹⁹ and their use in applications, such as tribology and lubrication, nanocomposites, tissue scaffolds and surgical implants and drug delivery.^{140,500,501} For many applications, the presence or absence of nitrogen in the nanodiamond is relatively unimportant. Some nanodiamond synthesis methods (e.g., the detonation technique) will inevitably yield diamond particles containing high nitrogen concentrations, whereas nanodiamonds produced by milling high purity diamond will contain very little nitrogen. The presence of different nitrogen defects (e.g., $\text{NV}^{0/-}$, $\text{N}_2\text{V}^{0/-}$, N_3V) significantly alters the fluorescent properties of nanodiamonds,⁵⁰² while the fact that the fluorescence intensity can be modulated by the presence of nearby magnetic fields opens up a range of new technologies based on quantum sensing, as discussed below (section 4.4).

Aside from the quantum applications, their bright luminescence, combined with their readily modifiable surface and biocompatibility, make diamond nanoparticles containing fluorescent NV centers extremely promising for biomedical applications,⁵⁰³ and, in particular, for use as a biomarker to “tag” biomolecules of interest as they travel around within living organisms.^{504–508} Nanodiamond biomarkers have a number of advantages over competing luminescent probes, such as quantum dots, fluorescent proteins (e.g., green fluorescent protein, GFP) or organic dyes (e.g., Alexa Fluor, fluorescein). First, for imaging of medium- to long-term biological processes, the NV centers in NDs are stable and do not photobleach, unlike the luminescent centers in most of their competitors, which often emit intermittently (blink) and eventually reduce in intensity (bleach) until they become too faint to see.⁵⁰⁹ Second, for long-term exposure, quantum dots can leach their (potentially toxic) chemical components into the cell cytoplasm,⁵¹⁰ whereas ND has been shown to have very low toxicity to most cell types.^{499,500} Further, the emission

from NV-containing NDs is typically in the wavelength range 625–800 nm, which is ideal for penetrating through tissue—thus allowing observation via an external microscope—and well clear of the wavelengths at which cells autofluoresce (300–500 nm).⁵¹¹ The fact that the surface of NDs can be chemically functionalized is another big advantage, allowing the attachment of a wide variety of biologically interactive species, such as simple hydrophilic/hydrophobic groups, proteins, antibodies, anticancer drugs and even DNA strands (Figure 14). Thus, quite apart from applications to monitor and investigate physiological processes within cells, there is growing interest in the use of NDs for targeted delivery of biological payloads to modulate the function of certain cell types. For example, NDs have been chemically modified to seek out and bind to cancer cells, and then deliver a cargo of a specific anticancer drug directly to those cells without harming neighboring healthy cells.⁵¹²

The use of NV-containing NDs for biomarking is possible because of their nanosize; they are sufficiently small that they can pass through the various membranes surrounding living cell structures without causing the cells any apparent damage. Once inside the cell, they diffuse to all regions of the cytoplasm—except the nucleus, into which NDs seem unable to penetrate.^{513–517} As Figure 35a shows, illumination with a green excitation laser causes the NDs to fluoresce in the red (recall Figure 20); observation of this fluorescence using confocal microscopy has allowed three-dimensional imaging and reconstruction of trajectories taken by individual NDs within a cell (Figure 35b) and, recently, real time tracking of single-particles inside a cell.⁵¹⁸ Such studies are starting to provide valuable insights into the fluid currents within cells, as well as the mechanisms by which nutrients, waste products and other metabolic products are transported around living cells.⁵¹⁹

4.4. Quantum Technologies Based on the NV⁻ Defect in Diamond

4.4.1. Properties of the NV⁻ Defect in Diamond That Underpin Its Exploitation in Quantum Technologies.

The development of many modern technologies has been driven by the need to improve efficiency and speed. This has resulted in miniaturization, to such a point where many devices are reaching the limits imposed by quantum mechanics. This impasse has motivated the development of radical new technologies based on quantum coherence, which promise breakthroughs in computational power, secure communications, and sensitivity in metrology and analytical science. Among these, spins trapped in defects in solid state systems are attracting considerable attention because of their resilience to decoherence and their compatibility with scalable device engineering. The negatively charged nitrogen-vacancy defect in diamond is perceived to have great technological promise. Because of favorable excited state photophysics (specifically the state-selective intersystem crossing probabilities), the NV⁻ electron spin can be optically initialized into the $m_S = 0$ ground state.⁵²⁰ As discussed in section 3.5.4.1, microwave excitation of the ground state $m_S = 0$ to $m_S = \pm 1$ transition results in a 30% reduction in the NV⁻ photoluminescence emission, allowing for optical determination of the spin state—even at room temperature.⁵²¹ The weakness of the spin–orbit coupling and the high Debye temperature of diamond ensures that the NV⁻ electron spin has an exceptionally long spin–lattice relaxation time (T_2 can reach 5 ms at room temperature and exceed hours at cryogenic temperatures).^{522,523} Dephasing

of the spin state can be mitigated by reducing the concentration of unwanted paramagnetic impurities and of ¹³C spins. In isotopically purified samples, T_2^* (the time scale of magnetic fluctuations) can exceed 100 μ s at room temperature, and dynamical decoupling can extend spin coherence to the homogeneous dephasing time T_2 .^{202,524} The NV⁻ electron polarization can be transferred to and from nearby nuclear spins using radio frequency and microwave excitation. The nuclear spins have very long coherence times⁵²⁵ and, as such, provide robust quantum memories.

As illustrated in Figure 20, NV centers located within a diamond lattice behave as isolated “chromophores”, with a set of energy levels distinct from those of the diamond. When excited with a burst of photons from a laser, a single NV will absorb only one photon. When it subsequently relaxes, the NV will re-emit only a single photon (with reduced energy), and this photon emerges with a specific optically readable spin.³⁰⁶ The photon can be captured in a suitable optical waveguide and transported where required. After a suitable delay, the NV resets, and can absorb and re-emit another photon. Thus, NV centers act as excellent sources of single photons,⁵²⁶ underpinning a host of applications involving quantum computing and quantum information processing.⁵²⁷

Many of these applications involve the curious phenomenon of quantum entanglement.⁵²⁸ When two particles (or photons) are brought together, their wave functions can mix (entangle), such that when the particles separate, each retains some information about their partner. In the case of two photons emitted from separate NV centers, their spins can become entangled if the photons are brought together in the same waveguide. When separated again, the spin of one photon can be instantaneously determined by observing the spin of the second photon, regardless of separation distance. In this regard, the entangled photons form a quantum bit (qubit). In contrast to a traditional binary computing bit, which can be either zero or one, a qubit is both 1 and 0 at the same time. Coupling two or more qubits allows multiple complex calculations to be done simultaneously, rather than sequentially, potentially offering greatly increased computational speeds. The more qubits that can be entangled, the greater the computational power: recent results in diamond have demonstrated a robust 10-qubit register comprised of nuclear spins coupled to an NV⁻ center.⁵²⁹ This is one of the driving forces behind the fabrication of grids of equally spaced NV centers in diamond, such as those shown in Figure 22b.

There are a growing number of reviews on applications of the NV⁻ defect to quantum technologies,^{288,297,315,341,530–532} and we do not attempt to reprise this information here but simply highlight some of the more widely investigated applications.

4.4.2. NV⁻ Defect in Diamond and Quantum Networks.

The NV⁻ combines a spin–light interface with control of local nuclear memories. Such an interface is essential for shared entanglement between spatially separated nodes in a quantum network and represents the essential resource for quantum key distribution and quantum cloud computing. In 2013, a breakthrough experiment established entanglement between two NV⁻ spins separated by 3 m,⁵³³ and the same team then went on to demonstrate the first loophole-free Bell test (i.e., a Bell experiment that leaves no room for explanations based on experimental imperfections) using two NV⁻ defects separated by 1.3 km.⁵³⁴

4.4.3. NV⁻ Defect in Diamond and Quantum Computing. Scaling a quantum computer to the large number of qubits required to outperform classical algorithms is a significant challenge and one which requires the ability to correct the inevitable errors that arise due to the delicate, analogue nature of quantum states. There have been impressive demonstrations of error correction in NV⁻-based systems,^{535,536} while proof-of-principle demonstrations with NV⁻ quantum registers have deduced the energy structure of a HeH⁺ cation.⁵³⁷ This work provides an important step toward a fully scalable solid-state implementation of a quantum chemistry simulator that might eventually find application in fields ranging from drug discovery to materials science.

4.4.4. NV⁻ Magnetometry. It is the room temperature optical readout of the magnetic resonance of the ground-state spin of the NV⁻ center in diamond that provides the exceptional capabilities for detection and imaging of magnetic fields. For scanning probe NV⁻ magnetometry, a single NV⁻ defect is integrated into the tip (either in a nanodiamond grafted to the tip or an all-diamond scanning probe) of an atomic force microscope with appropriate optical excitation and detection (see Figure 36).^{297,538–541} An alternate approach

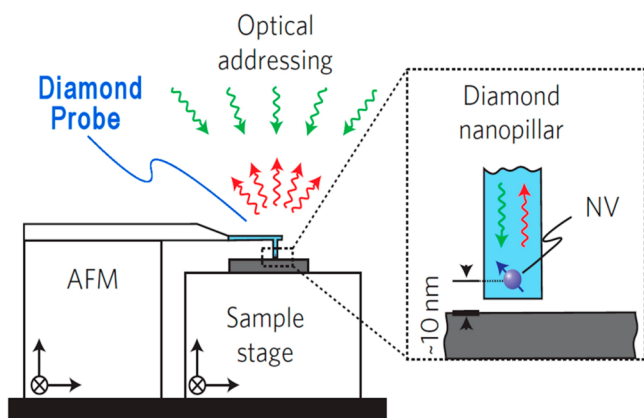


Figure 36. Schematic diagram of a nanoscopic scanning magnetometer. A single NV⁻ center is mounted to the end of an AFM tip and scanned over the surface of a sample, while optically detected magnetic resonance from the NV⁻ center is simultaneously measured. Lateral precision provided by the AFM is significantly higher than the optical diffraction limit, allowing nanoscale magnetic fields on approximately a nanometer scale to be mapped. Adapted from ref 541. Copyright 2012 Springer Nature Publishing AG.

is to have a diamond chip with a two-dimensional array of NV⁻ defects localized close to the surface, such that each is used as a pixel for measuring external magnetic fields in close proximity and an image reconstructed.⁵⁴² Both approaches combine high spatial resolution (relying on the close proximity of the NV⁻ defect to the sample surface) with high magnetic field sensitivity (e.g., AC ~ 10 nT Hz^{-1/2}, DC ~ 50 nT Hz^{-1/2}).²⁹⁷ Applications include mapping of heterogeneous magnetic materials,⁵⁴³ living cells (magnetotactic bacteria)⁵⁴⁴ and a wide range of advanced materials such as magnetic insulators undergoing spin injection,⁵⁴⁵ skyrmions,⁵⁴⁶ and graphene.⁵⁴⁷

Single NV-based magnetometers presently provide the highest-spatial-resolution magnetometry available. The exceptional sensitivity of NV-based magnetometers can be increased further by simultaneously sampling an ensemble of NV centers, rather than a single center, at the expense of spatial resolution.

Excellent far-field (i.e., magnetic field not varying over length scales comparable to the size of the diamond sensor) detection sensitivities have been demonstrated in the sub-pT Hz^{-1/2} range for AC measurements^{300,319,548} and in the sub-nT Hz^{-1/2} range at frequencies below 100 Hz.⁵⁴⁹ The NV⁻ magnetometer is calibration free, offers full vector readout (not just magnitude) and offers an exceptionally high dynamic range. This combination of properties is proving transformational for a wide variety of magnetometry applications, including all-magnetic navigation, geological surveys, current sensing, and locating underground/underwater magnetic anomalies.⁵⁵⁰

4.4.5. NV⁻ Defect and the Future of NMR and MRI. Nuclear magnetic resonance (NMR) and magnetic resonance imaging (MRI) are essential techniques that continue to enable breakthroughs in chemistry, biology, medicine, and materials science. NMR is commonly used to extract molecular-level information in a wide variety of physical, chemical, and biological scenarios. MRI is widely used to form pictures of the anatomy and the physiological processes of the body. The Achilles heel of the traditional magnetic resonance approaches remains the limited sensitivity, despite advances to higher magnetic fields and the use of dynamic nuclear polarization (DNP).^{551,552}

Several strategies of DNP have been proposed to generate large, nonthermal spin-polarized nuclear spin state distributions to enhance sensitivity. In single-crystal diamond containing a significant population of ¹³C nuclei (nuclear spin $I = 1/2$), polarization can be established within seconds, at room temperature, by optical pumping of NV⁻ centers.^{553,554} Nuclear spins associated with the ¹³C isotope in diamond possess long spin–lattice relaxation times, which facilitate a number of applications. For example, improved DNP strategies show that robust optical (via NV⁻ centers) nuclear polarization of diamond nanocrystals is feasible; appropriately functionalized, they form promising contrast agents for MRI⁵⁵⁵ and facilitate nanoscale hyperpolarized NMR spectroscopy of liquids.⁵⁵⁶ Although optical nuclear polarization using NV⁻ centers in diamond has attracted considerable attention, other nitrogen-related defects, when used in combination, offer alternate routes for nuclear hyperpolarization that may even prove more versatile than the NV⁻ center.³⁸⁴

Diamond-based DNP is undoubtedly useful but, in some ways, may be seen as simply enhancing the old approach to NMR and MRI. Today, researchers are realizing the possibility of utilizing NV⁻ centers in diamond as ultrasensitive magnetometers to detect NMR signals from nano- to micron-scale samples using low-cost equipment which can be assembled and operated by nonspecialists.^{557–559} Furthermore, with new protocols, spectral resolution comparable to conventional NMR can be achieved.^{560,561} Given the pace of recent progress, it is not fanciful to think that portable, relatively low cost, high sensitivity/resolution spectrometers, delivering on-chip NMR analysis, could be realized in the not too distant future.

4.4.6. NV⁻ Defect and Thermometry. The measurement of temperature variations on nanometer length scales is challenging, but a probe with subdegree temperature resolution would be very useful in many areas of biological, chemical, materials, and device research. To this end, recent studies have demonstrated nanoscale thermometry with optical readout using the temperature variation of the zero-field splitting associated with the electron spin of the NV⁻ defect in diamond.^{562,563} Sensitivities of a few mK were achieved in an

ultrapure bulk diamond. Experiments employing NV^- defects in nanodiamonds were able to measure the temperature inside a living cell and encouraged the hope that it should soon be possible to measure the heat produced by chemical interactions involving just a few molecules.⁵⁶⁴ Other novel NV^- -based methodologies for thermometry have also been proposed and applications demonstrated but these again are outside the scope of this Review.^{549,565–567}

4.4.7. NV^- Defect and Electric Field Sensing. Single NV^- defect centers in diamond can be used to sense electric fields via the electric-field dependent shifts of the energy levels.⁵⁶⁸ Using one NV^- center as an electrometer, Dolde et al.⁵⁶⁹ demonstrated detection of the single excess electron that determines the charge state of another NV^- center located ~ 25 nm away under ambient conditions. This work showed that an NV^- center could be used to detect the electric field of a single electron at a distance of ~ 150 nm within 1 s of averaging, suggesting the possibility of detecting the charge states of molecules/radicals near the surface of the diamond.

4.4.8. Hybrid Quantum Devices Involving a Solid-State Spin and a Macroscopic Mechanical Oscillator. There is also great interest in hybrid quantum devices involving a solid-state spin and a macroscopic mechanical oscillator, since such devices provide opportunities to mediate interactions between disparate quantum bits and to explore the quantum regime of macroscopic mechanical objects.⁵³² Several examples of coupling an NV^- center to a nanomechanical oscillator have already appeared^{570–573} and, with ever-improving diamond synthesis, processing, and nanofabrication, such hybrid devices can be expected to find a wealth of applications in quantum information processing.

4.4.9. Diamond Masers. The final novel NV^- -center based application reported in this section is a magnetic-field tunable maser based on optical pumping of ensembles of NV^- centers in diamond that works continuously under ambient conditions.⁵⁷⁴ Most previous maser technologies have required cryogenic refrigeration and high-vacuum systems, and been restricted to niche applications. This diamond maser paves the way for much wider exploitation of this technology which could find application in metrology, communications, quantum physics, and medicine.

5. SUMMARY AND PROSPECTIVE

Research activity that falls under the umbrella of “diamond science” has increased near-exponentially over the past few decades. Once largely the preserve of geoscientists and gemologists, the advent of lab-based growth methods (HPHT synthesis and, particularly, CVD) has led to huge advances in the availability of diamond samples grown under well-defined and well-controlled conditions. This, in turn, allows creation of diamond with user-selected doping levels, enriched or depleted in ^{13}C (relative to natural abundance). Notable examples include boron-doped diamond, which is enabling new applications in electrochemistry and analytical chemistry, and—central to this Review—single-crystal diamond with nitrogen-doping levels ranging from far below 1 ppm (so-called “electronic grade” material) to well in excess of 1000 ppm.

Access to such material has heralded quantitative advances in our knowledge and understanding of nitrogen-containing defects in diamond and their interconversion and aggregation which, in turn, has encouraged new thinking about natural diamond formation and underpins much of the instrumenta-

tion used to separate and/or identify natural and lab-grown diamonds. Section 3 summarizes contemporary knowledge relating to nitrogen-containing defects in diamond, and highlights some of the challenges that remain. But the availability of well-characterized nitrogen-doped diamond has also served to spawn completely new areas of research and new applications—many of which are summarized in section 4. For example, nitrogen-doped nanodiamonds have properties (e.g., (photo)chemical stability and biocompatibility) that encourage their use as fluorescent probes for particle tracking in heterogeneous environments. But it is the remarkable spin/photophysics of one specific nitrogen-containing defect in diamond, the NV^- defect, that is really starting to change science—impacting on a range of quantum technologies and offering new opportunities for magnetometry and thermometry on the nanoscale. There can be little doubt that the recent explosion of interest in diamond science will continue, and that nitrogen-doped diamond will be pivotal to that growth.

AUTHOR INFORMATION

Corresponding Author

Michael N. R. Ashfold – School of Chemistry, University of Bristol, Bristol BS8 1TS, U.K.; orcid.org/0000-0001-5762-7048; Email: mike.ashfold@bristol.ac.uk

Authors

Jonathan P. Goss – School of Engineering, University of Newcastle, Newcastle upon Tyne NE1 7RU, U.K.

Ben L. Green – Department of Physics, University of Warwick, Coventry CV4 7AL, U.K.

Paul W. May – School of Chemistry, University of Bristol, Bristol BS8 1TS, U.K.; orcid.org/0000-0002-5190-7847

Mark E. Newton – Department of Physics, University of Warwick, Coventry CV4 7AL, U.K.

Chloe V. Peaker – Gemological Institute of America, New York, New York 10036, United States

Complete contact information is available at:
<https://pubs.acs.org/10.1021/acs.chemrev.9b00518>

Notes

The authors declare no competing financial interest.

Biographies

Mike Ashfold obtained his PhD from the University of Birmingham in 1978. After postdoctoral research at the University of Oxford, he was appointed as a Lecturer at the University of Bristol, where he was promoted to a Chair in Physical Chemistry in 1992 and currently holds the Leverhulme Chair of Chemistry. He was elected to the Fellowship of the Royal Society in 2009. His research interests include plasma diagnosis (particularly in the context of diamond CVD), molecular photophysics, and spectroscopy.

Jonathan Goss used computational techniques to research into defects in diamond in his PhD (Exeter University, 1997), followed by postdoctoral projects modelling low-pressure plasma in Dublin City University and further atomistic modelling in Exeter before taking up an EPSRC Advanced Research Fellowship in Newcastle University in 2002. He is currently a Senior Lecturer in the School of Engineering, using a range of computational methods to study diamond (point defects, surfaces, and devices), as well as a range of technologically relevant materials, including Si, Ge, III-Vs, metal oxides, graphene, and CZTS.

Ben Green is a Royal Academy of Engineering Research Fellow based at Warwick University. Ben gained his PhD at Warwick University in 2013 and joined the R&D team at Element Six, Ltd., before returning to academia in 2015 as part of the Network Quantum Information Technology Quantum Hub. His primary research interests involve the identification, characterization, and subsequent exploitation of technologically useful point defects in diamond, driven by fundamental research into their optical, spin, and electronic properties.

Paul May held a Ramsay Memorial Fellowship (1992–4) and a Royal Society University Research Fellowship (1994–9) in the School of Chemistry at the University of Bristol prior to appointment to a Lectureship. He was promoted to Professor there in 2010, where he cofounded the Bristol CVD diamond group (with Mike Ashfold) in 1991. He has published >200 peer reviewed articles, 180 of which are on the subject of diamond/DLC films, and has given invited and contributed talks at >50 international conferences. He has also written a collection of short science-fiction stories and two popular science books, the latest of which is entitled *Molecules that Amaze Us*.

Mark Newton has been working in the field of diamond science and technology for 30 years. He has held academic posts at King's College London, Oxford University and, for the last 14 years, at Warwick University where he holds a Chair in Physics. His research interests include the physics and exploitation of defects in diamond, and the development of diamond-based technologies. He is director of the UK Engineering and Physical Sciences Research Council (EPSRC) Centre for Doctoral Training (CDT) in Diamond Science and Technology (DST).

Chloe Peaker obtained her PhD degree in 2018 under the primary supervision of Jonathan Goss at Newcastle University, UK. The thesis was partially sponsored by De Beers and focused on a systematic density functional theory study of the N_nVH_m (where $n + m \leq 4$) group of defects in diamond and their interplay in aggregation processes. Following a postdoctoral project at Warwick University pursuing experimental counterparts to theoretical results, she is currently a postdoctoral research fellow at the Gemological Institute of America (GIA) branching out in both experimental and theoretical research on point defects in diamond and other gemstones.

ACKNOWLEDGMENTS

The authors acknowledge financial support from EPSRC (Grants EP/K018388/1, EP/L015315/1, EP/M508305/1) and from Element Six, Ltd. M.N.R.A. is very grateful for the numerous insights provided by long-term collaborator Dr. Yuri Mankelevich (Skobeltsyn Institute of Nuclear Physics, Lomonosov Moscow State University). B.L.G. acknowledges funding from the Royal Academy of Engineering and is grateful to Dr. Ben Breeze (University of Warwick) for useful discussions. B.L.G. and M.E.N. are grateful to Dr. David Fisher for insightful discussions regarding the N₂ and N₃ transitions in diamond. C.V.P. thanks Karen V. Smit for useful discussions. No new data were created specifically for this study.

REFERENCES

(1) Shirey, S. B.; Shigley, J. E. Recent Advances in Understanding the Geology of Diamonds. *Gems Gemol.* **2013**, *49*, 188–222.
(2) Smith, E. M.; Shirey, S. B.; Richardson, S. H.; Nestola, F.; Bullock, E. S.; Wang, J. H.; Wang, W. Y. Blue Boron-Bearing Diamonds from Earth's Lower Mantle. *Nature* **2018**, *560*, 84–87.

(3) Mikhail, S.; Howell, D. A. Petrological Assessment of Diamond as a Recorder of the Mantle Nitrogen Cycle. *Am. Mineral.* **2016**, *101*, 780–787.
(4) Collins, A. T. Intrinsic and Extrinsic Absorption and Luminescence in Diamond. *Phys. B* **1993**, *185*, 284–296.
(5) Kaiser, W.; Bond, W. L. Nitrogen, a Major Impurity in Common Type-I Diamond. *Phys. Rev.* **1959**, *115*, 857–863.
(6) Boyd, S. R.; Kiflawi, I.; Woods, G. S. The Relationship between Infrared-Absorption and the A Defect Concentration in Diamond. *Philos. Mag. B* **1994**, *69*, 1149–1153.
(7) Boyd, S. R.; Kiflawi, I.; Woods, G. S. Infrared-Absorption by the B-Nitrogen Aggregate in Diamond. *Philos. Mag. B* **1995**, *72*, 351–361.
(8) Chrenko, R. M.; Tuft, R. E.; Strong, H. M. Transformation of the State of Nitrogen in Diamond. *Nature* **1977**, *270*, 141–144.
(9) Taylor, W. R.; Canil, D.; Milledge, H. J. Kinetics of Ib to Ia Nitrogen Aggregation in Diamond. *Geochim. Cosmochim. Acta* **1996**, *60*, 4725–4733.
(10) Breeding, C. M.; Shigley, J. E. The “Type” Classification System of Diamonds and Its Importance in Gemology. *Gems Gemol.* **2009**, *45*, 96–111.
(11) Mikhail, S.; Sverjensky, D. A. Nitrogen Speciation in Upper Mantle Fluids and the Origin of Earth's Nitrogen-Rich Atmosphere. *Nat. Geosci.* **2014**, *7*, 816–819.
(12) Smith, E. M.; Shirey, S. B.; Nestola, F.; Bullock, E. S.; Wang, J. H.; Richardson, S. H.; Wang, W. Large Gem Diamonds from Metallic Liquid in Earth's Deep Mantle. *Science* **2016**, *354*, 1403–1405.
(13) Danilenko, V. V. On the History of the Discovery of Nanodiamond Synthesis. *Phys. Solid State* **2004**, *46*, 595–599.
(14) Bundy, F. P.; Hall, H. T.; Strong, H. M.; Wentorf, R. H. Man-Made Diamonds. *Nature* **1955**, *176*, 51–55.
(15) Barnard, A. S. *The Diamond Formula*; Butterworth-Heinemann: Oxford, 2000.
(16) Bovenkerk, H. P.; Bundy, F. P.; Hall, H. T.; Strong, H. M.; Wentorf, R. H. Preparation of Diamond. *Nature* **1959**, *184*, 1094–1098.
(17) Dobrinets, I. A.; Vins, V. G.; Zaitsev, A. M. *HPHT-Treated Diamonds*, Springer Series in Materials Science 181; Springer-Verlag: Berlin, 2013.
(18) D'Haensens-Johansson, U. F. S.; Katrusha, A.; Moe, K. S.; Johnson, P.; Wang, W. Y. Large Colorless HPHT-Grown Synthetic Gem Diamonds from New Diamond Technology, Russia. *Gems Gemol.* **2015**, *51*, 260–279.
(19) Eaton-Magaña, S.; Shigley, J. E.; Breeding, C. M. Observations on HPHT-Grown Synthetic Diamonds: A Review. *Gems Gemol.* **2017**, *53*, 262–284.
(20) Berman, R.; Simon, F. On the Graphite-Diamond Equilibrium. *Z. Electrochem.* **1955**, *59*, 333–338.
(21) Peaker, C. V. First Principles Study of Point Defects in Diamond. Ph.D. Thesis, University of Newcastle, UK, 2018; <https://theses.ncl.ac.uk/jspui/handle/10443/4224>.
(22) Palyanov, Y. N.; Borzdov, Y. M.; Khokhryakov, A. F.; Kupriyanov, I. N.; Sokol, A. G. Effect of Nitrogen Impurity on Diamond Growth Processes. *Cryst. Growth Des.* **2010**, *10*, 3169–3175.
(23) Chen, L. C.; Miao, X. Y.; Ma, H. G.; Guo, L. S.; Wang, Z. K.; Yang, Z. Q.; Fang, C.; Jia, X. P. Synthesis and Characterization of Diamonds with Different Nitrogen Concentrations under High Pressure and High Temperature Conditions. *CrystEngComm* **2018**, *20*, 7164–7169.
(24) Liu, X. B.; Jia, X. P.; Fang, C.; Ma, H.-A. Diamond Crystallization and Growth in N–H Enriched Environment under HPHT Conditions. *CrystEngComm* **2016**, *18*, 8506–8515.
(25) Fang, C.; Zhang, Y. W.; Zhang, Z. F.; Shan, C. X.; Shen, W. X.; Jia, X. P. Preparation of ‘Natural’ Diamonds by HPHT Annealing of Synthetic Diamonds. *CrystEngComm* **2018**, *20*, 505–511.
(26) Spitsyn, B. V.; Bouilov, L. L.; Derjaguin, B. V. Diamond and Diamond-Like Films – Deposition from the Vapor-Phase, Structure and Properties. *Prog. Cryst. Growth Charact.* **1988**, *17*, 79–170 and references therein.

- (27) Angus, J. C.; Will, H. A.; Stanko, W. S. Growth of Diamond Seed Crystals by Vapor Deposition. *J. Appl. Phys.* **1968**, *39*, 2915–2922.
- (28) Matsumoto, S.; Sato, Y.; Tsutsumi, M.; Setaka, N. Growth of Diamond Particles from Methane-Hydrogen Gas. *J. Mater. Sci.* **1982**, *17*, 3106–3112.
- (29) Matsumoto, S.; Sato, Y.; Kamo, M.; Setaka, N. Vapor Deposition of Diamond Particles from Methane. *Jpn. J. Appl. Phys.* **1982**, *21*, L183–L185.
- (30) Kamo, M.; Sato, Y.; Matsumoto, S.; Setaka, N. Diamond Synthesis from Gas-Phase in Microwave Plasma. *J. Cryst. Growth* **1983**, *62*, 642–644.
- (31) Goodwin, D. G.; Butler, J. E. Theory of Diamond Chemical Vapor Deposition. In *Handbook of Industrial Diamonds and Diamond Films*; Prelas, M. A., Popovici, G., Bigelow, L. K., Eds.; Marcel Dekker, Inc.: New York, 1997; pp 527–581.
- (32) Gicquel, A.; Hassouni, K.; Silva, F.; Achard, J. CVD Diamond Films: from Growth to Applications. *Curr. Appl. Phys.* **2001**, *1*, 479–496.
- (33) Achard, J.; Silva, F.; Tallaire, A.; Bonnin, X.; Lombardi, G.; Hassouni, K.; Gicquel, A. High Quality MPACVD Diamond Single Crystal Growth: High Microwave Power Density Regime. *J. Phys. D: Appl. Phys.* **2007**, *40*, 6175–6188.
- (34) Butler, J. E.; Mankelevich, Y. A.; Cheesman, A.; Ma, J.; Ashfold, M. N. R. Understanding the Chemical Vapor Deposition of Diamond: Recent Progress. *J. Phys.: Condens. Matter* **2009**, *21*, 364201.
- (35) Balmer, R. S.; Brandon, J. R.; Clewes, S. L.; Dhillon, H. K.; Dodson, J. M.; Friel, I.; Inglis, P. N.; Madgwick, T. D.; Markham, M. L.; Mollart, T. P.; et al. Chemical Vapour Deposition Synthetic Diamond: Materials, Technology and Applications. *J. Phys.: Condens. Matter* **2009**, *21*, 364221.
- (36) Gracio, J. J.; Fan, Q. H.; Madaleno, J. C. Diamond Growth by Chemical Vapour Deposition. *J. Phys. D: Appl. Phys.* **2010**, *43*, 374017.
- (37) Tallaire, A.; Achard, J.; Silva, F.; Brinza, O.; Gicquel, A. Growth of Large Size Diamond Single Crystals by Plasma Assisted Chemical Vapour Deposition: Recent Achievements and Remaining Challenges. *C. R. Phys.* **2013**, *14*, 169–184.
- (38) May, P. W. Diamond Thin Films: A 21st Century Material. *Philos. Trans. R. Soc., A* **2000**, *358*, 473–495.
- (39) Leeds, S. M. Characterisation of the Gas-Phase Environment in a Microwave Plasma Enhanced Diamond Chemical Vapour Deposition Reactor using Molecular Beam Mass Spectrometry, PhD Thesis, University of Bristol, UK, 1999; <http://www.chm.bris.ac.uk/pt/diamond/stuthesis/begin.htm>.
- (40) Ashfold, M. N. R.; May, P. W.; Rego, C. A.; Everitt, N. M. Thin Film Diamond by Chemical Vapour Deposition Methods. *Chem. Soc. Rev.* **1994**, *23*, 21–30.
- (41) Ramesham, R.; Roppel, T.; Johnson, R. W.; et al. Characterization of polycrystalline diamond thin films grown on various substrates. *Thin Solid Films* **1992**, *212*, 96–103.
- (42) Yugo, S.; Kanai, T.; Kimura, T.; Muto, T. Generation of Diamond Nuclei by Electric-Field in Plasma Chemical Vapor-Deposition. *Appl. Phys. Lett.* **1991**, *58*, 1036–1038.
- (43) Stoner, B. R.; Ma, G. H. M.; Wolter, S. D.; Glass, J. T. Characterization of Bias-Enhanced Nucleation of Diamond on Silicon by *In Vacuo* Surface-Analysis and Transmission Electron-Microscopy. *Phys. Rev. B: Condens. Matter Mater. Phys.* **1992**, *45*, 11067–11084.
- (44) Williams, O. A. Nanocrystalline Diamond. *Diamond Relat. Mater.* **2011**, *20*, 621–640.
- (45) Gruen, D. M. Nanocrystalline Diamond Films. *Annu. Rev. Mater. Sci.* **1999**, *29*, 211–259.
- (46) Shenderova, O. A.; Gruen, D. M. *Ultrananocrystalline Diamond: Synthesis, Properties and Applications*, 2nd ed.; Elsevier, 2012.
- (47) Butler, J. E.; Sumant, A. V. The CVD of Nanodiamond Materials. *Chem. Vap. Deposition* **2008**, *14*, 145–160.
- (48) Wild, C.; Koidl, P.; Müller-Seibert, M.; Walcher, H.; Kohl, R.; Herres, N.; Locher, R.; Samlenski, R.; Brenn, R. Chemical Vapor Deposition and Characterization of Smooth {100}-Faceted Diamond Films. *Diamond Relat. Mater.* **1993**, *2*, 158–168.
- (49) Jin, S.; Moustakas, T. D. Effect of Nitrogen on the Growth of Diamond Films. *Appl. Phys. Lett.* **1994**, *65*, 403–405.
- (50) Schreck, M.; Asmussen, J.; Shikata, S.; Arnault, J.-C.; Fujimori, N. Large-Area High-Quality Single Crystal Diamond. *MRS Bull.* **2014**, *39*, 504–510.
- (51) Ardon, T.; McElhenny, G. CVD Layer Grown on Natural Diamond. *Gems Gemol* **2019**, *55* (1), 91–101.
- (52) Onstad, E.; Clarke, D. *How Man-Made Diamonds have Grown to Threaten Natural Gems*; Reuters Business News, 2018; <https://uk.reuters.com/article/uk-diamonds-debeers-synthetic/how-man-made-diamonds-have-grown-to-threaten-natural-gems-idUKKCN10K0NB>.
- (53) Yamada, H.; Chayahara, A.; Mokuno, Y.; Tsubouchi, N.; Shikata, S. Uniform Growth and Repeatable Fabrication of Inch-Sized Wafers of Single Crystal Diamond. *Diamond Relat. Mater.* **2013**, *33*, 27–31.
- (54) Yamada, H.; Chayahara, A.; Mokuno, Y.; Kato, Y.; Shikata, S. A 2-in. Mosaic Made of a Single-Crystal Diamond. *Appl. Phys. Lett.* **2014**, *104*, 102110.
- (55) Schreck, M.; Gsell, S.; Brescia, R.; Fischer, M. Ion Bombardment Induced Buried Lateral Growth: The Key Mechanism for the Synthesis of Single Crystal Diamond Wafers. *Sci. Rep.* **2017**, *7*, 44462.
- (56) Gallheber, B.-C.; Fischer, M.; Mayr, M.; Straub, J.; Schreck, M. Growth, Stress, and Defects of Heteroepitaxial Diamond on Ir/YSZ/Si(111). *J. Appl. Phys.* **2018**, *123*, 225302.
- (57) Ashfold, M. N. R.; May, P. W.; Petherbridge, J. R.; Rosser, K. N.; Smith, J. A.; Mankelevich, Yu.A.; Suetin, N. V. Unravelling Aspects of the Gas Phase Chemistry Involved in Diamond Chemical Vapour Deposition. *Phys. Chem. Chem. Phys.* **2001**, *3*, 3471–3485.
- (58) Gicquel, A.; Chenevier, M.; Hassouni, K.; Tserepi, A.; Dubus, M. Validation of Actinometry for Estimating Relative Hydrogen Atom Densities and Electron Energy Evolution in Plasma Assisted Diamond Deposition Reactors. *J. Appl. Phys.* **1998**, *83*, 7504–7521.
- (59) Hassouni, K.; Gicquel, A.; Capitelli, M.; Loureiro, J. Chemical Kinetics and Energy Transfer in Moderate Pressure H₂ Plasmas used in Diamond MPACVD. *Plasma Sources Sci. Technol.* **1999**, *8*, 494–512.
- (60) Lombardi, G.; Hassouni, K.; Benedic, F.; Mohasseb, F.; Ropcke, J.; Gicquel, A. Spectroscopic Diagnostics and Modelling of Ar/H₂/CH₄ Microwave Discharges used for Nanocrystalline Diamond Deposition. *J. Appl. Phys.* **2004**, *96*, 6739–6751.
- (61) Lombardi, G.; Hassouni, K.; Stancu, G. D.; Mechold, D.; Ropcke, J.; Gicquel, A. Modelling of Microwave Discharges of H₂ admixed with CH₄ for Diamond Deposition. *J. Appl. Phys.* **2005**, *98*, 053303.
- (62) Mankelevich, Yu.A.; Ashfold, M. N. R.; Ma, J. Plasma-Chemical Processes in Microwave Plasma Enhanced Chemical Vapour Deposition Reactors Operating with C/H/Ar Gas Mixtures. *J. Appl. Phys.* **2008**, *104*, 113304.
- (63) Ma, J.; Richley, J. C.; Ashfold, M. N. R.; Mankelevich, Yu.A. Probing the Plasma Chemistry in a Microwave Reactor used for Diamond Chemical Vapour Deposition by Cavity Ring Down Spectroscopy. *J. Appl. Phys.* **2008**, *104*, 103305.
- (64) Ma, J.; Ashfold, M. N. R.; Mankelevich, Yu.A. Validating Optical Emission Spectroscopy as a Diagnostic of Microwave Activated CH₄/Ar/H₂ Plasmas used for Diamond Chemical Vapor Deposition. *J. Appl. Phys.* **2009**, *105*, 043302.
- (65) Hassouni, K.; Silva, F.; Gicquel, A. Modelling of Diamond Deposition Microwave Cavity Generated Plasmas. *J. Phys. D: Appl. Phys.* **2010**, *43*, 153001.
- (66) Gicquel, A.; Derkaoui, N.; Rond, C.; Benedic, F.; Cicala, G.; Moneger, D.; Hassouni, K. Quantitative Analysis of Diamond Deposition Reactor Efficiency. *Chem. Phys.* **2012**, *398*, 239–247.
- (67) Richley, J. C.; Fox, O. J. L.; Ashfold, M. N. R.; Mankelevich, Yu.A. Combined Experimental and Modeling Studies of Microwave Activated CH₄/H₂/Ar Plasmas for Microcrystalline, Nanocrystalline

and Ultrananocrystalline Diamond Deposition. *J. Appl. Phys.* **2011**, *109*, 063307.

(68) Ashfold, M. N. R.; Mahoney, E. J. D.; Mushtaq, S.; Truscott, B. S.; Mankelevich, Yu.A. What [Plasma used for Growing] Diamond can Shine Like Flame? *Chem. Commun.* **2017**, *53*, 10482–10495.

(69) May, P. W.; Ashfold, M. N. R.; Mankelevich, Yu.A. Microcrystalline, Nanocrystalline, and Ultrananocrystalline Diamond Chemical Vapor Deposition: Experiment and Modelling of the Factors Controlling Growth Rate, Nucleation and Crystal Size. *J. Appl. Phys.* **2007**, *101*, 053115.

(70) Pate, B. B. The Diamond Surface – Atomic and Electronic Structure. *Surf. Sci.* **1986**, *165*, 83–142.

(71) Thoms, B. D.; Butler, J. E. HREELS and LEED of H/C(100) – the 2×1 Monohydride Dimer Row Reconstruction. *Surf. Sci.* **1995**, *328*, 291–301.

(72) Bobrov, K.; Mayne, A.; Comtet, G.; Dujardin, G.; Hellner, L.; Hoffman, A. Atomic-Scale Visualization and Surface Electronic Structure of the Hydrogenated Diamond C(100)-(2 × 1):H Surface. *Phys. Rev. B: Condens. Matter Mater. Phys.* **2003**, *68*, 195416.

(73) Garrison, B.; Dawnkaski, E. J.; Srivastava, D.; Brenner, D. W. Molecular-Dynamics Simulations of Dimer Opening on a Diamond (001)(2 × 1) Surface. *Science* **1992**, *255*, 835–838.

(74) Cheesman, A.; Harvey, J. N.; Ashfold, M. N. R. Studies of Carbon Incorporation on the Diamond (100) Surface during Chemical Vapor Deposition Using Density Functional Theory. *J. Phys. Chem. A* **2008**, *112*, 11436–11448.

(75) Butler, J. E.; Oleynik, I. A Mechanism for Crystal Twinning in the Growth of Diamond by Chemical Vapour Deposition. *Philos. Trans. R. Soc., A* **2008**, *366*, 295–310.

(76) Netto, A.; Frenklach, M. Kinetic Monte Carlo Simulations of CVD Diamond Growth – Interplay among Growth, Etching, and Migration. *Diamond Relat. Mater.* **2005**, *14*, 1630–1646.

(77) Rodgers, W. J.; May, P. W.; Allan, N. L.; Harvey, J. N. Three-Dimensional Kinetic Monte Carlo Simulations of Diamond Chemical Vapor Deposition. *J. Chem. Phys.* **2015**, *142*, 214707.

(78) Tallaire, A.; Collins, A. T.; Charles, D.; Achard, J.; Sussmann, R.; Gicquel, A.; Newton, M. E.; Edmonds, A. M.; Cruddace, R. J. Characterisation of High Quality Thick Single-Crystal Diamond Grown by CVD with a Low Nitrogen Addition. *Diamond Relat. Mater.* **2006**, *15*, 1700–1707.

(79) Kaminskii, A. A.; Lux, O.; Ralchenko, V. G.; Bolshakov, A. P.; Rhee, H.; Eichler, H. J.; Shirakawa, A.; Yoneda, H. High-Order Stokes and Anti-Stokes Raman Generation in Monoisotopic CVD ¹²C-Diamond. *Phys. Status Solidi RRL* **2016**, *10*, 471–474.

(80) Müller-Seibert, W.; Wörner, E.; Fuchs, F.; Wild, C.; Koidl, P. Nitrogen Induced Increase of Growth Rate in Chemical Vapor Deposition of Diamond. *Appl. Phys. Lett.* **1996**, *68*, 759–760.

(81) Yan, C.-S.; Vohra, Y. K.; Mao, H.-K.; Hemley, R. J. Very High Growth Rate Chemical Vapor Deposition of Single-Crystal Diamond. *Proc. Natl. Acad. Sci. U. S. A.* **2002**, *99*, 12523–12525.

(82) Chayahara, A.; Mokuno, Y.; Horino, Y.; Takasu, Y.; Kato, H.; Yoshikawa, H.; Fujimori, N. The Effect of Nitrogen Addition during High-Rate Homoepitaxial Growth of Diamond by Microwave Plasma CVD. *Diamond Relat. Mater.* **2004**, *13*, 1954–1958.

(83) Liu, Y.; Raabe, D. Influence of Nitrogen Doping on Growth Rate and Texture Evolution of Chemical Vapor Deposition Thin Films. *Appl. Phys. Lett.* **2009**, *94*, 021119.

(84) Achard, J.; Silva, F.; Brinza, O.; Tallaire, A.; Gicquel, A. Coupled Effect of Nitrogen Addition and Surface Temperature on the Morphology and the Kinetics of Thick CVD Diamond Single Crystals. *Diamond Relat. Mater.* **2007**, *16*, 685–689.

(85) Dunst, S.; Sternschulte, H.; Schreck, M. Growth Rate Enhancement by Nitrogen in Diamond Chemical Vapor Deposition – A Catalytic Effect. *Appl. Phys. Lett.* **2009**, *94*, 224101.

(86) Lu, J.; Gu, Y.; Grotjohn, T. A.; Schuelke, T.; Asmussen, J. Experimentally Defining the Safe and Efficient, High Pressure Microwave Plasma Assisted CVD Operating Regime for Single Crystal Diamond Synthesis. *Diamond Relat. Mater.* **2013**, *37*, 17–28.

(87) Bogdanov, S.; Vikharev, A.; Gorbachev, A.; Muchnikov, A.; Radishev, D.; Ovechkin, N.; Parshin, V. Growth-rate Enhancement of High-quality, Low-loss CVD-produced Diamond Disks Grown for Microwave Windows Application. *Chem. Vap. Deposition* **2014**, *20*, 32–38.

(88) Yamada, H.; Chayahara, A.; Mokuno, Y. Effects of Intentionally Introduced Nitrogen and Substrate Temperature on Growth of Diamond Bulk Single Crystals. *Jpn. J. Appl. Phys.* **2016**, *55*, 01AC07.

(89) Locher, R.; Wild, C.; Herres, N.; Behr, D.; Koidl, P. Nitrogen Stabilized 100 Texture in Chemical Vapour Deposited Diamond Films. *Appl. Phys. Lett.* **1994**, *65*, 34–36.

(90) Cao, G. Z.; Schermer, J. J.; van Enckevort, W. J. P.; Elst, W. A. L. M.; Giling, L. J. Growth of {100} Textured Diamond Films by the Addition of Nitrogen. *J. Appl. Phys.* **1996**, *79*, 1357–1364.

(91) Tang, C. J.; Fernandes, A. J. S.; Costa, F.; Pinto, J. L. Effect of Microwave Power and Nitrogen Addition on the Formation of {100} Faceted Diamond from Microcrystalline to Nanocrystalline. *Vacuum* **2011**, *85*, 1130–1134.

(92) Ashkinazi, E. E.; Khmel'nitskii, R. A.; Sedov, V. S.; Khomich, A. A.; Khomich, A. V.; Ralchenko, V. G. Morphology of Diamond Layers Grown on Different Facets of Single Crystal Diamond Substrates by a Microwave Plasma CVD in CH₄-H₂-N₂ Gas Mixtures. *Crystals* **2017**, *7*, 166.

(93) Truscott, B. S.; Kelly, M. W.; Potter, K. J.; Johnson, M.; Ashfold, M. N. R.; Mankelevich, Yu.A. Microwave Plasma-Activated Chemical Vapor Deposition of Nitrogen-Doped Diamond, I: N₂/H₂ and NH₃/H₂ Plasmas. *J. Phys. Chem. A* **2015**, *119*, 12962–12976.

(94) Yamada, H. Numerical Simulations to Study Growth of Single-Crystal Diamond by Using Microwave Plasma Chemical Vapor Deposition with Reactive (H, C, N) Species. *Jpn. J. Appl. Phys.* **2012**, *51*, 090105.

(95) Truscott, B. S.; Kelly, M. W.; Potter, K. J.; Ashfold, M. N. R.; Mankelevich, Yu.A. Microwave Plasma-Activated Chemical Vapor Deposition of Nitrogen-Doped Diamond, II: CH₄/N₂/H₂ Plasmas. *J. Phys. Chem. A* **2016**, *120*, 8537–8549.

(96) Kelly, M. W.; Halliwell, S. C.; Rodgers, W. J.; Pattle, J. D.; Harvey, J. N.; Ashfold, M. N. R. Theoretical Investigations of the Reactions of N- and O-Containing Species on a C(100):H 2 × 1 Reconstructed Diamond Surface. *J. Phys. Chem. A* **2017**, *121*, 2046–2055.

(97) Van Regemorter, T.; Larsson, K. Effect of a NH Coadsorbate on the CH₃ (or CH₂) Adsorption to a Surface Step on Diamond (100). *J. Phys. Chem. C* **2009**, *113*, 19891–19896.

(98) Van Regemorter, T.; Larsson, K. A. Theoretical Study of Nitrogen-Induced Effects on Initial Steps of Diamond CVD Growth. *Chem. Vap. Deposition* **2008**, *14*, 224–231.

(99) Van Regemorter, T.; Larsson, K. Effect of Substitutional N on Important Chemical Vapor Deposition Growth Steps. *J. Phys. Chem. A* **2009**, *113*, 3274–3284.

(100) Yiming, Z.; Larsson, F.; Larsson, K. Effect of CVD Diamond Growth by Doping with Nitrogen. *Theor. Chem. Acc.* **2014**, *133*, 1432.

(101) Edmonds, A. M.; D'Haensens-Johansson, U. F. S.; Cruddace, R. J.; Newton, M. E.; Fu, K. M. C.; Santori, C.; Beausoleil, R. G.; Twitchen, D. J.; Markham, M. L. Production of Oriented Nitrogen-Vacancy Color Centers in Synthetic Diamond. *Phys. Rev. B: Condens. Matter Mater. Phys.* **2012**, *86*, 035201.

(102) Michl, J.; Teraji, T.; Zaiser, S.; Jakobi, I.; Waldherr, G.; Dolde, F.; Neumann, P.; Doherty, M. W.; Manson, N. B.; Isoya, J.; et al. Perfect Alignment and Preferential Orientation of Nitrogen-Vacancy Centers during Chemical Vapor Deposition Diamond Growth on (111) Surfaces. *Appl. Phys. Lett.* **2014**, *104*, 102407.

(103) Lesik, M.; Tétienne, J. P.; Tallaire, A.; Achard, J.; Mille, V.; Gicquel, A.; Roch, J. F.; Jacques, V. Perfect Preferential Orientation of Nitrogen-Vacancy Defects in a Synthetic Diamond Sample. *Appl. Phys. Lett.* **2014**, *104*, 113107.

(104) Fukui, T.; Doi, Y.; Miyazaki, T.; Miyamoto, Y.; Kato, H.; Matsumoto, T.; Makino, T.; Yamasaki, S.; Morimoto, R.; Tokuda, N.; et al. Perfect Selective Alignment of Nitrogen-Vacancy Centers in Diamond. *Appl. Phys. Express* **2014**, *7*, 055201.

- (105) Ozawa, H.; Tahara, K.; Ishiwata, H.; Hatano, M.; Iwasaki, T. Formation of Perfectly Aligned Nitrogen-Vacancy-Center Ensembles in Chemical-Vapour-Deposition-Grown Diamond (111). *Appl. Phys. Express* **2017**, *10*, 045501.
- (106) Ishiwata, H.; Nakajima, M.; Tahara, K.; Ozawa, H.; Iwasaki, T.; Hatano, M. Perfectly Aligned Shallow Ensemble Nitrogen-Vacancy Centers in (111) Diamond. *Appl. Phys. Lett.* **2017**, *111*, 043103.
- (107) Tallaire, A.; Mayer, L.; Brinza, O.; Pinault-Thaury, M. A.; Debuisschert, T.; Achard, J. Highly Photostable NV Centre Ensembles in CVD Diamond Produced by using N₂O as the Doping Gas. *Appl. Phys. Lett.* **2017**, *111*, 143101.
- (108) Miyazaki, T.; Miyamoto, Y.; Makino, T.; Kato, H.; Yamasaki, S.; Fukui, T.; Doi, Y.; Tokuda, N.; Hatano, M.; Mizuoichi, N. Atomistic Mechanism of Perfect Alignment of Nitrogen-Vacancy Centers in Diamond. *Appl. Phys. Lett.* **2014**, *105*, 261601.
- (109) Karin, T.; Dunham, S.; Fu, K.-M. Alignment of the Diamond Nitrogen Vacancy Center by Strain Engineering. *Appl. Phys. Lett.* **2014**, *105*, 053106.
- (110) Ma, J.; Richley, J. C.; Davies, D. R. W.; Ashfold, M. N. R.; Mankelevich, Yu. A. Spectroscopic and Modeling Investigations of the Gas Phase Chemistry and Composition in Microwave Plasma Activated B₂H₆/CH₄/Ar/H₂ Gas Mixtures. *J. Phys. Chem. A* **2010**, *114*, 10076–10089.
- (111) May, P. W.; Ludlow, W. J.; Hannaway, M.; Heard, P. J.; Smith, J. A.; Rosser, K. N. Raman and Conductivity Studies of Boron Doped Microcrystalline Diamond, Facetted Nanocrystalline Diamond and Cauliflower Diamond Films. *Diamond Relat. Mater.* **2008**, *17*, 105–117.
- (112) Zhang, G.; Zeleznik, M.; Vanacken, J.; May, P. W.; Moshchalkov, V. V. Metal-Bosonic Insulator-Superconductor Transition in Boron-Doped Granular Diamond. *Phys. Rev. Lett.* **2013**, *110*, 077001.
- (113) Achard, J.; Silva, F.; Issaoui, R.; Brinza, O.; Tallaire, A.; Schneider, H.; Isoird, K.; Ding, H.; Koné, S.; Pinault, M. A.; et al. Thick Boron Doped Diamond Single Crystals for High Power Electronics. *Diamond Relat. Mater.* **2011**, *20*, 145–152.
- (114) Truscott, B. S.; Turner, C.; May, P. W. High-Pressure DC Glow Discharges in Hollow Diamond Cathodes. *Plasma Sources Sci. Technol.* **2016**, *25*, 025005.
- (115) Nistor, P. A.; May, P. W. Diamond Thin Films: Giving Biomedical Applications a New Shine. *J. R. Soc., Interface* **2017**, *14*, 20170382.
- (116) Granger, M. C.; Witek, M.; Xu, J. S.; Wang, J.; Hupert, M.; Hanks, A.; Koppang, M. D.; Butler, J. E.; Lucazeau, G.; Mermoux, M.; et al. Standard Electrochemical Behavior of High-Quality, Boron-Doped Polycrystalline Diamond Thin-Film Electrodes. *Anal. Chem.* **2000**, *72*, 3793–3804.
- (117) Luong, J. H. T.; Male, K. B.; Glennon, J. D. Boron-Doped Diamond Electrode: Synthesis, Characterization, Functionalization and Analytical Applications. *Analyst* **2009**, *134*, 1965–1979.
- (118) Macpherson, J. V. A Practical Guide to Using Boron Doped Diamond in Electrochemical Research. *Phys. Chem. Chem. Phys.* **2015**, *17*, 2935–2949.
- (119) Chaplin, B. P. Critical Review of Electrochemical Advanced Oxidation Processes for Water Treatment Applications. *Environ. Sci. Proc. Impacts* **2014**, *16*, 1182–1203.
- (120) Kalish, R. The Search for Donors in Diamond. *Diamond Relat. Mater.* **2001**, *10*, 1749–1755.
- (121) Koeck, F. A. M.; Garguilo, J. M.; Nemanich, R. J. On the Thermionic Emission from Nitrogen-Doped Diamond Films with Respect to Energy Conversion. *Diamond Relat. Mater.* **2004**, *13*, 2052–2055.
- (122) Kataoka, M.; Zhu, C.; Koeck, F. A. M.; Nemanich, R. J. Thermionic Electron Emission from Nitrogen-Doped Homoepitaxial Diamond. *Diamond Relat. Mater.* **2010**, *19*, 110–113.
- (123) Majchrowicz, D.; Kosowska, M.; Sankaran, K. J.; Struk, P.; Wąsowicz, M.; Sobaszek, M.; Haenen, K.; Jędrzejewska-Szczerska, M. Nitrogen-Doped Diamond Film for Optical Investigation of Hemoglobin Concentration. *Materials* **2018**, *11*, 109.
- (124) Descamps, C.; Tromson, D.; Guerrero, M. J.; Mer, C.; Rzepka, E.; Nesladek, M.; Bergonzo, P. Nitrogen-Doped Diamond: Thermoluminescence and Dosimetric Applications. *Diamond Relat. Mater.* **2006**, *15*, 833–837.
- (125) Jackson, M. J.; Ahmed, W. Fabrication and Wear of Nitrogen-Doped Diamond Microtools. *Int. J. Nanomanuf.* **2007**, *1*, 439–453.
- (126) Croot, A.; Othman, M. Z.; Conejeros, S.; Fox, N. A.; Allan, N. L. A Theoretical Study of Substitutional Boron–Nitrogen Clusters in Diamond. *J. Phys.: Condens. Matter* **2018**, *30*, 425501.
- (127) Halliwell, S. C.; May, P. W.; Fox, N. A.; Othman, M. Z. Investigations of the Co-Doping of Boron and Lithium into CVD Diamond Thin Films. *Diamond Relat. Mater.* **2017**, *76*, 115–122.
- (128) Othman, M. Z.; May, P. W.; Fox, N. A.; Heard, P. J. Incorporation of Lithium and Nitrogen into CVD Diamond Thin Films. *Diamond Relat. Mater.* **2014**, *44*, 1–7.
- (129) Bhattacharyya, S.; Auciello, O.; Birrell, J.; Carlisle, J. A.; Curtiss, L. A.; Goyette, A. N.; Gruen, D. M.; Krauss, A. R.; Schlueter, J.; Sumant, A.; et al. Synthesis and Characterization of Highly-Conducting Nitrogen-Doped Ultrananocrystalline Diamond Films. *Appl. Phys. Lett.* **2001**, *79*, 1441–1443.
- (130) Williams, O. A.; Zimmermann, T.; Kubovic, M.; Denisenko, A.; Kohn, E.; Jackman, R. B.; Gruen, D. M. Electronic Properties and Applications of Ultrananocrystalline Diamond. In *Synthesis, Properties and Applications of Ultrananocrystalline Diamond*, NATO Science Series Series II: Mathematics, Physics and Chemistry; Gruen, D. M., Shenderova, O. A., Vul', A. Y., Eds.; Springer: Dordrecht, 2005; Vol. 192, pp 373–382.
- (131) Birrell, J.; Carlisle, J. A.; Auciello, O.; Gruen, D. M.; Gibson, J. M. Morphology and Electronic Structure in Nitrogen-Doped Ultrananocrystalline Diamond. *Appl. Phys. Lett.* **2002**, *81*, 2235–2237.
- (132) Auciello, O.; Sumant, A. V. Status Review of the Science and Technology of Ultrananocrystalline diamond (UNCD™) Films and Application to Multifunctional Devices. *Diamond Relat. Mater.* **2010**, *19*, 699–718.
- (133) Williams, O. A. Ultrananocrystalline Diamond for Electronic Applications. *Semicond. Sci. Technol.* **2006**, *21*, R49–R56.
- (134) Nunn, N.; Torelli, M.; McGuire, G.; Shenderova, O. Nanodiamond: A High Impact Nanomaterial. *Curr. Opin. Solid State Mater. Sci.* **2017**, *21*, 1–9.
- (135) Filik, J. Diamondoid Hydrocarbons. In *Carbon Based Nanomaterials*, Materials Science Foundations (monograph series); Ali, N., Öchsner, A., Ahmed, W., Eds.; Trans Tech, Switzerland, 2010; Chapter 1, pp 65–66, 1–26.
- (136) Dahl, J. E.; Liu, S. G.; Carlson, R. M. K. Isolation and Structure of Higher Diamondoids, Nanometer-Sized Diamond Molecules. *Science* **2003**, *299*, 96–99.
- (137) Dahl, J. E. P.; Moldovan, J. M.; Peakman, T. M.; Clardy, J. C.; Lobkovsky, E.; Olmstead, M. M.; May, P. W.; Davis, T. J.; Steeds, J. W.; Peters, K. E.; et al. Isolation and Structural Proof of the Large Diamond Molecule, Cyclohexamantane (C₂₆H₃₀). *Angew. Chem., Int. Ed.* **2003**, *42*, 2040–2044.
- (138) Gunawan, M. A.; Hierso, J.-C.; Poinot, D.; Fokin, A. A.; Fokina, N. A.; Tkachenko, B. A.; Schreiner, P. R. Diamondoids: Functionalization and Subsequent Applications of Perfectly Defined Molecular Cage Hydrocarbons. *New J. Chem.* **2014**, *38*, 28–41.
- (139) Sivaraman, G.; Fyta, M. Chemically Modified Diamondoids as Biosensors for DNA. *Nanoscale* **2014**, *6*, 4225–4232.
- (140) Mochalin, V. N.; Shenderova, O.; Ho, D.; Gogotsi, Y. The properties and applications of nanodiamonds. *Nat. Nanotechnol.* **2012**, *7*, 11–23.
- (141) Kuznetsov, V. L.; Aleksandrov, M. N.; Zagoruiko, I. V.; Chuvilin, A. L.; Moroz, E. M.; Kolomiichuk, V. N.; Likhoholov, V. A.; Brylyakov, P. M.; Sakovitch, G. V. Study of Ultradispersed Diamond Powders Obtained Using Explosive Energy. *Carbon* **1991**, *29*, 665–668.

- (142) Dolmatov, V.; Veretennikova, M.; Marchukov, V.; Sushchev, V. Currently Available Methods of Industrial Nanodiamond Synthesis. *Phys. Solid State* **2004**, *46*, 611–615.
- (143) Shakun, A.; Vuorinen, J.; Hoikkanen, M.; Poikelispää, M.; Das, A. Hard Nanodiamonds in Soft Rubbers: Past, Present and Future – A Review. *Composites, Part A* **2014**, *64*, 49–69.
- (144) Vlasov, I. I.; Shenderova, O.; Turner, S.; Lebedev, O. I.; Basov, A. A.; Sildos, I.; Rahn, M.; Shiryayev, A. A.; van Tendeloo, G. Nitrogen and Luminescent Nitrogen-Vacancy Defects in Detonation Nanodiamond. *Small* **2010**, *6*, 687–694.
- (145) Shenderova, O. A.; Vlasov, I. I.; Turner, S.; Van Tendeloo, G.; Orlinskii, S. B.; Shiryayev, A. A.; Khomich, A. A.; Sulyanov, S. N.; Jelezko, F.; Wrachtrup, J. Nitrogen Control in Nanodiamond Produced by Detonation Shock-Wave-Assisted Synthesis. *J. Phys. Chem. C* **2011**, *115*, 14014–14024.
- (146) Krueger, A. The Structure and Reactivity of Nanoscale Diamond. *J. Mater. Chem.* **2008**, *18*, 1485–1492.
- (147) Krueger, A.; Ozawa, M.; Jarre, G.; Liang, Y.; Stegk, J.; Lu, L. Deagglomeration and Functionalisation of Detonation Diamond. *Phys. Status Solidi A* **2007**, *204*, 2881–2887.
- (148) Barnard, A. S.; Russo, S. P.; Snook, I. K. Coexistence of Bucky Diamond with Nanodiamond and Fullerene Carbon Phases. *Phys. Rev. B: Condens. Matter Mater. Phys.* **2003**, *68*, 073406.
- (149) Barnard, A. S.; Sternberg, M. Substitutional Nitrogen in Nanodiamond and Bucky-Diamond Particles. *J. Phys. Chem. B* **2005**, *109*, 17107–17112.
- (150) Krueger, A.; Lang, D. Functionality is Key: Recent Progress in the Surface Modification of Nanodiamond. *Adv. Funct. Mater.* **2012**, *22*, 890–906.
- (151) Williams, O. A.; Hees, J.; Dieker, C.; Jäger, W.; Kirste, L.; Nebel, C. E. Size-Dependent Reactivity of Diamond Nanoparticles. *ACS Nano* **2010**, *4*, 4824–4830.
- (152) Liu, Y.; Gu, Z.; Margrave, J. L.; Khabashesku, V. N. Functionalization of Nanoscale Diamond Powder: Fluoro-, Alkyl-, Amino-, and Amino Acid-Nanodiamond Derivatives. *Chem. Mater.* **2004**, *16*, 3924–3930.
- (153) Krüger, A.; Liang, Y.; Jarre, G.; Stegk, J. Surface Functionalisation of Detonation Diamond Suitable for Biological Applications. *J. Mater. Chem.* **2006**, *16*, 2322–2328.
- (154) Yeap, W. S.; Chen, S.; Loh, K. P. Detonation Nanodiamond: An Organic Platform for the Suzuki Coupling of Organic Molecules. *Langmuir* **2009**, *25*, 185–191.
- (155) Hens, S. C.; Cunningham, G.; Tyler, T.; Moseenkov, S.; Kuznetsov, V.; Shenderova, O. Nanodiamond Bioconjugate Probes and their Collection by Electrophoresis. *Diamond Relat. Mater.* **2008**, *17*, 1858–1866.
- (156) Mochalin, V. N.; Gogotsi, Y. Wet Chemistry Route to Hydrophobic Blue Fluorescent Nanodiamond. *J. Am. Chem. Soc.* **2009**, *131*, 4594–4595.
- (157) Boudou, J.-P.; Curmi, P. A.; Jelezko, F.; Wrachtrup, J.; Aubert, P.; Sennour, M.; Balasubramanian, G.; Reuter, R.; Thorel, A.; Gaffet, E. High Yield Fabrication of Fluorescent Nanodiamonds. *Nanotechnology* **2009**, *20*, 235602; **2009**, *20*, 359801.
- (158) Yang, L.; May, P. W.; Yin, L.; Smith, J. A.; Rosser, K. N. Growth of Diamond Nanocrystals by Pulsed Laser Ablation of Graphite in Liquid. *Diamond Relat. Mater.* **2007**, *16*, 725–729.
- (159) Amans, D.; Chenu, A.; Ledoux, G.; Dujardin, C.; Reynaud, C.; Sublemontier, O.; Masenelli-Varlot, K.; Guillois, O. Nanodiamond Synthesis by Pulsed Laser Ablation in Liquids. *Diamond Relat. Mater.* **2009**, *18*, 177–180.
- (160) Ray Techniques, Ltd. Nanodiamond technologies. <http://www.nanodiamond.co.il/>.
- (161) Yang, L.; May, P. W.; Yin, L.; Huang, Y.; Smith, J. A.; Scott, T. B. Symmetric Organization of Self-Assembled Carbon Nitride. *Nanotechnology* **2007**, *18*, 335605.
- (162) Dresselhaus, M. S.; Kalish, R. *Ion Implantation in Diamond, Graphite and Related Materials*; Springer Science: Berlin, 2013.
- (163) Braunstein, G.; Kalish, R. Effective *p*-type Doping of Diamond by Boron Ion Implantation. *J. Appl. Phys.* **1983**, *54*, 2106–2108.
- (164) Praver, S.; Uzan-Saguy, C.; Braunstein, G.; Kalish, R. Can *n*-type Doping of Diamond be Achieved by Li or Na Ion-Implantation? *Appl. Phys. Lett.* **1993**, *63*, 2502–2504.
- (165) Meijer, J.; Burchard, B.; Domhan, M.; Wittmann, C.; Gaebel, T.; Popa, I.; Jelezko, F.; Wrachtrup, J. Generation of Single Color Centers by Focused Nitrogen Implantation. *Appl. Phys. Lett.* **2005**, *87*, 261909.
- (166) Rabeau, J. R.; Reichart, P.; Tamanyan, G.; Jamieson, D. N.; Praver, S.; Jelezko, F.; Gaebel, T.; Popa, I.; Domhan, M.; Wrachtrup, J. Implantation of Labelled Single Nitrogen Vacancy Centers in Diamond using ¹⁵N. *Appl. Phys. Lett.* **2006**, *88*, 023113.
- (167) Weis, C. D.; Schuh, A.; Batra, A.; Persaud, A.; Rangelow, I. W.; Bokor, J.; Lo, C. C.; Cabrini, S.; Sideras-Haddad, E.; Fuchs, G. D.; et al. Single Atom Doping for Quantum Device Development in Diamond and Silicon. *J. Vac. Sci. Technol. B. Microelec. Nanometer Struct. Proc. Meas. Phenom.* **2008**, *26*, 2596–2600.
- (168) Naydenov, B.; Reinhard, F.; Lämmle, A.; Richter, V.; Kalish, R.; D’Haenens-Johansson, U. F. S.; Newton, M.; Jelezko, F.; Wrachtrup, J. Increasing the Coherence Time of Single Electron Spins in Diamond by High Temperature Annealing. *Appl. Phys. Lett.* **2010**, *97*, 242511.
- (169) Kalish, R.; Uzan-Saguy, C.; Philosoph, B.; Richter, V.; Lagrange, J. P.; Gheeraert, E.; Deneuille, A.; Collins, A. T. Nitrogen Doping of Diamond by Ion Implantation. *Diamond Relat. Mater.* **1997**, *6*, 516–520.
- (170) Deák, P.; Aradi, B.; Kaviani, M.; Frauenheim, T.; Gali, A. Formation of NV Centers in Diamond: A Theoretical Study Based on Calculated Transitions and Migration of Nitrogen and Vacancy Related Defects. *Phys. Rev. B: Condens. Matter Mater. Phys.* **2014**, *89*, 075203.
- (171) Iakubovskii, K.; Adriaenssens, G. J. Trapping of Vacancies by Defects in Diamond. *J. Phys.: Condens. Matter* **2001**, *13*, 6015–6018.
- (172) Dyer, H. B.; Raal, F. A.; Du Preez, L.; Loubser, J. H. N. Optical Absorption Features Associated with Paramagnetic Nitrogen in Diamond. *Philos. Mag.* **1965**, *11*, 763–774.
- (173) Mildren, R. P. Intrinsic Optical Properties of Diamond. In *Optical Engineering of Diamond*, Mildren, R. P., Rabeau, J., Eds.; Wiley Online Books, 2013; pp 1–34.
- (174) Hainschwang, T. Gemstone Analysis by Spectroscopy. In *Encyclopedia of Spectroscopy and Spectrometry*, 3rd ed.; Lindon, J. C., Tranter, G. E., Koppenaal, D. W., Eds.; Elsevier, 2017; pp 18–24.
- (175) Zaitsev, A. M. *Optical Properties of Diamond*; Springer: Berlin, 2001.
- (176) Dischler, B. *Handbook of Spectral Lines in Diamond*; Springer: Berlin, 2012.
- (177) Kaplyanskii, A. A. Noncubic Centers in Cubic Crystals and Their Piezospectroscopic Investigation. *Opt. Spectrosc.* **1964**, *16*, 329–337.
- (178) Kaplyanskii, A. A. Computation of Deformation of Splitting of Spectral Transitions in Cubic Crystals. *Opt. Spectrosc.* **1964**, *16*, 557–565.
- (179) Hughes, A. E.; Runciman, W. A. Uniaxial Stress Splitting of Doubly Degenerate States of Tetragonal and Trigonal Centres in Cubic Crystals. *Proc. Phys. Soc., London* **1967**, *90*, 827–838.
- (180) Davies, G.; Nazaré, M. H. Uniaxial Stress Splitting of *e* to *e* Transitions at Trigonal Centres in Cubic Crystals: The 594 nm Band in Diamond. *J. Phys. C: Solid State Phys.* **1980**, *13*, 4127–4136.
- (181) Mohammed, K.; Davies, G.; Collins, A. T. Uniaxial Stress Splitting of Photoluminescence Transitions at Optical Centres in Cubic Crystals: Theory and Application to Diamond. *J. Phys. C: Solid State Phys.* **1982**, *15*, 2779–2788.
- (182) Runciman, W. A. Stress Spectra of Defects in Diamond. *Proc. Phys. Soc., London* **1965**, *86*, 629–636.
- (183) Green, B. L.; Doherty, M. W.; Nako, E.; Manson, N. B.; D’Haenens-Johansson, U. F. S.; Williams, S. D.; Twitchen, D. J.; Newton, M. E. Electronic Structure of the Neutral Silicon-Vacancy Center in Diamond. *Phys. Rev. B: Condens. Matter Mater. Phys.* **2019**, *99*, 161112.

- (184) Rogers, L. J.; Doherty, M. W.; Barson, M. S. J.; Onoda, S.; Ohshima, T.; Manson, N. B. Singlet Levels of the NV⁻ Centre in Diamond. *New J. Phys.* **2015**, *17*, 013048.
- (185) de Sa, E. S.; Davies, G. Uniaxial Stress Studies of the 2.498 eV (H4), 2.417 and 2.536 eV Vibronic Bands in Diamond. *Proc. R. Soc. London, Ser. A* **1977**, *357*, 231–251.
- (186) Sternschulte, H.; Thonke, K.; Gerster, J.; Limmer, W.; Sauer, R.; Spitzer, J.; Münzinger, P. C. Uniaxial Stress and Zeeman Splitting of the 1.681 eV Optical Center in a Homoepitaxial CVD Diamond Film. *Diamond Relat. Mater.* **1995**, *4*, 1189–1192.
- (187) Davies, G.; Hamer, M. F. Optical Studies of the 1.945 eV Vibronic Band in Diamond. *Proc. R. Soc. London, Ser. A* **1976**, *348*, 285–298.
- (188) Smith, H. E.; Davies, G.; Newton, M. E.; Kanda, H. Structure of the Self-Interstitial in Diamond. *Phys. Rev. B: Condens. Matter Mater. Phys.* **2004**, *69*, 045203.
- (189) Walker, J. Optical Absorption and Luminescence in Diamond. *Rep. Prog. Phys.* **1979**, *42*, 1605–1659.
- (190) McCluskey, M. D. Local Vibrational Modes of Impurities in Semiconductors. *J. Appl. Phys.* **2000**, *87*, 3593–3617.
- (191) Woods, G. S.; Collins, A. T. The 1450 cm⁻¹ Infrared Absorption in Annealed, Electron-Irradiated Type I Diamonds. *J. Phys. C: Solid State Phys.* **1982**, *15*, L949–L952.
- (192) Woods, G. S.; Collins, A. T. Infrared Absorption Spectra of Hydrogen Complexes in Type I Diamonds. *J. Phys. Chem. Solids* **1983**, *44*, 471–475.
- (193) Kiflawi, I.; Fisher, D.; Kanda, H.; Sittas, G. The Creation of the 3107 cm⁻¹ Hydrogen Absorption Peak in Synthetic Diamond Single Crystals. *Diamond Relat. Mater.* **1996**, *5*, 1516–1518.
- (194) Goss, J. P.; Briddon, P. R.; Hill, V.; Jones, R.; Rayson, M. J. Identification of the Structure of the 3107 cm⁻¹ H-Related Defect in Diamond. *J. Phys.: Condens. Matter* **2014**, *26*, 145801.
- (195) Davies, G.; Stavola, M. Optical Measurements of Point Defects. *Semiconductors and Semimetals* **1998**, *51B*, 1–92.
- (196) Hughes, A. E. Isotope Shifts for Zero-Phonon and Phonon-Assisted Transitions in Lithium Fluoride. *Proc. Phys. Soc., London* **1966**, *88*, 449–462.
- (197) Collins, A. T.; Davies, G.; Kanda, H.; Woods, G. S. Spectroscopic Studies of Carbon-13 Synthetic Diamond. *J. Phys. C: Solid State Phys.* **1988**, *21*, 1363–1376.
- (198) Davies, G.; Kiflawi, I.; Sittas, G.; Kanda, H. The Effects of Carbon and Nitrogen Isotopes on the 'N3' Optical Transition in Diamond. *J. Phys.: Condens. Matter* **1997**, *9*, 3871–3879.
- (199) Iakoubovskii, K.; Davies, G. Vibronic Effects in the 1.4-eV Optical Center in Diamond. *Phys. Rev. B: Condens. Matter Mater. Phys.* **2004**, *70*, 245206.
- (200) Clark, C. D.; Kanda, H.; Kiflawi, I.; Sittas, G. Silicon Defects in Diamond. *Phys. Rev. B: Condens. Matter Mater. Phys.* **1995**, *51*, 16681–16688.
- (201) D'Haenens-Johansson, U. F. S.; Edmonds, A. M.; Green, B. L.; Newton, M. E.; Davies, G.; Martineau, P. M.; Khan, R. U. A.; Twitchen, D. J. Optical Properties of the Neutral Silicon Split-Vacancy Center in Diamond. *Phys. Rev. B: Condens. Matter Mater. Phys.* **2011**, *84*, 245208.
- (202) Balasubramanian, G.; Neumann, P.; Twitchen, D.; Markham, M.; Kolesov, R.; Mizuochi, N.; Isoya, J.; Achard, J.; Beck, J.; Tisler, J.; et al. Ultralong Spin Coherence Time in Isotopically Engineered Diamond. *Nat. Mater.* **2009**, *8*, 383–387.
- (203) Green, B. L.; Mottishaw, S.; Breeze, B. G.; Edmonds, A. M.; D'Haenens-Johansson, U. F. S.; Doherty, M. W.; Williams, S. D.; Twitchen, D. J.; Newton, M. E. Neutral Silicon-Vacancy Center in Diamond: Spin Polarization and Lifetimes. *Phys. Rev. Lett.* **2017**, *119*, 096402.
- (204) Rose, B. C.; Huang, D.; Zhang, Z.-H.; Stevenson, P.; Tyrshkin, A. M.; Sangtawesin, S.; Srinivasan, S.; Loudin, L.; Markham, M. L.; Edmonds, A. M.; et al. Observation of an Environmentally Insensitive Solid-State Spin Defect in Diamond. *Science* **2018**, *361*, 60–63.
- (205) Weil, J. A.; Bolton, J. R. *Electron Paramagnetic Resonance*, 2nd ed.; John Wiley & Sons: Hoboken, 2007.
- (206) Abragam, A.; Bleaney, B. *Electron Paramagnetic Resonance of Transition Ions*, 2nd ed.; Dover Publications, Inc.: New York, 2015.
- (207) Poole, C. P. *Electron Spin Resonance*, 2nd ed.; Dover Publications, Inc.: New York, 1983.
- (208) Eaton, G. R.; Eaton, S. S.; Barr, D. P.; Weber, R. T. *Quantitative EPR*; Springer: New York, 2010.
- (209) Eaton, S. S.; Eaton, G. R. The World as Viewed by and with Unpaired Electrons. *J. Magn. Reson.* **2012**, *223*, 151–163.
- (210) Loubser, J. H. N.; van Wyk, J. A. Electron Spin Resonance in the Study of Diamond. *Rep. Prog. Phys.* **1978**, *41*, 1201–1248.
- (211) Newton, M. E. Electron Paramagnetic Resonance of Radiation Damage Centres in Diamond. In *Properties and Growth of Diamond*; Davies, G., Ed.; IEE - Inspec, 1994; p 153.
- (212) Newton, M. E. EPR, ENDOR and EPR Imaging of Defects in Diamond. In *Electron Paramagnetic Resonance*; The Royal Society of Chemistry, 2007; Vol. 20, pp 131–156.
- (213) Impurities and Defects in Group IV Elements, IV–IV and III–V Compounds. Part a: Group IV Elements; *Landolt–Börnstein–Group III Condensed Matter*; Madelung, O., Rössler, U., Schulz, M., Eds.; Springer: Berlin, 2002; 41A2a.
- (214) Nadolinny, V.; Komarovskikh, A.; Palyanov, Y. Incorporation of Large Impurity Atoms into the Diamond Crystal Lattice: EPR of Split-Vacancy Defects in Diamond. *Crystals* **2017**, *7*, 237.
- (215) Mitchell, D. G.; Tseitlin, M.; Quine, R. W.; Meyer, V.; Newton, M. E.; Schnegg, A.; George, B.; Eaton, S. S.; Eaton, G. R. X-Band Rapid-Scan EPR of Samples with Long Electron Spin Relaxation Times: A Comparison of Continuous Wave, Pulse and Rapid-Scan EPR. *Mol. Phys.* **2013**, *111*, 2664–2673.
- (216) Loubser, J. H. N.; Van Wyk, J. A. Optical Spin-Polarisation in a Triplet State in Irradiated and Annealed Type 1b Diamonds. *Diam. Res.* **1977**, *11*, 11–14.
- (217) Hepp, C.; Müller, T.; Waselowski, V.; Becker, J. N.; Pingault, B.; Sternschulte, H.; Steinmüller-Nethl, D.; Gali, A.; Maze, J. R.; Atatüre, M.; et al. Electronic Structure of the Silicon Vacancy Color Center in Diamond. *Phys. Rev. Lett.* **2014**, *112*, 036405.
- (218) Pingault, B.; Becker, J. N.; Schulte, C. H. H.; Arend, C.; Hepp, C.; Godde, T.; Tartakovskii, A. I.; Markham, M.; Becher, C.; Atatüre, M. All-Optical Formation of Coherent Dark States of Silicon-Vacancy Spins in Diamond. *Phys. Rev. Lett.* **2014**, *113*, 263601.
- (219) Siyushev, P.; Metsch, M. H.; Ijaz, A.; Binder, J. M.; Bhaskar, M. K.; Sukachev, D. D.; Sipahigil, A.; Evans, R. E.; Nguyen, C. T.; Lukin, M. D.; et al. Optical and Microwave Control of Germanium-Vacancy Center Spins in Diamond. *Phys. Rev. B: Condens. Matter Mater. Phys.* **2017**, *96*, 081201.
- (220) Thiering, G.; Gali, A. Ab Initio Magneto-Optical Spectrum of Group-IV-Vacancy Color Centers in Diamond. *Phys. Rev. X* **2018**, *8*, 021063.
- (221) Lee, S.; Widmann, M.; Rendler, T.; Doherty, M. W.; Babinec, T. M.; Yang, S.; Eyer, M.; Siyushev, P.; Hausmann, B. J. M.; Loncar, M.; et al. Readout and Control of a Single Nuclear Spin with a Metastable Electron Spin Ancilla. *Nat. Nanotechnol.* **2013**, *8*, 487–492.
- (222) Douglas, I. N.; Runciman, W. A. The Magnetic Circular Dichroism Spectrum of the GR1 Line in Irradiated Diamonds. *J. Phys. C: Solid State Phys.* **1977**, *10*, 2253–2259.
- (223) Douglas, I. N.; Runciman, W. A. Application of Magnetic Circular Dichroism Spectroscopy to the Optical Spectra of Natural and Irradiated Diamonds. *Phys. Chem. Miner.* **1977**, *1*, 129–136.
- (224) Jelezko, F.; Wrachtrup, J. Single Defect Centres in Diamond: A Review. *Phys. Status Solidi A* **2006**, *203*, 3207–3225.
- (225) Pezzagna, S.; Meijer, J. Single-Ion Implantation in Diamond with a High Lateral Resolution: A Key Technology for the Fabrication of Quantum Devices. In *Comprehensive Hard Materials*; Sarin, V. K., Ed.; Elsevier: Oxford, UK, 2014; pp 321–336.
- (226) Zapol, P.; Sternberg, M.; Curtiss, L. A.; Frauenheim, T.; Gruen, D. M. Tight-Binding Molecular-Dynamics Simulation of

Impurities in Ultrananocrystalline Diamond Grain Boundaries. *Phys. Rev. B: Condens. Matter Mater. Phys.* **2001**, *65*, 454031.

(227) Heyd, J.; Scuseria, G. E.; Ernzerhof, M. Hybrid Functionals Based on a Screened Coulomb Potential. *J. Chem. Phys.* **2003**, *118*, 8207–8215.

(228) Thiering, G.; Gali, A. Theory of the Optical Spin-Polarization Loop of the Nitrogen-Vacancy Center in Diamond. *Phys. Rev. B: Condens. Matter Mater. Phys.* **2018**, *98*, 085207.

(229) Thiering, G.; Gali, A. The $(e_g \otimes e_u) \otimes e_g$ Product Jahn–Teller Effect in the Neutral Group-IV Vacancy Quantum Bits in Diamond. *npj Comput. Mater.* **2019**, *5*, 18.

(230) Hertkorn, J.; Wrachtrup, J.; Fyta, M. Vacancy Defect Centers in Diamond: Influence of Surface Termination. *Eur. Phys. J.: Spec. Top.* **2019**, *227*, 1591–1601.

(231) Goss, J. P.; Briddon, P. R.; Pinto, H.; Jones, R. Optically Active Point Defects in High Quality Single Crystal Diamond. *Phys. Status Solidi A* **2010**, *207*, 2049–2053.

(232) Liggins, S.; Newton, M. E.; Goss, J. P.; Briddon, P. R.; Fisher, D. Identification of the Dinitrogen (001) Split Interstitial H1a in Diamond. *Phys. Rev. B: Condens. Matter Mater. Phys.* **2010**, *81*, 085214.

(233) Goss, J. P.; Briddon, P. R.; Jones, R.; Sque, S. Donor and Acceptor States in Diamond. *Diamond Relat. Mater.* **2004**, *13*, 684–690.

(234) Häußler, S.; Thiering, G.; Dietrich, A.; Waasem, N.; Teraji, T.; Isoya, J.; Iwasaki, T.; Hatano, M.; Jelezko, F.; Gali, A.; et al. Photoluminescence Excitation Spectroscopy of SiV- and GeV- Color Center in Diamond. *New J. Phys.* **2017**, *19*, 063036.

(235) Pfender, M.; Aslam, N.; Simon, P.; Antonov, D.; Thiering, G.; Burk, S.; Fávoro De Oliveira, F.; Denisenko, A.; Fedder, H.; Meijer, J.; et al. Protecting a Diamond Quantum Memory by Charge State Control. *Nano Lett.* **2017**, *17*, 5931–5937.

(236) Goldman, M. L.; Sipahigil, A.; Doherty, M. W.; Yao, N. Y.; Bennett, S. D.; Markham, M.; Twitchen, D. J.; Manson, N. B.; Kubanek, A.; Lukin, M. D. Phonon-Induced Population Dynamics and Intersystem Crossing in Nitrogen-Vacancy Centers. *Phys. Rev. Lett.* **2015**, *114*, 145502.

(237) Atumi, M. K.; Goss, J. P.; Briddon, P. R.; Rayson, M. J. Atomistic Modeling of the Polarization of Nitrogen Centers in Diamond Due to Growth Surface Orientation. *Phys. Rev. B: Condens. Matter Mater. Phys.* **2013**, *88*, 245301.

(238) Zou, Y.; Larsson, K. Effect of Boron Doping on the CVD Growth Rate of Diamond. *J. Phys. Chem. C* **2016**, *120*, 10658–10666.

(239) Etmimi, K.; Ahmed, M.; Briddon, P.; Goss, J.; Gsies, A. Nitrogen-Pair Paramagnetic Defects in Diamond: A Density Functional Study. *Phys. Rev. B: Condens. Matter Mater. Phys.* **2009**, *79*, 205207.

(240) Gali, A.; Fyta, M.; Kaxiras, E. *Ab Initio* Supercell Calculations on Nitrogen-Vacancy Center in Diamond: Electronic Structure and Hyperfine Tensors. *Phys. Rev. B: Condens. Matter Mater. Phys.* **2008**, *77*, 155206.

(241) Peaker, C. V.; Atumi, M. K.; Goss, J. P.; Briddon, P. R.; Horsfall, A. B.; Rayson, M. J.; Jones, R. Assignment of ^{13}C Hyperfine Interactions in the P1-Center in Diamond. *Diamond Relat. Mater.* **2016**, *70*, 118–123.

(242) Meng, Y.-F.; Yan, C.-S.; Lai, J.; Krasnicki, S.; Shu, H.; Yu, T.; Liang, Q.; Mao, H.-K.; Hemley, R. J. Enhanced Optical Properties of Chemical Vapor Deposited Single Crystal Diamond by Low-Pressure/High-Temperature Annealing. *Proc. Natl. Acad. Sci. U. S. A.* **2008**, *105*, 17620–17625.

(243) Kazuchits, N. M.; Rusetsky, M. S.; Kazuchits, V. N.; Zaitsev, A. M. Aggregation of Nitrogen in Synthetic Diamonds Annealed at High Temperature without Stabilizing Pressure. *Diamond Relat. Mater.* **2016**, *64*, 202–207.

(244) Kazuchits, N. M.; Rusetsky, M. S.; Kazuchits, V. N.; Korolik, O. V.; Kumar, V.; Moe, K. S.; Wang, W.; Zaitsev, A. M. Comparison of HPHT and LPHT Annealing of Ib Synthetic Diamond. *Diamond Relat. Mater.* **2019**, *91*, 156–164.

(245) Khan, R. U. A.; Martineau, P. M.; Cann, B. L.; Newton, M. E.; Twitchen, D. J. Charge Transfer Effects, Thermo and Photochromism in Single Crystal CVD Synthetic Diamond. *J. Phys.: Condens. Matter* **2009**, *21*, 364214.

(246) Mäki, J.-M.; Tuomisto, F.; Varpula, A.; Fisher, D.; Khan, R. U. A.; Martineau, P. M. Time Dependence of Charge Transfer Processes in Diamond Studied with Positrons. *Phys. Rev. Lett.* **2011**, *107*, 217403.

(247) Cox, A.; Newton, M. E.; Baker, J. M. ENDOR Studies on the N1 Di-Nitrogen Centre in Diamond. *J. Phys.: Condens. Matter* **1992**, *4*, 8119–8130.

(248) Newton, M. E.; Baker, J. M. ENDOR Studies on the W7 Di-Nitrogen Centre in Brown Diamond. *J. Phys.: Condens. Matter* **1991**, *3*, 3591–3603.

(249) Mineeva, R. M.; Titkov, S. V.; Speransky, A. V. Structural Defects in Natural Plastically Deformed Diamonds: Evidence from EPR Spectroscopy. *Geol. Ore Deposits* **2009**, *51*, 233–242.

(250) Mehandru, S. P.; Anderson, A. B. The Migration of Interstitial H in Diamond and its Pairing with Substitutional B and N: Molecular Orbital Theory. *J. Mater. Res.* **1994**, *9*, 383–395.

(251) Burns, R. C.; Cvetkovic, V.; Dodge, C. N.; Evans, D. J. F.; Rooney, M.-L. T.; Spear, P. M.; Welbourn, C. M. Growth-Sector Dependence of Optical Features in Large Synthetic Diamonds. *J. Cryst. Growth* **1990**, *104*, 257–279.

(252) Samlenski, R.; Haug, C.; Brenn, R.; Wild, C.; Locher, R.; Koidl, P. Incorporation of Nitrogen in Chemical Vapor Deposition Diamond. *Appl. Phys. Lett.* **1995**, *67*, 2798–2800.

(253) Briddon, P. R.; Jones, R. Theory of Impurities in Diamond. *Phys. B* **1993**, *185*, 179–189.

(254) Smith, W. V.; Sorokin, P. P.; Gelles, I. L.; Lasher, G. J. Electron-Spin Resonance of Nitrogen Donors in Diamond. *Phys. Rev.* **1959**, *115*, 1546–1552.

(255) Zhang, S.; Ke, S. C.; Zvanut, M. E.; Tohver, H. T.; Vohra, Y. K. G. Tensor for Substitutional Nitrogen in Diamond. *Phys. Rev. B: Condens. Matter Mater. Phys.* **1994**, *49*, 015392.

(256) Barklie, R. C.; Guven, J. ^{13}C Hyperfine Structure and Relaxation Times of the P1 Centre in Diamond. *J. Phys. C: Solid State Phys.* **1981**, *14*, 3621–3631.

(257) Cox, A.; Newton, M. E.; Baker, J. M. ^{13}C , ^{14}N and ^{15}N ENDOR Measurements on the Single Substitutional Nitrogen Centre (P1) in Diamond. *J. Phys.: Condens. Matter* **1994**, *6*, 551–563.

(258) Cook, R. J.; Whiffen, D. H. Electron Nuclear Double Resonance Study of a Nitrogen Centre in Diamond. *Proc. R. Soc. London. Ser. A* **1966**, *295*, 99–106.

(259) Tucker, O. D.; Newton, M. E.; Baker, J. M. EPR and N^{14} Electron-Nuclear Double-Resonance Measurements on the Ionized Nearest-Neighbor Dinitrogen Center in Diamond. *Phys. Rev. B: Condens. Matter Mater. Phys.* **1994**, *50*, 15586–15596.

(260) Loubser, J. H. N.; van Ryneveld, W. P. The Dynamic Jahn–Teller and Other Effects in the High-Temperature Electron Spin Resonance Spectrum of Nitrogen in Diamond. *Br. J. Appl. Phys.* **1967**, *18*, 1029–1031.

(261) Ammerlaan, C. A. J.; Burgemeister, E. A. Reorientation of Nitrogen in Type-Ib Diamond by Thermal Excitation and Tunneling. *Phys. Rev. Lett.* **1981**, *47*, 954–957.

(262) van Wyk, J. A.; Reynhardt, E. C.; High, G. L.; Kiflawi, I. The Dependences of ESR Line Widths and Spin-Spin Relaxation Times of Single Nitrogen Defects on the Concentration of Nitrogen Defects in Diamond. *J. Phys. D: Appl. Phys.* **1997**, *30*, 1790–1793.

(263) Reynhardt, E. C.; High, G. L.; van Wyk, J. A. Temperature Dependence of Spin-Spin and Spin-Lattice Relaxation Times of Paramagnetic Nitrogen Defects in Diamond. *J. Chem. Phys.* **1998**, *109*, 8471–8477.

(264) Nadolinny, V. A.; Yeliseyev, A. P.; Baker, J. M.; Twitchen, D. J.; Newton, M. E.; Hofstaetter, A.; Feigelson, B. EPR Spectra of Separated Pairs of Substitutional Nitrogen Atoms in Diamond with a High Concentration of Nitrogen. *Phys. Rev. B: Condens. Matter Mater. Phys.* **1999**, *60*, 5392–5403.

- (265) Woods, G. S.; Van Wyk, J. A.; Collins, A. T. The Nitrogen Content of Type Ib Synthetic Diamond. *Philos. Mag. B* **1990**, *62*, 589–595.
- (266) Collins, A. T.; Woods, G. S. An Anomaly in the Infrared Absorption Spectrum of Synthetic Diamond. *Philos. Mag. B* **1982**, *46*, 77–83.
- (267) Samoilovich, M. I.; Bezrukov, G. N.; Butuzov, V. P.; Podol'skikh, L. D. Peculiarities in Electron Paramagnetic Resonance and Infrared Spectra of Diamonds Alloyed with the Isotope N¹⁵. *Soviet Physics Doklady* **1975**, *19*, 409–410.
- (268) Jones, R.; Briddon, P. R.; Öberg, S. First-Principles Theory of Nitrogen Aggregates in Diamond. *Philos. Mag. Lett.* **1992**, *66*, 67–74.
- (269) Liggins, S. Identification of Point Defects in Treated Single Crystal Diamond. Ph.D. Thesis, University of Warwick, UK, 2011; <http://webcat.warwick.ac.uk/record=b2491628~S15>.
- (270) Farrer, R. G. On the Substitutional Nitrogen Donor in Diamond. *Solid State Commun.* **1969**, *7*, 685–688.
- (271) Rosa, J.; Vaněček, M.; Nešládek, M.; Stals, L. M. Photoionization Cross-Section of Dominant Defects in CVD Diamond. *Diamond Relat. Mater.* **1999**, *8*, 721–724.
- (272) Ulbricht, R.; van der Post, S. T.; Goss, J. P.; Briddon, P. R.; Jones, R.; Khan, R. U. A.; Bonn, M. Single Substitutional Nitrogen Defects Revealed as Electron Acceptor States in Diamond Using Ultrafast Spectroscopy. *Phys. Rev. B: Condens. Matter Mater. Phys.* **2011**, *84*, 165202.
- (273) Jones, R.; Goss, J. P.; Briddon, P. R. Acceptor Level of Nitrogen in Diamond and the 270 nm Absorption Band. *Phys. Rev. B: Condens. Matter Mater. Phys.* **2009**, *80*, 033205.
- (274) Lawson, S. C.; Fisher, D.; Hunt, D. C.; Newton, M. E. On the Existence of Positively Charged Single-Substitutional Nitrogen in Diamond. *J. Phys.: Condens. Matter* **1998**, *10*, 6171–6180.
- (275) Evans, T.; Qi, Z. The Kinetics of the Aggregation of Nitrogen Atoms in Diamond. *Proc. R. Soc. London, Ser. A* **1982**, *381*, 159–178.
- (276) Davies, G. The A Nitrogen Aggregate in Diamond-Its Symmetry and Possible Structure. *J. Phys. C: Solid State Phys.* **1976**, *9*, L537–L542.
- (277) Sutherland, G. B. B. M.; Blackwell, D. E.; Simeral, W. G. The Problem of the Two Types of Diamond. *Nature* **1954**, *174*, 901–904.
- (278) Baranov, P. G.; Il'in, I. V.; Soltamova, A. A.; Vul', A. Y.; Kidalov, S. V.; Shakhov, F. M.; Mamin, G. V.; Orlinkii, S. B.; Salakhov, M. K. Electron Spin Resonance Detection and Identification of Nitrogen Centers in Nanodiamonds. *JETP Lett.* **2009**, *89*, 409–413.
- (279) Kiflawi, I.; Mainwood, A.; et al. Nitrogen Interstitials in Diamond. *Phys. Rev. B: Condens. Matter Mater. Phys.* **1996**, *54*, 16719–16726.
- (280) Felton, S.; Cann, B. L.; Edmonds, A. M.; Liggins, S.; Cruddace, R. J.; Newton, M. E.; Fisher, D.; Baker, J. M. Electron Paramagnetic Resonance Studies of Nitrogen Interstitial Defects in Diamond. *J. Phys.: Condens. Matter* **2009**, *21*, 364212.
- (281) Atumi, M. K.; Goss, J. P.; Briddon, P. R.; Shrif, F. E.; Rayson, M. J. Hyperfine Interactions at Nitrogen Interstitial Defects in Diamond. *J. Phys.: Condens. Matter* **2013**, *25*, 065802.
- (282) Goss, J. P.; Briddon, P. R.; Papagiannidis, S.; Jones, R. Interstitial Nitrogen and its Complexes in Diamond. *Phys. Rev. B: Condens. Matter Mater. Phys.* **2004**, *70*, 235208.
- (283) Coulson, C.; Kearsley, M. Colour Centres in Irradiated Diamonds. I. *Proc. R. Soc. A Math. Phys. Eng. Sci.* **1957**, *241*, 433–454.
- (284) Coulson, C. A.; Larkins, F. P. Isolated Single Vacancy in Diamond - I. Electronic Structure. *J. Phys. Chem. Solids* **1971**, *32*, 2245–2257.
- (285) Felton, S.; Edmonds, A. M.; Newton, M. E.; Martineau, P. M.; Fisher, D.; Twitchen, D. J. Electron Paramagnetic Resonance Studies of the Neutral Nitrogen Vacancy in Diamond. *Phys. Rev. B: Condens. Matter Mater. Phys.* **2008**, *77*, 081201.
- (286) Hauf, M. V.; Grotz, B.; Naydenov, B.; Dankerl, M.; Pezzagna, S.; Meijer, J.; Jelezko, F.; Wrachtrup, J.; Stutzmann, M.; Reinhard, F.; et al. Chemical Control of the Charge State of Nitrogen-Vacancy Centers in Diamond. *Phys. Rev. B: Condens. Matter Mater. Phys.* **2011**, *83*, 081304.
- (287) Doherty, M. W.; Manson, N. B.; Delaney, P.; Jelezko, F.; Wrachtrup, J.; Hollenberg, L. C. L. The Nitrogen-Vacancy Colour Centre in Diamond. *Phys. Rep.* **2013**, *528*, 1–45.
- (288) Schirhagl, R.; Chang, K.; Loretz, M.; Degen, C. L. Nitrogen-Vacancy Centers in Diamond: Nanoscale Sensors for Physics and Biology. *Annu. Rev. Phys. Chem.* **2014**, *65*, 83–105.
- (289) Fu, K. M. C.; Santori, C.; Barclay, P. E.; Rogers, L. J.; Manson, N. B.; Beausoleil, R. G. Observation of the Dynamic Jahn-Teller Effect in the Excited States of Nitrogen-Vacancy Centers in Diamond. *Phys. Rev. Lett.* **2009**, *103*, 256404.
- (290) Stanwix, P. L.; Pham, L. M.; Maze, J. R.; Le Sage, D.; Yeung, T. K.; Cappellaro, P.; Hemmer, P. R.; Yacoby, A.; Lukin, M. D.; Walsworth, R. L. Coherence of Nitrogen-Vacancy Electronic Spin Ensembles in Diamond. *Phys. Rev. B: Condens. Matter Mater. Phys.* **2010**, *82*, 201201.
- (291) Sukachev, D. D.; Sipahigil, A.; Nguyen, C. T.; Bhaskar, M. K.; Evans, R. E.; Jelezko, F.; Lukin, M. D. Silicon-Vacancy Spin Qubit in Diamond: A Quantum Memory Exceeding 10 Ms with Single-Shot State Readout. *Phys. Rev. Lett.* **2017**, *119*, 223602.
- (292) Sipahigil, A.; Evans, R. E.; Sukachev, D. D.; Burek, M. J.; Borregaard, J.; Bhaskar, M. K.; Nguyen, C. T.; Pacheco, J. L.; Atikian, H. A.; Meuwly, C.; et al. An Integrated Diamond Nanophotonics Platform for Quantum-Optical Networks. *Science* **2016**, *354*, 847–850.
- (293) Christle, D. J.; Falk, A. L.; Andrich, P.; Klimov, P. V.; Hassan, J. U.; Son, N. T.; Janzén, E.; Ohshima, T.; Awschalom, D. D. Isolated Electron Spins in Silicon Carbide with Millisecond Coherence Times. *Nat. Mater.* **2015**, *14*, 160–163.
- (294) Widmann, M.; Lee, S. Y.; Rendler, T.; Son, N. T.; Fedder, H.; Paik, S.; Yang, L. P.; Zhao, N.; Yang, S.; Booker, I.; et al. Coherent Control of Single Spins in Silicon Carbide at Room Temperature. *Nat. Mater.* **2015**, *14*, 164–168.
- (295) Exarhos, A. L.; Hopper, D. A.; Patel, R. N.; Doherty, M. W.; Bassett, L. C. Magnetic-Field-Dependent Quantum Emission in Hexagonal Boron Nitride at Room Temperature. *Nat. Commun.* **2019**, *10*, 222.
- (296) Maze, J. R.; Gali, A.; Togan, E.; Chu, Y.; Trifonov, A.; Kaxiras, E.; Lukin, M. D. Properties of Nitrogen-Vacancy Centers in Diamond: The Group Theoretic Approach. *New J. Phys.* **2011**, *13*, 025025.
- (297) Rondin, L.; Tetienne, J.-P. P.; Hingant, T.; Roch, J.-F. F.; Maletinsky, P.; Jacques, V. Magnetometry with Nitrogen-Vacancy Defects in Diamond. *Rep. Prog. Phys.* **2014**, *77*, 056503.
- (298) Rondin, L.; Dantelle, G.; Slablab, A.; Grosshans, F.; Treussart, F.; Bergonzo, P.; Perruchas, S.; Gacoin, T.; Chaigneau, M.; Chang, H. C.; et al. Surface-Induced Charge State Conversion of Nitrogen-Vacancy Defects in Nanodiamonds. *Phys. Rev. B: Condens. Matter Mater. Phys.* **2010**, *82*, 115449.
- (299) Davies, G. Dynamic Jahn-Teller Distortions at Trigonal Optical Centres in Diamond. *J. Phys. C: Solid State Phys.* **1979**, *12*, 2551–2566.
- (300) Acosta, V. M.; Bauch, E.; Jarmola, A.; Zipp, L. J.; Ledbetter, M. P.; Budker, D. Broadband Magnetometry by Infrared-Absorption Detection of Nitrogen-Vacancy Ensembles in Diamond. *Appl. Phys. Lett.* **2010**, *97*, 174104.
- (301) Hauf, M. V.; Simon, P.; Aslam, N.; Pfender, M.; Neumann, P.; Pezzagna, S.; Meijer, J.; Wrachtrup, J.; Stutzmann, M.; Reinhard, F.; et al. Addressing Single Nitrogen-Vacancy Centers in Diamond with Transparent in-Plane Gate Structures. *Nano Lett.* **2014**, *14*, 2359–2364.
- (302) Meara, C. J.; Rayson, M. J.; Briddon, P. R.; Goss, J. P. A Density Functional Theory Study on Magnetically Detecting Positively Charged Nitrogen-Vacancy Center in Diamond. *Phys. Rev. B: Condens. Matter Mater. Phys.* **2019**, *100*, 104108.
- (303) Barson, M. S. J.; Krausz, E.; Manson, N. B.; Doherty, M. W. The Fine Structure of the Neutral Nitrogen-Vacancy Center in Diamond. *Nanophotonics* **2019**, *8*, 1985–1991.

- (304) Gali, A. Theory of the Neutral Nitrogen-Vacancy Center in Diamond and Its Application to the Realization of a Qubit. *Phys. Rev. B: Condens. Matter Mater. Phys.* **2009**, *79*, 235210.
- (305) Collins, A. T. The Fermi Level in Diamond. *J. Phys.: Condens. Matter* **2002**, *14*, 3743–3750.
- (306) Gruber, A.; Dräbenstedt, A.; Tietz, C.; Wrachtrup, J.; von Borczyskowski, C. Scanning Confocal Optical Microscopy and Magnetic Resonance on Single Defect Centers. *Science* **1997**, *276*, 2012–2014.
- (307) Aslam, N.; Waldherr, G.; Neumann, P.; Jelezko, F.; Wrachtrup, J. Photo-Induced Ionization Dynamics of the Nitrogen Vacancy Defect in Diamond Investigated by Single-Shot Charge State Detection. *New J. Phys.* **2013**, *15*, 013064.
- (308) Manson, N. B.; Hedges, M.; Barson, M. S. J.; Ahlefeldt, R.; Doherty, M. W.; Abe, H.; Ohshima, T.; Sellars, M. J. NV–N⁺ Pair Centre in 1b Diamond. *New J. Phys.* **2018**, *20*, 113037.
- (309) Bourgeois, E.; Jarmola, A.; Siyushev, P.; Gulka, M.; Hruby, J.; Jelezko, F.; Budker, D.; Nesladek, M. Photoelectric Detection of Electron Spin Resonance of Nitrogen-Vacancy Centres in Diamond. *Nat. Commun.* **2015**, *6*, 8577.
- (310) Bourgeois, E.; Londero, E.; Buczak, K.; Hruby, J.; Gulka, M.; Balasubramanian, Y.; Wachter, G.; Stursa, J.; Dobes, K.; Aumayr, F.; et al. Enhanced Photoelectric Detection of NV Magnetic Resonances in Diamond under Dual-Beam Excitation. *Phys. Rev. B: Condens. Matter Mater. Phys.* **2017**, *95*, 041402.
- (311) Gulka, M.; Bourgeois, E.; Hruby, J.; Siyushev, P.; Wachter, G.; Aumayr, F.; Hemmer, P. R.; Gali, A.; Jelezko, F.; Trupke, M.; et al. Pulsed Photoelectric Coherent Manipulation and Detection of N-V Center Spins in Diamond. *Phys. Rev. Appl.* **2017**, *7*, 044032.
- (312) Siyushev, P.; Nesladek, M.; Bourgeois, E.; Gulka, M.; Hruby, J.; Yamamoto, T.; Trupke, M.; Teraji, T.; Isoya, J.; Jelezko, F. Photoelectrical Imaging and Coherent Spin-State Readout of Single Nitrogen-Vacancy Centers in Diamond. *Science* **2019**, *363*, 728–731.
- (313) Davies, G.; Lawson, S. C.; Collins, A. T.; Mainwood, A.; Sharp, S. J. Vacancy-Related Centers in Diamond. *Phys. Rev. B: Condens. Matter Mater. Phys.* **1992**, *46*, 13157–13170.
- (314) Newton, M. E.; Campbell, B. A.; Twitchen, D. J.; Baker, J. M.; Anthony, T. R. Recombination-Enhanced Diffusion of Self-Interstitial Atoms and Vacancy–Interstitial Recombination in Diamond. *Diamond Relat. Mater.* **2002**, *11*, 618–622.
- (315) Schröder, T.; Mouradian, S. L.; Zheng, J.; Trusheim, M. E.; Walsh, M.; Chen, E. H.; Li, L.; Bayn, I.; Englund, D. Quantum Nanophotonics in Diamond [Invited]. *J. Opt. Soc. Am. B* **2016**, *33*, B65–B83.
- (316) Mouradian, S. L.; Schröder, T.; Poitras, C. B.; Li, L.; Goldstein, J.; Chen, E. H.; Walsh, M.; Cardenas, J.; Markham, M. L.; Twitchen, D. J.; et al. Scalable Integration of Long-Lived Quantum Memories into a Photonic Circuit. *Phys. Rev. X* **2015**, *5*, 031009.
- (317) Dolde, F.; Jakobi, I.; Naydenov, B.; Zhao, N.; Pezzagna, S.; Trautmann, C.; Meijer, J.; Neumann, P.; Jelezko, F.; Wrachtrup, J. Room-Temperature Entanglement between Single Defect Spins in Diamond. *Nat. Phys.* **2013**, *9*, 139–143.
- (318) Lühmann, T.; Raatz, N.; John, R.; Lesik, M.; Rödiger, J.; Portail, M.; Wildanger, D.; Kleißler, F.; Nordlund, K.; Zaitsev, A.; et al. Screening and Engineering of Colour Centres in Diamond. *J. Phys. D: Appl. Phys.* **2018**, *51*, 483002.
- (319) Acosta, V. M.; Bauch, E.; Ledbetter, M. P.; Santori, C.; Fu, K.-M.M.C.; Barclay, P. E.; Beausoleil, R. G.; Linget, H.; Roch, J. F.; Treussart, F.; et al. Diamonds with a High Density of Nitrogen-Vacancy Centers for Magnetometry Applications. *Phys. Rev. B: Condens. Matter Mater. Phys.* **2009**, *80*, 115202.
- (320) Zhang, C.; Yuan, H.; Zhang, N.; Xu, L. X.; Li, B.; Cheng, G. D.; Wang, Y.; Gui, Q.; Fang, J. C. Dependence of High Density Nitrogen-Vacancy Center Ensemble Coherence on Electron Irradiation Doses and Annealing Time. *J. Phys. D: Appl. Phys.* **2017**, *50*, S05104.
- (321) McLellan, C. A.; Myers, B. A.; Kraemer, S.; Ohno, K.; Awschalom, D. D.; Bleszynski Jayich, A. C. Patterned Formation of Highly Coherent Nitrogen-Vacancy Centers Using a Focused Electron Irradiation Technique. *Nano Lett.* **2016**, *16*, 2450–2454.
- (322) Kleinsasser, E. E.; Stanfield, M. M.; Banks, J. K. Q.; Zhu, Z.; Li, W. D.; Acosta, V. M.; Watanabe, H.; Itoh, K. M.; Fu, K. M. C. High Density Nitrogen-Vacancy Sensing Surface Created via He⁺ Ion Implantation of ¹²C Diamond. *Appl. Phys. Lett.* **2016**, *108*, 202401.
- (323) Naydenov, B.; Kolesov, R.; Batalov, A.; Meijer, J.; Pezzagna, S.; Rogalla, D.; Jelezko, F.; Wrachtrup, J. Engineering Single Photon Emitters by Ion Implantation in Diamond. *Appl. Phys. Lett.* **2009**, *95*, 181109.
- (324) Alghannam, F.; Hemmer, P. Engineering of Shallow Layers of Nitrogen Vacancy Colour Centres in Diamond Using Plasma Immersion Ion Implantation. *Sci. Rep.* **2019**, *9*, 5870.
- (325) Chen, Y.-C.; Salter, P. S.; Knauer, S.; Weng, L.; Frangeskou, A. C.; Stephen, C. J.; Ishmael, S. N.; Dolan, P. R.; Johnson, S.; Green, B. L.; et al. Laser Writing of Coherent Colour Centres in Diamond. *Nat. Photonics* **2017**, *11*, 77–80.
- (326) Chen, Y.-C.; Griffiths, B.; Weng, L.; Nicley, S.; Ishmael, S. N.; Lekhai, Y.; Johnson, S.; Stephen, C. J.; Green, B. L.; Morley, G. W.; et al. Laser Writing of Individual Atomic Defects in a Crystal with Near-Unity Yield. *Optica* **2019**, *6*, 662–667.
- (327) Kononenko, V. V.; Vlasov, I. I.; Gololobov, V. M.; Kononenko, T. V.; Semenov, T. A.; Khomich, A. A.; Shershulin, V. A.; Krivobok, V. S.; Konov, V. I. Nitrogen-Vacancy Defects in Diamond Produced by Femtosecond Laser Nanoablation Technique. *Appl. Phys. Lett.* **2017**, *111*, 081101.
- (328) Capelli, M.; Heffernan, A. H.; Ohshima, T.; Abe, H.; Jeske, J.; Hope, A.; Greentree, A. D.; Reineck, P.; Gibson, B. C. Increased Nitrogen-Vacancy Centre Creation Yield in Diamond Through Electron Beam Irradiation at High Temperature. *Carbon* **2019**, *143*, 714–719.
- (329) Ohno, K.; Heremans, F. J.; Bassett, L. C.; Myers, B. A.; Toyli, D. M.; Bleszynski Jayich, A. C.; Palmström, C. J.; Awschalom, D. D. Engineering Shallow Spins in Diamond with Nitrogen Delta-Doping. *Appl. Phys. Lett.* **2012**, *101*, 082413.
- (330) van Dam, S. B.; Walsh, M.; Degen, M. J.; Bersin, E.; Mouradian, S. L.; Galiullin, A.; Ruf, M.; Ijspeert, M.; Taminiau, T. H.; Hanson, R.; et al. Optical Coherence of Diamond Nitrogen-Vacancy Centers Formed by Ion Implantation and Annealing. *Phys. Rev. B: Condens. Matter Mater. Phys.* **2019**, *99*, 161203.
- (331) Fávoro de Oliveira, F.; Antonov, D.; Wang, Y.; Neumann, P.; Momenzadeh, S. A.; Häußermann, T.; Pasquarelli, A.; Denisenko, A.; Wrachtrup, J. Tailoring Spin Defects in Diamond by Lattice Charging. *Nat. Commun.* **2017**, *8*, 15409.
- (332) Spinicelli, P.; Dréau, A.; Rondin, L.; Silva, F.; Achard, J.; Xavier, S.; Bansropun, S.; Debuisschert, T.; Pezzagna, S.; Meijer, J.; et al. Engineered Arrays of Nitrogen-Vacancy Color Centers in Diamond Based on Implantation of CN – Molecules through Nanoapertures. *New J. Phys.* **2011**, *13*, 025014.
- (333) Hui, Y. Y.; Cheng, C. L.; Chang, H. C. Nanodiamonds for Optical Bioimaging. *J. Phys. D: Appl. Phys.* **2010**, *43*, 374021.
- (334) Tallaire, A.; Lesik, M.; Jacques, V.; Pezzagna, S.; Mille, V.; Brinza, O.; Meijer, J.; Abel, B.; Roch, J. F.; Gicquel, A.; et al. Temperature Dependent Creation of Nitrogen-Vacancy Centers in Single Crystal CVD Diamond Layers. *Diamond Relat. Mater.* **2015**, *51*, 55–60.
- (335) Rogers, L. J.; Jahnke, K. D.; Doherty, M. W.; Dietrich, A.; McGuinness, L. P.; Müller, C.; Teraji, T.; Sumiya, H.; Isoya, J.; Manson, N. B.; et al. Electronic Structure of the Negatively Charged Silicon-Vacancy Center in Diamond. *Phys. Rev. B: Condens. Matter Mater. Phys.* **2014**, *89*, 235101.
- (336) Pinto, H.; Jones, R.; Palmer, D. W.; Goss, J. P.; Briddon, P. R.; Öberg, S. On the Diffusion of NV Defects in Diamond. *Phys. Status Solidi A* **2012**, *209*, 1765–1768.
- (337) Osterkamp, C.; Mangold, M.; Lang, J.; Balasubramanian, P.; Teraji, T.; Naydenov, B.; Jelezko, F. Engineering Preferentially-Aligned Nitrogen-Vacancy Centre Ensembles in CVD Grown Diamond. *Sci. Rep.* **2019**, *9*, 5786.

- (338) Appel, P.; Neu, E.; Ganzhorn, M.; Barfuss, A.; Batzer, M.; Gratz, M.; Tschöpe, A.; Maletinsky, P. Fabrication of all Diamond Scanning Probes for Nanoscale Magnetometry. *Rev. Sci. Instrum.* **2016**, *87*, 063703.
- (339) Lukosz, W.; Kunz, R. Light-Emission by Magnetic and Electric Dipoles close to a Plane Interface. 1. Total Radiated Power. *J. Opt. Soc. Am.* **1977**, *67*, 1607–1615.
- (340) Hausmann, B. J.; Khan, M.; Zhang, Y.; Babinec, T. M.; Martinick, K.; McCutcheon, M.; Hemmer, P. R.; Lončar, M. Fabrication of Diamond Nanowires for Quantum Information Processing Applications. *Diamond Relat. Mater.* **2010**, *19*, 621–629.
- (341) Bernardi, E.; Nelz, R.; Sonusen, S.; Neu, E. Nanoscale Sensing using Point Defects in Single-Crystal Diamond: Recent Progress on Nitrogen Vacancy Center-Based Sensors. *Crystals* **2017**, *7*, 124.
- (342) Lawson, S. C.; Davies, G.; Collins, A. T.; Mainwood, A. The “H2” Optical Transition in Diamond: The Effects of Uniaxial Stress Perturbations, Temperature and Isotopic Substitution. *J. Phys.: Condens. Matter* **1992**, *4*, 3439–3452.
- (343) Dale, M. W. Colour Centres on Demand in Diamond, Ph.D. Thesis, University of Warwick, UK, 2015; <http://webcat.warwick.ac.uk/record=b2870881~S1>.
- (344) Davies, G.; Nazaré, M. H.; Hamer, M. F. The H3 (2.463 eV) Vibronic Band in Diamond: Uniaxial Stress Effects and the Breakdown of Mirror Symmetry. *Proc. R. Soc. London, Ser. A* **1976**, *351*, 245–265.
- (345) van Wyk, J. A.; Woods, G. S. Electron Spin Resonance of Excited States of the H3 and H4 Centres in Irradiated Type Ia Diamonds. *J. Phys.: Condens. Matter* **1995**, *7*, 5901–5911.
- (346) Clark, C. D.; Ditchburn, R. W.; Dyer, H. B. The Absorption Spectra of Irradiated Diamonds after Heat Treatment. *Proc. R. Soc. London A. Math. Phys. Sci.* **1956**, *237*, 75–89.
- (347) Collins, A. T. A. Spectroscopic Survey of Naturally-Occurring Vacancy-Related Colour Centres in Diamond. *J. Phys. D: Appl. Phys.* **1982**, *15*, 1431–1438.
- (348) Davies, G. No Phonon Lineshapes and Crystal Strain Fields in Diamonds. *J. Phys. C: Solid State Phys.* **1970**, *3*, 2474–2486.
- (349) Davies, G.; Crossfield, M. Luminescence Quenching and Zero-Phonon Line Broadening Associated with Defect Interactions in Diamond. *J. Phys. C: Solid State Phys.* **1973**, *6*, L104–L108.
- (350) Crossfield, M. D.; Davies, G.; Collins, A. T.; Lightowlers, E. C. The Role of Defect Interactions in Reducing the Decay Time of H3 Luminescence in Diamond. *J. Phys. C: Solid State Phys.* **1974**, *7*, 1909–1917.
- (351) Jones, R.; Goss, J. P.; Pinto, H.; Palmer, D. W. Diffusion of Nitrogen in Diamond and the Formation of A-Centres. *Diamond Relat. Mater.* **2015**, *53*, 35–39.
- (352) Collins, A. T. Vacancy Enhanced Aggregation of Nitrogen in Diamond. *J. Phys. C: Solid State Phys.* **1980**, *13*, 2641–2650.
- (353) Green, B. L.; Dale, M. W.; Newton, M. E.; Fisher, D. Electron Paramagnetic Resonance of the N_2V^- Defect in ^{15}N -Doped Synthetic Diamond. *Phys. Rev. B: Condens. Matter Mater. Phys.* **2015**, *92*, 165204.
- (354) Dodge, C. N. An Optical Study of Sintered and Black Diamond, Ph.D. Thesis, University of Reading, UK, 1986.
- (355) Collins, A. T. The Characterisation of Point Defects in Diamond by Luminescence Spectroscopy. *Diamond Relat. Mater.* **1992**, *1*, 457–469.
- (356) Erasmus, R. M. Optical Properties and Mechanical Stress State in Cubic Boron Nitride and Diamond. Ph.D. Thesis, University of the Witwatersrand, South Africa, 2013; <http://hdl.handle.net/10539/12572>.
- (357) Hanley, P. L.; Kiflawi, I.; Lang, A. R. On Topographically Identifiable Sources of Cathodoluminescence in Natural Diamonds. *Philos. Trans. R. Soc. A Math. Phys. Eng. Sci.* **1977**, *284*, 329–368.
- (358) Lang, A. R. Defects in Natural Diamonds: Recent Observations by New Methods. *J. Cryst. Growth* **1977**, *42*, 625–631.
- (359) Bangert, U.; Barnes, R.; Gass, M. H.; Bleloch, A. L.; Godfrey, I. S. Vacancy Clusters, Dislocations and Brown Colouration in Diamond. *J. Phys.: Condens. Matter* **2009**, *21*, 364208.
- (360) Fritsch, E. The Nature of Diamonds. In *The Nature of Diamonds*; Harlow, G. E., Ed.; Cambridge University Press, 1998; pp 23–47.
- (361) Collins, A. T.; Kanda, H.; Kitawaki, H. Colour Changes Produced in Natural Brown Diamonds by High-Pressure, High-Temperature Treatment. *Diamond Relat. Mater.* **2000**, *9*, 113–122.
- (362) Welbourn, C. M.; Cooper, M. A.; Spear, P. M. De Beers Natural versus Synthetic Diamond Verification Instruments. *Gems Gemol.* **1996**, *32*, 156–169.
- (363) Hsu, J. H.; Su, W. D.; Yang, K. L.; Tzeng, Y. K.; Chang, H. C. Nonblinking Green Emission from Single H3 Color Centers in Nanodiamonds. *Appl. Phys. Lett.* **2011**, *98*, 193116.
- (364) Kolesov, R.; Lasse, S.; Rothfuchs, C.; Wieck, A. D.; Xia, K.; Kornher, T.; Wrachtrup, J. Superresolution Microscopy of Single Rare-Earth Emitters in YAG and H3 Centers in Diamond. *Phys. Rev. Lett.* **2018**, *120*, 033903.
- (365) Aharonovich, I.; Castelletto, S.; Simpson, D. A.; Su, C.-H.; Greentree, A. D.; Prawer, S. Diamond-Based Single-Photon Emitters. *Rep. Prog. Phys.* **2011**, *74*, 076501.
- (366) Udvarhelyi, P.; Londero, E.; Gali, A.; et al. Ab Initio Theory of the N_2V Defect in Diamond for Quantum Memory Implementation. *Phys. Rev. B: Condens. Matter Mater. Phys.* **2017**, *96*, 155211.
- (367) Pereira, E.; Monteiro, T. Delayed Luminescence of the H3 Centre in Diamond. *J. Lumin.* **1991**, *48–49*, 814–818.
- (368) Collins, A. T. Excited States of the H3 Vibronic Centre in Diamond. *J. Phys. C: Solid State Phys.* **1983**, *16*, 6691–6694.
- (369) Rand, S. C.; Deshazer, L. G. Visible Color-Center Laser in Diamond. *Opt. Lett.* **1985**, *10*, 481–483.
- (370) du Preez, L. Electron Paramagnetic Resonance and Optical Investigations of Defect Centres in Diamond, Ph.D. Thesis, University of the Witwatersrand, Johannesburg, South Africa, 1965; <http://hdl.handle.net/10539/20866>.
- (371) Mita, Y.; Nisida, Y.; Suito, K.; Onodera, A.; Yazu, S. Photochromism of H2 and H3 Centres in Synthetic Type Ib Diamonds. *J. Phys.: Condens. Matter* **1990**, *2*, 8567–8574.
- (372) Mita, Y.; Ohno, Y.; Adachi, Y.; Kanehara, H.; Nisida, Y.; Nakashima, T. Recovery Process of Photochromism of H2 and H3 Centres in Diamond. *Diamond Relat. Mater.* **1993**, *2*, 768–772.
- (373) Crowther, P. A.; Dean, P. J. Phonon Interactions, Piezo-Optical Properties and the Inter-Relationship of the N3 and N9 Absorption-Emission Systems in Diamond. *J. Phys. Chem. Solids* **1967**, *28*, 1115–1136.
- (374) Thomaz, M. F.; Davies, G. The Decay Time of N3 Luminescence in Natural Diamond. *Proc. R. Soc. London, Ser. A* **1978**, *362*, 405–419.
- (375) Collins, A. T.; Connor, A.; Ly, C.-H.; Shareef, A.; Spear, P. M. High-Temperature Annealing of Optical Centers in Type-I Diamond. *J. Appl. Phys.* **2005**, *97*, 083517.
- (376) King, J. M.; Shigley, J. E.; Gelb, T. H.; Guhin, S. S.; Hall, M.; Wang, W. Characterization and Grading of Natural-Color Yellow Diamonds. *Gems Gemol.* **2005**, *41*, 88–115.
- (377) Jones, R.; Goss, J. P.; Briddon, P. R.; Öberg, S. N2 and N4 Optical Transitions in Diamond: A Breakdown of the Vacancy Model. *Phys. Rev. B: Condens. Matter Mater. Phys.* **1997**, *56*, R1654–R1656.
- (378) Davies, G.; Welbourn, C. M.; Loubser, J. H. N. Optical and Electron Paramagnetic Effects in Yellow Type Ia Diamonds. *Diam. Res.* **1978**, *21*, 23–30.
- (379) Loubser, J. H. N.; Wright, A. C. J. Endor of P2. *Diam. Res.* **1973**, *16*, 4.
- (380) van Wyk, J. A. Carbon-13 Hyperfine Interaction of the Unique Carbon of the P2 (ESR) or N3 (Optical) Centre in Diamond. *J. Phys. C Solid State Phys.* **1982**, *15*, L981–L983.
- (381) van Wyk, J. A.; Loubser, J. H. N. ENDOR of the P2 Centre in Type-Ia Diamonds. *J. Phys.: Condens. Matter* **1993**, *5*, 3019–3026.
- (382) Green, B. L.; Breeze, B. G.; Newton, M. E. Electron Paramagnetic Resonance and Photochromism of N_3V^0 in Diamond. *J. Phys.: Condens. Matter* **2017**, *29*, 225701.

- (383) Mita, Y.; Kanehara, H.; Nisida, Y.; Okada, M. Photochromic Behaviour of the N3 Centre in Neutron-irradiated and Annealed Type-Ib Diamond. *Philos. Mag. Lett.* **1997**, *76*, 93–98.
- (384) Green, B. L.; Breeze, B. G.; Rees, G. J.; Hanna, J. V.; Chou, J. P.; Ivády, V.; Gali, A.; Newton, M. E. All-Optical Hyperpolarization of Electron and Nuclear Spins in Diamond. *Phys. Rev. B: Condens. Matter Mater. Phys.* **2017**, *96*, 054101.
- (385) Davies, G.; Summersgill, I. Nitrogen-Dependent Optical Properties of Diamond. *Diam. Res.* **1973**, *16*, 6.
- (386) Fisher, D. Brown Diamonds and High Pressure High Temperature Treatment. *Lithos* **2009**, *112*, 619–624.
- (387) Fisher, D.; Sibley, S. J.; Kelly, C. J. Brown Colour in Natural Diamond and Interaction between the Brown Related and Other Colour-Inducing Defects. *J. Phys.: Condens. Matter* **2009**, *21*, 364213.
- (388) Allen, B. P.; Evans, T. Aggregation of Nitrogen in Diamond, Including Platelet Formation. *Proc. R. Soc. London, Ser. A* **1981**, *375*, 93–104.
- (389) Davies, G. The Effect of Nitrogen Impurity on the Annealing of Radiation Damage in Diamond. *J. Phys. C: Solid State Phys.* **1972**, *5*, 2534–2542.
- (390) Mainwood, A. Nitrogen and Nitrogen-Vacancy Complexes and Their Formation in Diamond. *Phys. Rev. B: Condens. Matter Mater. Phys.* **1994**, *49*, 7934–7940.
- (391) Hunt, D.; Twitchen, D.; Newton, M.; Baker, J.; et al. Identification of the Neutral Carbon <100>-Split Interstitial in Diamond. *Phys. Rev. B: Condens. Matter Mater. Phys.* **2000**, *61*, 3863–3876.
- (392) Clark, C. D.; Walker, J. The Neutral Vacancy in Diamond. *Proc. R. Soc. London, Ser. A* **1973**, *334*, 241–257.
- (393) Davies, G. Charge States of the Vacancy in Diamond. *Nature* **1977**, *269*, 498–500.
- (394) Isoya, J.; Kanda, H.; Uchida, Y.; Lawson, S. C.; Yamasaki, S.; Itoh, H.; Morita, Y. EPR Identification of the Negatively Charged Vacancy in Diamond. *Phys. Rev. B: Condens. Matter Mater. Phys.* **1992**, *45*, 1436–1439.
- (395) Watt, G. A.; Newton, M. E.; Baker, J. M. EPR and Optical Imaging of the Growth-Sector Dependence of Radiation-Damage Defect Production in Synthetic Diamond. *Diamond Relat. Mater.* **2001**, *10*, 1681–1683.
- (396) Goss, J. P.; Coomer, B. J.; Shaw, T. D.; Briddon, P. R.; Rayson, M.; Öberg, S.; et al. Self-Interstitial Aggregation in Diamond. *Phys. Rev. B: Condens. Matter Mater. Phys.* **2001**, *63*, 195208.
- (397) Prins, J. F. On the Annihilation of Vacancies by Diffusing Interstitial Atoms in Diamond. *Diamond Relat. Mater.* **2000**, *9*, 1835–1839.
- (398) Kiflawi, I.; Collins, A. T.; Iakoubovskii, K.; Fisher, D. Electron Irradiation and the Formation of Vacancy–Interstitial Pairs in Diamond. *J. Phys.: Condens. Matter* **2007**, *19*, 046216.
- (399) Woods, G. S. Infrared Absorption Studies of the Annealing of Irradiated Diamonds. *Philos. Mag. B* **1984**, *50*, 673–688.
- (400) Fisher, D.; Lawson, S. C. The Effect of Nickel and Cobalt on the Aggregation of Nitrogen in Diamond. *Diamond Relat. Mater.* **1998**, *7*, 299–304.
- (401) Charles, S. J.; Butler, J. E.; Feygelson, B. N.; Newton, M. E.; Carroll, D. L.; Steeds, J. W.; Darwish, H.; Yan, C. S.; Mao, H. K.; Hemley, R. J. Characterization of Nitrogen Doped Chemical Vapor Deposited Single Crystal Diamond before and after High Pressure, High Temperature Annealing. *Phys. Status Solidi Appl. Res.* **2004**, *201*, 2473–2485.
- (402) Kanda, H.; Jia, X. Change of Luminescence Character of Ib Diamonds with HPHT Treatment. *Diamond Relat. Mater.* **2001**, *10*, 1665–1669.
- (403) Brozel, M. R.; Evans, T.; Stephenson, R. F. Partial Dissociation of Nitrogen Aggregates in Diamond by High Temperature-High Pressure Treatments. *Proc. R. Soc. London, Ser. A* **1978**, *361*, 109–127.
- (404) Goss, J. P.; Coomer, B. J.; Jones, R.; Fall, C. J.; Briddon, P. R.; Öberg, S. Extended Defects in Diamond: The Interstitial Platelet. *Phys. Rev. B: Condens. Matter Mater. Phys.* **2003**, *67*, 165208.
- (405) Jones, R.; Hounscome, L. S.; Fujita, N.; Öberg, S.; Briddon, P. R. Electrical and Optical Properties of Multivacancy Centres in Diamond. *Phys. Status Solidi A* **2007**, *204*, 3059–3064.
- (406) Hudson, P. R. W.; Tsong, I. S. T. Hydrogen Impurity in Natural Gem Diamond. *J. Mater. Sci.* **1977**, *12*, 2389–2395.
- (407) Sideras-Haddad, E.; Connell, S. E.; Sellschop, J. P. F.; Machi, I. Z.; Rebuli, D.; Maclear, R. D.; Doyle, D. P. Hydrogen and Oxygen Chemistry and Dynamics in Diamond Studied by Nuclear Microscopic Techniques. *Nucl. Instrum. Methods Phys. Res., Sect. B* **2001**, *181*, 419–425.
- (408) Glover, C.; Newton, M. E.; Martineau, P.; Twitchen, D. J.; Baker, J. M. Hydrogen Incorporation in Diamond: The Nitrogen-Vacancy-Hydrogen Complex. *Phys. Rev. Lett.* **2003**, *90*, 185507.
- (409) Goss, J. P.; Briddon, P. R.; Jones, R.; Sque, S. The Vacancy-Nitrogen-Hydrogen Complex in Diamond: A Potential Deep Centre in Chemical Vapour Deposited Material. *J. Phys.: Condens. Matter* **2003**, *15*, S2903–S2911.
- (410) Shaw, M. J.; Briddon, P. R.; Goss, J. P.; Rayson, M. J.; Kerridge, A.; Harker, A. H.; Stoneham, A. M. Importance of Quantum Tunneling in Vacancy-Hydrogen Complexes in Diamond. *Phys. Rev. Lett.* **2005**, *95*, 105502.
- (411) Kerridge, A.; Harker, A. H.; Stoneham, A. M. Quantum Behaviour of Hydrogen and Muonium in Vacancy-Containing Complexes in Diamond. *J. Phys.: Condens. Matter* **2004**, *16*, 8743–8751.
- (412) Edmonds, A. M. Magnetic Resonance Studies of Point Defects in Single Crystal Diamond. PhD Thesis, University of Warwick, 2008; <http://webcat.warwick.ac.uk/record=b2248398-S9>.
- (413) Khan, R. U. A.; Cann, B. L.; Martineau, P. M.; Samartseva, J.; Freeth, J. J. P.; Sibley, S. J.; Hartland, C. B.; Newton, M. E.; Dhillon, H. K.; Twitchen, D. J. Colour-Causing Defects and Their Related Optoelectronic Transitions in Single Crystal CVD Diamond. *J. Phys.: Condens. Matter* **2013**, *25*, 275801.
- (414) Pinto, H.; Jones, R.; Goss, J. P.; Briddon, P. R. Point and Extended Defects in Chemical Vapour Deposited Diamond. *J. Phys. Conf. Ser.* **2011**, *281*, 012023.
- (415) Cruddace, R. J. Magnetic Resonance and Optical Studies of Point Defects in Single Crystal CVD Diamond. PhD Thesis, University of Warwick, 2007; <http://webcat.warwick.ac.uk/record=b2242706-S9>.
- (416) Martineau, P. M.; Lawson, S. C.; Taylor, A. J.; Quinn, S. J.; Evans, D. J. F.; Crowder, M. J. Identification of Synthetic Diamond Grown Using Chemical Vapour Deposition (CVD). *Gems Gemol.* **2004**, *40*, 2–25.
- (417) Fuchs, F.; Wild, C.; Schwarz, K.; Koidl, P. Hydrogen-Related IR Absorption in Chemical Vapour Deposited Diamond. *Diamond Relat. Mater.* **1995**, *4*, 652–656.
- (418) Hartland, C. B. A Study of Point Defects in CVD Diamond Using Electron Paramagnetic Resonance and Optical Spectroscopy. PhD Thesis, University of Warwick, UK, 2014; <http://webcat.warwick.ac.uk/record=b2754901-S1>.
- (419) Peaker, C. V.; Goss, J. P.; Briddon, P. R.; Horsfall, A. B.; Rayson, M. J. The Vacancy–Hydrogen Defect in Diamond: A Computational Study. *Phys. Status Solidi A* **2015**, *212*, 2431–2436.
- (420) Peaker, C. V.; Goss, J. P.; Briddon, P. R.; Horsfall, A. B.; Rayson, M. J. Di-Nitrogen–Vacancy–Hydrogen Defects in Diamond: A Computational Study. *Phys. Status Solidi A* **2015**, *212*, 2616–2620.
- (421) Wang, W.; Doering, P.; Tower, J.; Lu, R.; Eaton-Magaña, S.; Johnson, P.; Emerson, E.; Moses, T. M. Strongly Colored Pink CVD Lab-Grown Diamonds. *Gems Gemol.* **2010**, *46*, 4–17.
- (422) Felton, S.; Edmonds, A. M.; Newton, M. E.; Martineau, P. M.; Fisher, D.; Twitchen, D. J.; Baker, J. M. Hyperfine Interaction in the Ground State of the Negatively Charged Nitrogen Vacancy Center in Diamond. *Phys. Rev. B: Condens. Matter Mater. Phys.* **2009**, *79*, 075203.
- (423) Baker, J. M.; Newton, M. E. The Use of ENDOR to Identify the Atomic Structure of Defects in Diamond. *Appl. Magn. Reson.* **1994**, *7*, 209–235.

- (424) Gentile, F. S.; Salustro, S.; Causà, M.; Erba, A.; Carbonnière, P.; Dovesi, R. The VN_3H Defect in Diamond: A Quantum-Mechanical Characterization. *Phys. Chem. Chem. Phys.* **2017**, *19*, 22221–22229.
- (425) Chrenko, R. M.; McDonald, R. S.; Darrow, K. A. Infra-Red Spectra of Diamond Coat. *Nature* **1967**, *213*, 474–476.
- (426) Charette, J. J. Le Spectre Infra-Rouge a Grande Dispersion Des Trois Types de Diamants et Ses Variations En Fonction de La Temperature. *Physica* **1959**, *25*, 1303–1312.
- (427) Kohn, S. C.; Speich, L.; Smith, C. B.; Bulanova, G. P. FTIR Thermochronometry of Natural Diamonds: A Closer Look. *Lithos* **2016**, *265*, 148–158.
- (428) Fritsch, E.; Hainschwang, T.; Massi, L.; Rondeau, B. Hydrogen-Related Optical Centres in Natural Diamond: An Update. *New Diam. Front. Carbon Technol.* **2007**, *17*, 63–89.
- (429) Rondeau, B.; Fritsch, E.; Guiraud, M.; Chalain, J. P.; Notari, F. Three Historical “Asteriated” Hydrogen-Rich Diamonds: Growth History and Sector-Dependent Impurity Incorporation. *Diamond Relat. Mater.* **2004**, *13*, 1658–1673.
- (430) Zaitsev, A. M.; Moe, K. S.; Wang, W. Defect Transformations in Nitrogen-Doped CVD Diamond during Irradiation and Annealing. *Diamond Relat. Mater.* **2018**, *88*, 237–255.
- (431) De Weerd, F.; N. Kupriyanov, I. Report on the Influence of HPHT Annealing on the 3107 cm^{-1} Hydrogen Related Absorption Peak in Natural Type Ia Diamonds. *Diamond Relat. Mater.* **2002**, *11*, 714–715.
- (432) Jones, R. Dislocations, Vacancies and the Brown Colour of CVD and Natural Diamond. *Diamond Relat. Mater.* **2009**, *18*, 820–826.
- (433) Goss, J. P.; Jones, R.; Heggie, M. I.; Ewels, C. P.; Briddon, P. R.; Öberg, S. Theory of Hydrogen in Diamond. *Phys. Rev. B: Condens. Matter Mater. Phys.* **2002**, *65*, 115207.
- (434) Goss, J. P. Theory of Hydrogen in Diamond. *J. Phys.: Condens. Matter* **2003**, *15*, R551–R580.
- (435) Welbourn, C. M.; Rooney, M. L. T.; Evans, D. J. F. A Study of Diamonds of Cube and Cube-Related Shape from the Jwaneng Mine. *J. Cryst. Growth* **1989**, *94*, 229–252.
- (436) Atumi, M. K. First Principles Simulations of the Structure and Incorporation of Point Defects in Diamond. PhD Thesis, Newcastle University, UK, 2014; <http://theses.ncl.ac.uk/jspui/handle/10443/2447>.
- (437) Baker, J. M. Optical and EPR Centres Involving 3d Metals in Diamond. In *XI Feofilov Symposium on Spectroscopy of Crystals Activated by Rare-Earth and Transition Metal Ions*; 2002, Vol. 4766, pp 106–118.
- (438) Yelisseyev, A.; Kanda, H. Optical Centers Related to 3D Transition Metals in Diamond. *New Diam. Front. Carbon Technol.* **2007**, *17*, 127–178.
- (439) Collins, A. T. Spectroscopy of Defects and Transition Metals in Diamond. *Diamond Relat. Mater.* **2000**, *9*, 417–423.
- (440) Nadolinny, V. A.; Yelisseyev, A. P.; Baker, J. M.; Newton, M. E.; Twitchen, D. J.; Lawson, S. C.; Yuryeva, O. P.; Feigelson, B. N. A Study of ^{13}C Hyperfine Structure in the EPR of Nickel-Nitrogen-Containing Centres in Diamond and Correlation with Their Optical Properties. *J. Phys.: Condens. Matter* **1999**, *11*, 7357–7376.
- (441) Gaebel, T.; Popa, I.; Gruber, A.; Domhan, M.; Jelezko, F.; Wrachtrup, J. Stable Single-Photon Source in the Near Infrared. *New J. Phys.* **2004**, *6*, 98.
- (442) Sildos, I.; Loot, A.; Kiisk, V.; Puust, L.; Hizhnyakov, V.; Yelisseyev, A.; Osvet, A.; Vlasov, I. Spectroscopic Study of NE8 Defect in Synthetic Diamond for Optical Thermometry. *Diamond Relat. Mater.* **2017**, *76*, 27–30.
- (443) Thiering, G.; Londero, E.; Gali, A. Single Nickel-Related Defects in Molecular-Sized Nanodiamonds for Multicolor Bioimaging: An *Ab Initio* Study. *Nanoscale* **2014**, *6*, 12018–12025.
- (444) Pezzagna, S.; Rogalla, D.; Wildanger, D.; Meijer, J.; Zaitsev, A. Creation and Nature of Optical Centres in Diamond for Single-Photon Emission-Overview and Critical Remarks. *New J. Phys.* **2011**, *13*, 035024.
- (445) Palyanov, Y. N.; Kupriyanov, I. N.; Khokhryakov, A. F.; Ralchenko, V. G. Crystal Growth of Diamond. In *Handbook of Crystal Growth*; Rudolph, P., Ed.; Elsevier, 2015; pp 671–713.
- (446) Goss, J. P.; Jones, R.; Breuer, S. J.; Briddon, P. R.; Öberg, S. The Twelve-Line 1.682 eV Luminescence Center in Diamond and the Vacancy-Silicon Complex. *Phys. Rev. Lett.* **1996**, *77*, 3041–3044.
- (447) Isoya, J.; Kanda, H.; Norris, J. R.; Tang, J.; Bowman, M. K. Fourier-Transform and Continuous-Wave EPR Studies of Nickel in Synthetic Diamond: Site and Spin Multiplicity. *Phys. Rev. B: Condens. Matter Mater. Phys.* **1990**, *41*, 3905–3913.
- (448) Nadolinny, V. A.; Yelisseyev, A. P.; Yuryeva, O. P.; Feigelson, B. N. EPR Study of the Transformations in Nickel Containing Centres at Heated Synthetic Diamonds. *Appl. Magn. Reson.* **1997**, *12*, 543–554.
- (449) Gehlhoff, W.; Pereira, R. N. The Identity of the AB1 and NE4 Electron Paramagnetic Resonance Spectra in High-Pressure-High-Temperature Diamond. *J. Phys.: Condens. Matter* **2002**, *14*, 13751–13760.
- (450) Nadolinny, V. A.; Yelisseyev, A. P. Structure and Creation Conditions of Complex Nitrogen-Nickel Defects in Synthetic Diamonds. *Diamond Relat. Mater.* **1994**, *3*, 1196–1200.
- (451) Pereira, R. N.; Neves, A. J.; Gehlhoff, W.; Sobolev, N. A.; Rino, L.; Kanda, H. Annealing Study of the Formation of Nickel-Related Paramagnetic Defects in Diamond. *Diamond Relat. Mater.* **2002**, *11*, 623–626.
- (452) Neves, A. J.; Pereira, R.; Sobolev, N. A.; Nazaré, M. H.; Gehlhoff, W.; Naser, A.; Kanda, H. New Paramagnetic Centers in Annealed High-Pressure Synthetic Diamond. *Diamond Relat. Mater.* **2000**, *9*, 1057–1060.
- (453) Neves, A. J.; Pereira, R.; Sobolev, N. A.; Nazaré, M. H.; Gehlhoff, W.; Naser, A.; Kanda, H. New Paramagnetic Defects in Synthetic Diamonds Grown Using Nickel Catalyst. *Phys. B* **1999**, *273–274*, 651–654.
- (454) Iakoubovskii, K.; Stesmans, A.; Nouwen, B.; Adriaenssens, G. J. ESR and Optical Evidence for a Ni Vacancy Center in CVD Diamond. *Phys. Rev. B: Condens. Matter Mater. Phys.* **2000**, *62*, 16587–16594.
- (455) Goss, J. P.; Briddon, P. R.; Jones, R.; Öberg, S. The Lattice Location of Ni in Diamond: A Theoretical Study. *J. Phys.: Condens. Matter* **2004**, *16*, 4567–4578.
- (456) Nadolinny, V. A.; Baker, J. M.; Yuryeva, O. P.; Newton, M. E.; Twitchen, D. J.; Palyanov, Y. N. EPR Study of the Peculiarities of Incorporating Transition Metal Ions into the Diamond Structure. *Appl. Magn. Reson.* **2005**, *28*, 365–381.
- (457) Nadolinny, V. A.; Yelisseyev, A. P. New Paramagnetic Centres Containing Nickel Ions in Diamond. *Diamond Relat. Mater.* **1994**, *3*, 17–21.
- (458) Lawson, S. C.; Kanda, H. Nickel in Diamond: An Annealing Study. *Diamond Relat. Mater.* **1993**, *2*, 130–135.
- (459) Kupriyanov, I. N.; Gusev, V. A.; Borzdov, Y. M.; Kalinin, A. A.; Pal'yanov, Y. N. Photoluminescence Study of Annealed Nickel- and Nitrogen-Containing Synthetic Diamond. *Diamond Relat. Mater.* **1999**, *8*, 1301–1309.
- (460) Noble, C. J.; Pawlik, T.; Spaeth, J.-M. Electron Paramagnetic Resonance Investigations of Nickel Defects in Natural Diamonds. *J. Phys.: Condens. Matter* **1998**, *10*, 11781–11793.
- (461) Wrachtrup, J.; Jelezko, F. Processing Quantum Information in Diamond. *J. Phys.: Condens. Matter* **2006**, *18*, S807–S824.
- (462) Wolfer, M.; Kriele, A.; Williams, O. A.; Obloh, H.; Leancu, C. C.; Nebel, C. E. Nickel Doping of Nitrogen Enriched CVD-Diamond for the Production of Single Photon Emitters. *Phys. Status Solidi A* **2009**, *206*, 2012–2015.
- (463) Rabeau, J. R.; Chin, Y. L.; Prawer, S.; Jelezko, F.; Gaebel, T.; Wrachtrup, J. Fabrication of Single Nickel-Nitrogen Defects in Diamond by Chemical Vapor Deposition. *Appl. Phys. Lett.* **2005**, *86*, 131926.
- (464) Wu, E.; Rabeau, J. R.; Roger, G.; Treussart, F.; Zeng, H.; Grangier, P.; Prawer, S.; Roch, J. F. Room Temperature Triggered Single-Photon Source in the near Infrared. *New J. Phys.* **2007**, *9*, 434.

- (465) Wolfer, M.; Obloh, H.; Williams, O. A.; Leancu, C.-C.; Kirste, L.; Gheeraert, E.; Nebel, C. E. Doping of Single Crystalline Diamond with Nickel. *Phys. Status Solidi A* **2010**, *207*, 2054–2057.
- (466) Orwa, J. O.; Aharonovich, I.; Jelezko, F.; Balasubramanian, G.; Balog, P.; Markham, M.; Twitchen, D. J.; Greentree, A. D.; Prawer, S. Nickel Related Optical Centres in Diamond Created by Ion Implantation. *J. Appl. Phys.* **2010**, *107*, 093512.
- (467) Iwasaki, T.; Ishibashi, F.; Miyamoto, Y.; Doi, Y.; Kobayashi, S.; Miyazaki, T.; Tahara, K.; Jahnke, K. D.; Rogers, L. J.; Naydenov, B.; et al. Germanium-Vacancy Single Color Centers in Diamond. *Sci. Rep.* **2015**, *5*, 12882.
- (468) Trusheim, M. E.; Pingault, B.; Wan, N. H.; Gündoğan, M.; De Santis, L.; Debroux, R.; Gangloff, D.; Purser, C.; Chen, K. C.; Walsh, M.; et al. Transform-Limited Photons from a Coherent Tin-Vacancy Spin in Diamond. *Phys. Rev. Lett.* **2020**, *124*, 023602.
- (469) Nadolinny, V. A.; Yeliseyev, A. P.; Baker, J. M.; Twitchen, D. J.; Newton, M. E.; Feigelson, B. N.; Yuryeva, O. P. Mechanisms of Nitrogen Aggregation in Nickel- and Cobalt-Containing Synthetic Diamonds. *Diamond Relat. Mater.* **2000**, *9*, 883–886.
- (470) Kiflawi, I.; Kanda, H.; Mainwood, A. The Effect of Nickel and the Kinetics of the Aggregation of Nitrogen in Diamond. *Diamond Relat. Mater.* **1998**, *7*, 327–332.
- (471) Lawson, S. C.; Kanda, H.; Watanabe, K.; Kiflawi, I.; Sato, Y.; Collins, A. T. Spectroscopic Study of Cobalt-Related Optical Centers in Synthetic Diamond. *J. Appl. Phys.* **1996**, *79*, 4348–4357.
- (472) Johnston, K.; Mainwood, A. Transition Metals in Diamond: Do Chemical Trends Arise from *Ab Initio* Calculations? *Phys. B* **2001**, *308–310*, 565–568.
- (473) Johnston, K.; Mainwood, A.; Collins, A. T.; Davies, G.; Twitchen, D.; Newton, M.; Baker, J. M. Experimental and Theoretical Studies of Cobalt Defects in Diamond. *Diamond Relat. Mater.* **2000**, *9*, 424–427.
- (474) Johnston, K.; Mainwood, A.; Collins, A. T.; Davies, G.; Twitchen, D.; Baker, J. M.; Newton, M. Transition Metals in Diamond: Experimental and Theoretical Identification of Co-N Complexes. *Phys. B* **1999**, *273–274*, 647–650.
- (475) Twitchen, D.; Baker, J.; Newton, M.; Johnston, K. Identification of Cobalt on a Lattice Site in Diamond. *Phys. Rev. B: Condens. Matter Mater. Phys.* **2000**, *61*, 9–11.
- (476) Vins, V. G. On the Transformation of Optically Active Defects in Diamond Crystal Lattice. *Diamond Relat. Mater.* **2004**, *13*, 732–735.
- (477) Nadolinny, V. A.; Yuryeva, O. P.; Chepurov, A. I.; Shatsky, V. Titanium Ions in the Diamond Structure: Model and Experimental Evidence. *Appl. Magn. Reson.* **2009**, *36*, 109–113.
- (478) Nadolinny, V. A.; Yuryeva, O. P.; Shatsky, V. S.; Stepanov, A. S.; Golushko, V. V.; Rakhmanova, M. I.; Kupriyanov, I. N.; Kalinin, A. A.; Palyanov, Y. N.; Zedgenizov, D. New Data on the Nature of the EPR OK1 and N3 Centers in Diamond. *Appl. Magn. Reson.* **2009**, *36*, 97–108.
- (479) Nadolinny, V. A.; Golushko, V. V.; Yuryeva, O. P.; Rakhmanova, M. I.; Shatsky, V. S. A New Paramagnetic Nitrogen Center in Natural Titanium-Containing Diamonds. *Appl. Magn. Reson.* **2010**, *39*, 303–308.
- (480) Liang, Z. Z.; Jia, X.; Zhu, P. W.; Ma, H. A.; Zang, C. Y.; Qing, J. M.; Guan, Q. F. Effects of the Additive NaN₃ Added in Powder Catalysts on the Morphology and Inclusions of Diamonds Synthesized under HPHT. *Diamond Relat. Mater.* **2006**, *15*, 10–14.
- (481) Aharonovich, I.; Castelletto, S.; Johnson, B. C.; McCallum, J. C.; Simpson, D. A.; Greentree, A. D.; Prawer, S. Chromium Single-Photon Emitters in Diamond Fabricated by Ion Implantation. *Phys. Rev. B: Condens. Matter Mater. Phys.* **2010**, *81*, 121201.
- (482) Zaitsev, A. Vibronic Spectra of Impurity-Related Optical Centers in Diamond. *Phys. Rev. B: Condens. Matter Mater. Phys.* **2000**, *61*, 12909–12922.
- (483) Sankaran, K. J.; Panda, K.; Sundaravel, B.; Tai, N. H.; Lin, I. N. Enhancing Electrical Conductivity and Electron Field Emission Properties of Ultrananocrystalline Diamond Films by Copper Ion Implantation and Annealing. *J. Appl. Phys.* **2014**, *115*, 063701.
- (484) Sedov, V. S.; Khomich, A. A.; Ralchenko, V. G.; Martyanov, A. K.; Savin, S. S.; Poklonskaya, O. N.; Trofimov, N. S. Growth of Si-Doped Polycrystalline Diamond Films on AlN Substrates by Microwave Plasma Chemical Vapor Deposition. *J. Coating Sci. Technol.* **2015**, *2*, 38–45.
- (485) Goss, J. P.; Briddon, P. R.; Shaw, M. J. Density Functional Simulations of Silicon-Containing Point Defects in Diamond. *Phys. Rev. B: Condens. Matter Mater. Phys.* **2007**, *76*, 075204.
- (486) Stachel, T.; Harris, J. W. The Origin of Cratonic Diamonds - Constraints from Mineral Inclusions. *Ore Geol. Rev.* **2008**, *34*, 5–32.
- (487) Meyer, H. O. A. Chrome Pyrope: An Inclusion in Natural Diamond. *Science* **1968**, *160*, 1446–1447.
- (488) Meyer, H. O. A.; Boyd, F. R. Composition and Origin of Crystalline Inclusions in Natural Diamonds. *Geochim. Cosmochim. Acta* **1972**, *36*, 1255–1273.
- (489) Richardson, S. H.; Gurney, J. J.; Erlank, A. J.; Harris, J. W. Origin of Diamonds in Old Enriched Mantle. *Nature* **1984**, *310*, 198–202.
- (490) Taylor, W. R.; Jaques, A. L.; Ridd, M. Nitrogen-Defect Aggregation Characteristics of some Australasian Diamonds—Time-Temperature Constraints on the Source Regions of Pipe and Alluvial Diamonds. *Am. Mineral.* **1990**, *75*, 1290–1310.
- (491) Smit, K. V.; Shirey, S. B.; Wang, W. Type Ib Diamond Formation and Preservation in the West African Lithospheric Mantle: Re–Os Age Constraints from Sulphide Inclusions in Zimmi Diamonds. *Precambrian Res.* **2016**, *286*, 152–166.
- (492) Pearson, D. G.; Shirey, S. B.; Harris, J. W.; Carlson, R. W. Sulphide Inclusions in Diamonds from the Koffiefontein Kimberlite, S Africa: Constraints on Diamond Ages and Mantle Re–Os Systematics. *Earth Planet. Sci. Lett.* **1998**, *160*, 311–326.
- (493) Westerlund, K. J.; Shirey, S. B.; Richardson, S. H.; Carlson, R. W.; Gurney, J. J.; Harris, J. W. A Subduction Wedge Origin for Paleoproterozoic Peridotitic Diamonds and Harzburgites from the Panda Kimberlite, Slave Craton: Evidence from Re–Os Isotope Systematics. *Contrib. Mineral. Petrol.* **2006**, *152*, 275–294.
- (494) Shirey, S. B.; Richardson, S. H. Start of the Wilson Cycle at 3 Ga shown by Diamonds from Subcontinental Mantle. *Science* **2011**, *333*, 434–436.
- (495) Howell, D.; O'Neill, C. J.; Grant, K. J.; Griffin, W. L.; O'Reilly, S. Y.; Pearson, N. J.; Stern, R. A.; Stachel, T. Platelet Development in Cuboid Diamonds: Insights from Micro-FTIR Mapping. *Contrib. Mineral. Petrol.* **2012**, *164*, 1011–1025.
- (496) Smart, K. A.; Chacko, T.; Stachel, T.; Muehlenbachs, K.; Stern, R. A.; Heaman, L. M. Diamond Growth from Oxidized Carbon Sources Beneath the Northern Slave Craton, Canada: a $\delta^{13}\text{C}$ –N Study of Eclogite-Hosted Diamonds from the Jericho Kimberlite. *Geochim. Cosmochim. Acta* **2011**, *75*, 6027–6047.
- (497) Cartigny, P.; Palot, M.; Thomassot, E.; Harris, J. W. Diamond Formation: A Stable Isotope Perspective. *Annu. Rev. Earth Planet. Sci.* **2014**, *42*, 699–732.
- (498) Diamond Producers Association protocol to test the performance of diamond verification instruments in a consistent manner. <https://diamondproducers.com/assure/assure-directory/>.
- (499) Schrand, A. M.; Huang, H.; Carlson, C.; Schlager, J. J.; Osawa, E.; Hussain, S. M.; Dai, L. Are Diamond Nanoparticles Cytotoxic? *J. Phys. Chem. B* **2007**, *111*, 2–7.
- (500) Schrand, A. M.; Hens, S. A. C.; Shenderova, O. A. Nanodiamond Particles: Properties and Perspectives for Bioapplications. *Crit. Rev. Solid State Mater. Sci.* **2009**, *34*, 18–74.
- (501) Chow, E. K.; Zhang, X.-Q.; Chen, M.; Lam, R.; Robinson, E.; Huang, H.; Schaffer, D.; Osawa, E.; Goga, A.; Ho, D. Nanodiamond Therapeutic Delivery Agents Mediate Enhanced Chemoresistant Tumor Treatment. *Sci. Transl. Med.* **2011**, *3*, 73ra21.
- (502) Chang, H.-C.; Hsiao, W. W. -W.; Su, M.-C. *Fluorescent Nanodiamond*; Wiley-VCH, 2018.
- (503) Say, J. M.; van Vreden, C.; Reilly, D. J.; Brown, L. J.; Rabeau, J. R.; King, N. J. C. Luminescent nanodiamonds for biomedical applications. *Biophys. Rev.* **2011**, *3*, 171–184.

- (504) Fu, C.-C.; Lee, H.-Y.; Chen, K.; Lim, T.-S.; Wu, H.-Y.; Lin, P.-K.; Wei, P.-K.; Tsao, P.-H.; Chang, H.-C.; Fann, W. Characterization and Application of Single Fluorescent Nanodiamonds as Cellular Biomarkers. *Proc. Natl. Acad. Sci. U. S. A.* **2007**, *104*, 727–732.
- (505) Barnard, A. S. Diamond Standard in Diagnostics: Nanodiamond Biolabels Make Their Mark. *Analyst* **2009**, *134*, 1751–1764.
- (506) Mohan, N.; Chen, C.-S.; Hsieh, H.-H.; Wu, Y.-C.; Chang, H.-C. In Vivo Imaging and Toxicity Assessments of Fluorescent Nanodiamonds in *Caenorhabditis Elegans*. *Nano Lett.* **2010**, *10*, 3692–3699.
- (507) Wu, T. J.; Tzeng, Y. K.; Chang, W. W.; Cheng, C. A.; Kuo, Y.; Chien, C. H.; Chang, H. C.; Yu, J. Tracking the Engraftment and Regenerative Capabilities of Transplanted Lung Stem Cells using Fluorescent Nanodiamonds. *Nat. Nanotechnol.* **2013**, *8*, 682–689.
- (508) Hui, Y. Y.; Hsiao, W. W.-W.; Haziza, S.; Simonneau, M.; Treussart, F.; Chang, H.-C. Single Particle Tracking of Fluorescent Nanodiamonds in Cells and Organisms. *Curr. Opin. Solid State Mater. Sci.* **2017**, *21*, 35–42.
- (509) Lee, S. F.; Osborne, M. A. Photodynamics of a Single Quantum Dot: Fluorescence Activation, Enhancement, Intermittency, and Decay. *J. Am. Chem. Soc.* **2007**, *129*, 8936–8937.
- (510) Treussart, F.; Jacques, V.; Wu, E.; Gacoin, T.; Grangier, P.; Roch, J.-F. Photoluminescence of Single Colour Defects in 50 nm Diamond Nanocrystals. *Phys. B* **2006**, *376–377*, 926–929.
- (511) Billinton, N.; Knight, A. W. Seeing the Wood through the Trees: A Review of Techniques for Distinguishing Green Fluorescent Protein from Endogenous Autofluorescence. *Anal. Biochem.* **2001**, *291*, 175–197.
- (512) Ho, D.; Wang, C.-H. K.; Chow, E. K.-H. Nanodiamonds: The Intersection of Nanotechnology, Drug Development, and Personalized Medicine. *Science Advances* **2015**, *1*, No. e1500439.
- (513) Yu, S.-J.; Kang, M.-W.; Chang, H.-C.; Chen, K.-M.; Yu, Y.-C. Bright Fluorescent Nanodiamonds: No Photobleaching and Low Cytotoxicity. *J. Am. Chem. Soc.* **2005**, *127*, 17604–17605.
- (514) Chang, Y.-R.; Lee, H.-Y.; Chen, K.; Chang, C.-C.; Tsai, D.-S.; Fu, C.-C.; Lim, T.-S.; Tzeng, Y.-K.; Fang, C.-Y.; Han, C.-C.; et al. Mass Production and Dynamic Imaging of Fluorescent Nanodiamonds. *Nat. Nanotechnol.* **2008**, *3*, 284–288.
- (515) Chang, I. P.; Hwang, K. C.; Chiang, C.-S. Preparation of Fluorescent Magnetic Nanodiamonds and Cellular Imaging. *J. Am. Chem. Soc.* **2008**, *130*, 15476–15481.
- (516) Wee, T.-L.; Mau, Y.-W.; Fang, C.-Y.; Hsu, H.-L.; Han, C.-C.; Chang, H.-C. Preparation and Characterization of Green Fluorescent Nanodiamonds for Biological Applications. *Diamond Relat. Mater.* **2009**, *18*, 567–573.
- (517) Zhang, X.-Q.; Chen, M.; Lam, R.; Xu, X.; Osawa, E.; Ho, D. Polymer-Functionalized Nanodiamond Platforms as Vehicles for Gene Delivery. *ACS Nano* **2009**, *3*, 2609–2016.
- (518) Faklaris, O.; Garrot, D.; Joshi, V.; Boudou, J.-P.; Sauvage, T.; Curmi, P. A.; Treussart, F. Comparison of the Photoluminescence Properties of Semiconductor Quantum Dots and Non-Blinking Diamond Nanoparticles. Observation of the Diffusion of Diamond Nanoparticles in Living Cells. *J. Eur. Optical Soc.: Rapid Publ.* **2009**, *4*, 090325.
- (519) Claveau, S.; Bertrand, J.-R.; Treussart, F. Fluorescent Nanodiamond Applications for Cellular Process Sensing and Cell Tracking. *Micromachines* **2018**, *9*, 247.
- (520) Robledo, L.; Childress, L.; Bernien, H.; Hensen, B.; Alkemade, P. F. A.; Hanson, R. High-Fidelity Projective Read-out of a Solid-State Spin Quantum Register. *Nature* **2011**, *477*, 574–578.
- (521) Childress, L.; Gurudev Dutt, M. V.; Taylor, J. M.; Zibrov, A. S.; Jelezko, F.; Wrachtrup, J.; Hemmer, P. R.; Lukin, M. D. Coherent Dynamics of Coupled Electron and Nuclear Spin Qubits in Diamond. *Science* **2006**, *314*, 281–285.
- (522) Jarmola, A.; Acosta, V. M.; Jensen, K.; Chemerisov, S.; Budker, D. Temperature- and Magnetic-Field-Dependent Longitudinal Spin Relaxation in Nitrogen-Vacancy Ensembles in Diamond. *Phys. Rev. Lett.* **2012**, *108*, 197601.
- (523) Astner, T.; Gugler, J.; Angerer, A.; Wald, S.; Putz, S.; Mauser, N. J.; Trupke, M.; Sumiya, H.; Onoda, S.; Isoya, J.; et al. Solid-State Electron Spin Lifetime Limited by Phononic Vacuum Modes. *Nat. Mater.* **2018**, *17*, 313–317.
- (524) Bar-Gill, N.; Pham, L. M.; Jarmola, A.; Budker, D.; Walsworth, R. L. Solid-State Electronic Spin Coherence Time Approaching One Second. *Nat. Commun.* **2013**, *4*, 1743.
- (525) Gurudev Dutt, M. V.; Childress, L.; Jiang, L.; Togan, E.; Maze, J.; Jelezko, F.; Zibrov, A. S.; Hemmer, P. R.; Lukin, M. D. Quantum Register Based on Individual Electronic and Nuclear Spin Qubits in Diamond. *Science* **2007**, *316*, 1312–1316.
- (526) Kurtsiefer, C.; Mayer, S.; Zarda, P.; Weinfurter, H. Stable Solid-State Source of Single Photons. *Phys. Rev. Lett.* **2000**, *85*, 290–293.
- (527) Prawer, S.; Greentree, A. D. Diamond for Quantum Computing. *Science* **2008**, *320*, 1601–1602.
- (528) Horodecki, R.; Horodecki, P.; Horodecki, M.; Horodecki, K. Quantum Entanglement. *Rev. Mod. Phys.* **2009**, *81*, 865–942.
- (529) Bradley, C. E.; Randall, J.; Aboobeh, M. H.; Berrevoets, R. C.; Degen, M. J.; Bakker, M. A.; Markham, M.; Twitche, D. J.; Taminiau, T. H. A Ten-Qubit Solid-State Spin Register with Quantum Memory up to One Minute. *Phys. Rev. X* **2019**, *9*, 031045.
- (530) Awschalom, D. D.; Hanson, R.; Wrachtrup, J.; Zhou, B. B. Quantum Technologies with Optically Interfaced Solid-State Spins. *Nat. Photonics* **2018**, *12*, 516–527.
- (531) Casola, F.; van der Sar, T.; Yacoby, A. Probing Condensed Matter Physics with Magnetometry Based on Nitrogen-Vacancy Centres in Diamond. *Nat. Rev. Mater.* **2018**, *3*, 17088.
- (532) Lee, D.; Lee, K. W.; Cady, J. V.; Ovarthaiyapong, P.; Jayich, A. C. B. Topical Review: Spins and Mechanics in Diamond. *J. Opt.* **2017**, *19*, 033001.
- (533) Bernien, H.; Hensen, B.; Pfaff, W.; Koolstra, G.; Blok, M. S.; Robledo, L.; Taminiau, T. H.; Markham, M.; Twitche, D. J.; Childress, L.; et al. Herald Entanglement between Solid-State Qubits Separated by Three Metres. *Nature* **2013**, *497*, 86–90.
- (534) Hensen, B.; Bernien, H.; Dreau, A. E.; Reiserer, A.; Kalb, N.; Blok, M. S.; Ruitenberg, J.; Vermeulen, R. F. L.; Schouten, R. N.; Abellan, C.; et al. Loophole-Free Bell Inequality Violation Using Electron Spins Separated by 1.3 Kilometres. *Nature* **2015**, *526*, 682–686.
- (535) Waldherr, G.; Wang, Y.; Zaiser, S.; Jamali, M.; Schulte-Herbrueggen, T.; Abe, H.; Ohshima, T.; Isoya, J.; Du, J. F.; Neumann, P.; et al. Quantum Error Correction in a Solid-State Hybrid Spin Register. *Nature* **2014**, *506*, 204–207.
- (536) Taminiau, T. H.; Cramer, J.; van der Sar, T.; Dobrovitski, V. V.; Hanson, R. Universal Control and Error Correction in Multi-Qubit Spin Registers in Diamond. *Nat. Nanotechnol.* **2014**, *9*, 171–176.
- (537) Wang, Y.; Dolde, F.; Biamonte, J.; Babbush, R.; Bergholm, V.; Yang, S.; Jakobi, I.; Neumann, P.; Aspuru-Guzik, A.; Whitfield, J. D.; et al. Quantum Simulation of Helium Hydride Cation in a Solid-State Spin Register. *ACS Nano* **2015**, *9*, 7769–7774.
- (538) Balasubramanian, G.; Chan, I. Y.; Kolesov, R.; Al-Hmoud, M.; Tisler, J.; Shin, C.; Kim, C.; Wojcik, A.; Hemmer, P. R.; Krueger, A.; et al. Nanoscale Imaging Magnetometry with Diamond Spins under Ambient Conditions. *Nature* **2008**, *455*, 648–651.
- (539) Maze, J. R.; Stanwix, P. L.; Hodges, J. S.; Hong, S.; Taylor, J. M.; Cappellaro, P.; Jiang, L.; Dutt, M. V. G.; Togan, E.; Zibrov, A. S.; et al. Nanoscale Magnetic Sensing with an Individual Electronic Spin in Diamond. *Nature* **2008**, *455*, 644–647.
- (540) Taylor, J. M.; Cappellaro, P.; Childress, L.; Jiang, L.; Budker, D.; Hemmer, P. R.; Yacoby, A.; Walsworth, R.; Lukin, M. D. High-Sensitivity Diamond Magnetometer with Nanoscale Resolution. *Nat. Phys.* **2008**, *4*, 810–816.
- (541) Maletinsky, P.; Hong, S.; Grinolds, M.; Hausmann, B.; Lukin, M.; Walsworth, R.; Lončar, M.; Yacoby, A. A Robust Scanning Diamond Sensor for Nanoscale Imaging with Single Nitrogen-Vacancy Centres. *Nat. Nanotechnol.* **2012**, *7*, 320–324.

- (542) Steinert, S.; Dolde, F.; Neumann, P.; Aird, A.; Naydenov, B.; Balasubramanian, G.; Jelezko, F.; Wrachtrup, J. High Sensitivity Magnetic Imaging Using an Array of Spins in Diamond. *Rev. Sci. Instrum.* **2010**, *81*, 043705.
- (543) Fu, R. R.; Weiss, B. P.; Lima, E. A.; Harrison, R. J.; Bai, X.-N.; Desch, S. J.; Ebel, D. S.; Suavet, C.; Wang, H.; Glenn, D.; et al. Solar Nebula Magnetic Fields Recorded in the Semarkona Meteorite. *Science* **2014**, *346*, 1089–1092.
- (544) Le Sage, D.; Arai, K.; Glenn, D. R.; DeVience, S. J.; Pham, L. M.; Rahn-Lee, L.; Lukin, M. D.; Yacoby, A.; Komeili, A.; Walsworth, R. L. Optical Magnetic Imaging of Living Cells. *Nature* **2013**, *496*, 486–489.
- (545) Du, C.; van der Sar, T.; Zhou, T. X.; Upadhyaya, P.; Casola, F.; Zhang, H.; Onbasli, M. C.; Ross, C. A.; Walsworth, R. L.; Tserkovnyak, Y.; et al. Control and Local Measurement of the Spin Chemical Potential in a Magnetic Insulator. *Science* **2017**, *357*, 195–198.
- (546) Dovzhenko, Y.; Casola, F.; Schlotter, S.; Zhou, T. X.; Buttner, F.; Walsworth, R. L.; Beach, G. S. D.; Yacoby, A. Magnetostatic Twists in Room-Temperature Skyrmions Explored by Nitrogen-Vacancy Center Spin Texture Reconstruction. *Nat. Commun.* **2018**, *9*, 2712.
- (547) Brenneis, A.; Gaudreau, L.; Seifert, M.; Karl, H.; Brandt, M. S.; Huebl, H.; Garrido, J. A.; Koppens, F. H. L.; Holleitner, A. W. Ultrafast Electronic Readout of Diamond Nitrogen-Vacancy Centres Coupled to Graphene. *Nat. Nanotechnol.* **2015**, *10*, 135–139.
- (548) Wolf, T.; Neumann, P.; Nakamura, K.; Sumiya, H.; Ohshima, T.; Isoya, J.; Wrachtrup, J. Subpicotesla Diamond Magnetometry. *Phys. Rev. X* **2015**, *5*, 041001.
- (549) Clevenson, H.; Trusheim, M. E.; Teale, C.; Schroeder, T.; Braje, D.; Englund, D. Broadband Magnetometry and Temperature Sensing with a Light-Trapping Diamond Waveguide. *Nat. Phys.* **2015**, *11*, 393–397.
- (550) Clevenson, H.; Pham, L. M.; Teale, C.; Johnson, K.; Englund, D.; Braje, D. Robust High-Dynamic-Range Vector Magnetometry with Nitrogen-Vacancy Centers in Diamond. *Appl. Phys. Lett.* **2018**, *112*, 252406.
- (551) Maly, T.; Debelouchina, G. T.; Bajaj, V. S.; Hu, K.-N.; Joo, C.-G.; Mak-Jurkauskas, M. L.; Sirigiri, J. R.; van der Wel, P. C. A.; Herzfeld, J.; Temkin, R. J.; Griffin, R. G. Dynamic Nuclear Polarization at High Magnetic Fields. *J. Chem. Phys.* **2008**, *128*, 052211.
- (552) Ardenkjaer-Larsen, J.-H.; Boebinger, G. S.; Comment, A.; Duckett, S.; Edison, A. S.; Engelke, F.; Griesinger, C.; Griffin, R. G.; Hilty, C.; Maeda, H.; et al. Facing and Overcoming Sensitivity Challenges in Bio-molecular NMR Spectroscopy. *Angew. Chem., Int. Ed.* **2015**, *54*, 9162–9185.
- (553) King, J. P.; Coles, P. J.; Reimer, J. A. Optical Polarization of C-13 Nuclei in Diamond through Nitrogen Vacancy Centers. *Phys. Rev. B: Condens. Matter Mater. Phys.* **2010**, *81*, 073201.
- (554) Fischer, R.; Bretschneider, C. O.; London, P.; Budker, D.; Gershoni, D.; Frydman, L. Bulk Nuclear Polarization Enhanced at Room Temperature by Optical Pumping. *Phys. Rev. Lett.* **2013**, *111*, 057601.
- (555) Scheuer, J.; Schwartz, I.; Chen, Q.; Schulze-Sünninghausen, D.; Carl, P.; Höfer, P.; Retzker, A.; Sumiya, H.; Isoya, J.; Luy, B.; et al. Optically Induced Dynamic Nuclear Spin Polarisation in Diamond. *New J. Phys.* **2016**, *18*, 013040.
- (556) Chen, Q.; Schwarz, I.; Jelezko, F.; Retzker, A.; Plenio, M. B. Resonance-inclined Optical Nuclear Spin Polarization of Liquids in Diamond Structures. *Phys. Rev. B: Condens. Matter Mater. Phys.* **2016**, *93*, No. 060408(R).
- (557) Staudacher, T.; Shi, F.; Pezzagna, S.; Meijer, J.; Du, J.; Meriles, C. A.; Reinhard, F.; Wrachtrup, J. Nuclear Magnetic Resonance Spectroscopy on a 5 nm³ Sample Volume. *Science* **2013**, *339*, 561–563.
- (558) Mamin, H. J.; Kim, M.; Sherwood, M. H.; Rettner, C. T.; Ohno, K.; Awschalom, D. D.; Rugar, D. Nanoscale Nuclear Magnetic Resonance with a Nitrogen-Vacancy Spin Sensor. *Science* **2013**, *339*, 557–560.
- (559) Bucher, D. B.; Aude Craik, D. P. L.; Backlund, M. P.; Turner, M. J.; Ben Dor, O.; Glenn, D. R.; Walsworth, R. L. Quantum diamond spectrometer for nanoscale NMR and ESR spectroscopy. *Nat. Protoc.* **2019**, *14*, 2707–2747.
- (560) Glenn, D. R.; Bucher, D. B.; Lee, J.; Lukin, M. D.; Park, H.; Walsworth, R. L. High-Resolution Magnetic Resonance Spectroscopy Using a Solid-State Spin Sensor. *Nature* **2018**, *555*, 351–354.
- (561) Schwartz, I.; Roskopf, J.; Schmitt, S.; Tratzmiller, B.; Chen, Q.; McGuinness, L. P.; Jelezko, F.; Plenio, M. B. Blueprint for Nanoscale NMR. *Sci. Rep.* **2019**, *9*, 6938.
- (562) Kucsko, G.; Maurer, P. C.; Yao, N. Y.; Kubo, M.; Noh, H. J.; Lo, P. K.; Park, H.; Lukin, M. D. Nanometre-Scale Thermometry in a Living Cell. *Nature* **2013**, *500*, 54–58.
- (563) Toyli, D. M.; de las Casas, C. F.; Christle, D. J.; Dobrovitski, V. V.; Awschalom, D. D. Fluorescence Thermometry Enhanced by the Quantum Coherence of Single Spins in Diamond. *Proc. Natl. Acad. Sci. U. S. A.* **2013**, *110*, 8417–8421.
- (564) Neumann, P.; Jakobi, I.; Dolde, F.; Burk, C.; Reuter, R.; Waldherr, G.; Honert, J.; Wolf, T.; Brunner, A.; Shim, J. H.; et al. High-Precision Nanoscale Temperature Sensing Using Single Defects in Diamond. *Nano Lett.* **2013**, *13*, 2738–2742.
- (565) Tzeng, Y.-K.; Tsai, P.-C.; Liu, H.-Y.; Chen, O. Y.; Hsu, H.; Yee, F.-G.; Chang, M.-S.; Chang, H.-C. Time-Resolved Luminescence Nanothermometry with Nitrogen-Vacancy Centers in Nanodiamonds. *Nano Lett.* **2015**, *15*, 3945–3952.
- (566) Plakhotnik, T.; Doherty, M. W.; Cole, J. H.; Chapman, R.; Manson, N. B. All-Optical Thermometry and Thermal Properties of the Optically Detected Spin Resonances of the NV⁻ Center in Nanodiamond. *Nano Lett.* **2014**, *14*, 4989–4996.
- (567) Hsiao, W. W.-W.; Hui, Y. Y.; Tsai, P.-C.; Chang, H.-C. Fluorescent Nanodiamond: A Versatile Tool for Long-Term Cell Tracking, Super-Resolution Imaging, and Nanoscale Temperature Sensing. *Acc. Chem. Res.* **2016**, *49*, 400–407.
- (568) Dolde, F.; Fedder, H.; Doherty, M. W.; Noebauer, T.; Rempp, F.; Balasubramanian, G.; Wolf, T.; Reinhard, F.; Hollenberg, L. C. L.; Jelezko, F.; et al. Electric-Field Sensing Using Single Diamond Spins. *Nat. Phys.* **2011**, *7*, 459–463.
- (569) Dolde, F.; Doherty, M. W.; Michl, J.; Jakobi, I.; Naydenov, B.; Pezzagna, S.; Meijer, J.; Neumann, P.; Jelezko, F.; Manson, N. B.; et al. Nanoscale Detection of a Single Fundamental Charge in Ambient Conditions Using the NV⁻ Center in Diamond. *Phys. Rev. Lett.* **2014**, *112*, 097603.
- (570) Golter, D. A.; Oo, T.; Amezcua, M.; Stewart, K. A.; Wang, H. Optomechanical Quantum Control of a Nitrogen-Vacancy Center in Diamond. *Phys. Rev. Lett.* **2016**, *116*, 143602.
- (571) Barfuss, A.; Teissier, J.; Neu, E.; Nunnenkamp, A.; Maletinsky, P. Strong Mechanical Driving of a Single Electron Spin. *Nat. Phys.* **2015**, *11*, 820–824.
- (572) MacQuarrie, E. R.; Gosavi, T. A.; Jungwirth, N. R.; Bhave, S. A.; Fuchs, G. D. Mechanical Spin Control of Nitrogen-Vacancy Centers in Diamond. *Phys. Rev. Lett.* **2013**, *111*, 227602.
- (573) Arcizet, O.; Jacques, V.; Siria, A.; Poncharal, P.; Vincent, P.; Seidelin, S. A Single Nitrogen-Vacancy Defect Coupled to a Nanomechanical Oscillator. *Nat. Phys.* **2011**, *7*, 879–883.
- (574) Breeze, J. D.; Salvadori, E.; Sathian, J.; Alford, N. M.; Kay, C. W. M. Continuous-Wave Room-Temperature Diamond Maser. *Nature* **2018**, *555*, 493–496.